NEAR-INFRARED SPECTRAL DEPENDENCE ON TEMPERATURE FOR MAFIC MINERALS, METEORITES, AND LUNAR SOILS: IMPLICATIONS FOR ASTEROID AND LUNAR SCIENCE

A DISSERTATION SUBMITTED TO THE GRADUATE DIVISION OF THE UNIVERSITY OF HAWAI'I IN PARTIAL FULFILLMENT OF THE REQUIREMENTS FOR THE DEGREE OF

DOCTOR OF PHILOSOPHY

IN

GEOLOGY AND GEOPHYSICS

DECEMBER 2000

By

John L. Hinrichs

Dissertation Committee:
Paul G. Lucey, Chairperson
B. Ray Hawke
Jeffrey Bell
G. Jeffery Taylor
David Tholen

We certify that we have read this dissertation and that, in our opinion it is satisfactory in scope and quality as a dissertation for the degree of Doctor of Philosophy in Geology and Geophysics.

DISSERTATION COMMITTEE

Paul Lucey
Chairperson

Jeffrey T. Bell

Bernard Ray Hawke

MSP12

David J. Thaler

ABSTRACT

New measurements of the temperature dependent near-infrared spectra of mafic minerals are made with a new environment chamber apparatus. The new spectra have higher temperature and spectral resolution than earlier data. The radiation environment dominates the surface temperature of the powdered mineral samples in vacuo. Measurements of meteorites as asteroid proxies demonstrate the effect should be detectable with modern spaceborne and telescopic instrumentation within the temperature range expected across the asteroid belt and due to temperature differences produced by variation of solar insolation angle. Meteorite spectra show even larger change in the near-infrared between main-belt temperatures and terrestrial ambient. Near-infrared spectral measurements of lunar soils show insignificant sensitivity to temperature.

TABLE OF CONTENTS

LIST OF TABLES

LIST OF FIGURES

CHAPTER 1

Introduction

Variability of mafic minerals' near-infrared spectra as a function of temperature was investigated in the pioneering work of Ted Roush in his 1984 Master's Thesis[1]. Later, a series of papers Roush and Singer[2,3,4] detailed how the width, area, and placement of mafic silicate absorption features may change with changes of temperature and admonished the planetary community that remote sensing analysis of bodies such as asteroids may be in error if this effect is neglected. This paper extends the work of Roush and Singer with new, more reliable, measurements of mafic minerals and investigates the fine details involved in measurements of this type.

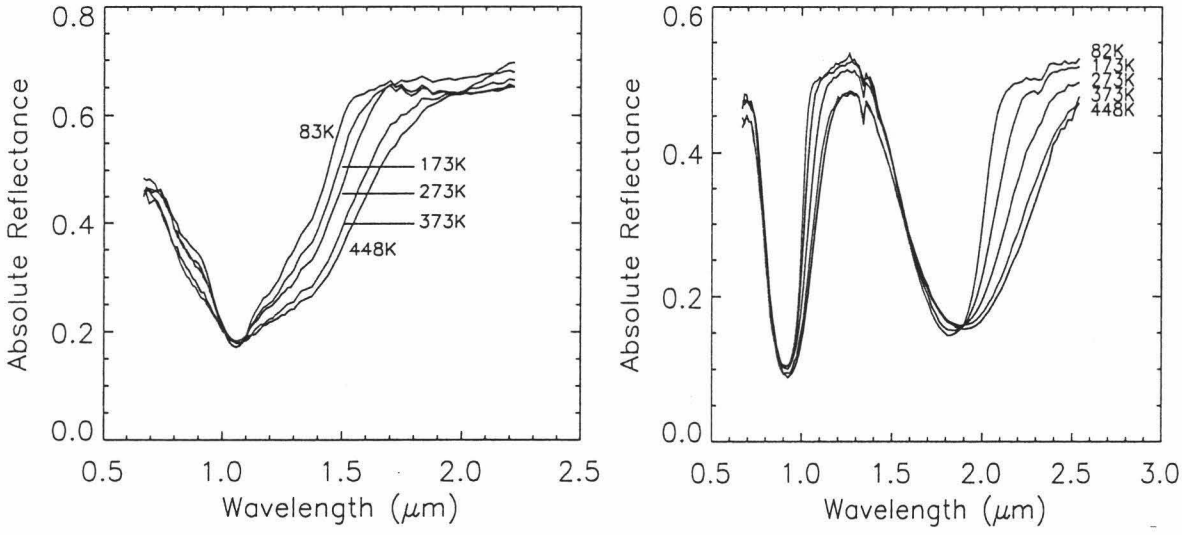

Figure 1.1. Results from Ted Roush's 1984 University of Hawaii Masters Thesis demonstrating the dependence of olivine and pyroxene near-infrared spectra to temperature. The left plot demonstrates this effect for a Fo 89 green sand beach olivine and the right plot shows the effect in a bronzite pyroxene.

There are details not addressed in the Roush and Singer work that cause the quantitative interpretation and validity of those measurements to be questioned. In particular, the detail of the samples' optical surface true thermodynamic temperature is

left open to question. We will show that the sample radiative environment, neglected in the previous work, is the primary factor to determine the optical surface temperature and we have made substantial advances in quantifying how much this parameter affects experimental results. With this knowledge we are able to revisit the Roush measurements and quantify the sensitivity to temperature that these NIR absorption features exhibit.

Figures 1.1 shows results from Roush's 1984 thesis for the minerals olivine and pyroxene. These data demonstrate how the mafic absorption features tend to broaden with increasing temperature and how the pyroxene band minima shift in wavelength.

The nature of these absorption features is discussed in many sources[5] and is believed to be due to electronic transitions between the d-orbitals of the Fe^{2+} cations within the mineral's crystal structure. Ordinarily a free standing Fe^{2+} ion has no preference for which d-orbitals are filled or partially filled (of course always in accordance with the Aufbau "building up" principle). When these ions are coordinated within a silicate crystal the symmetry between d-orbitals is broken and different orbitals will have higher or lower occupancy energy depending on its orientation to the electric field at the occupancy site. These small differences in energy between otherwise degenerate d-orbitals are responsible for the absorption seen in the infrared. Only metals in the transition series have partially filled d-orbitals so the magnesium component of a solid solution series does not produce these near-infrared absorptions. However, the relative amounts of Mg and Fe, as well as other elements, affect the average interatomic spacing and therefore do have secondary

effects on the absorption features. These secondary effects are exactly the diagnostic features that NIR remote sensing looks for to determine the chemistry of mafic silicates.

It is not unreasonable to assume that as the temperature of the mafic silicate changes, so too will the interatomic spacing and subsequently the crystal field. Consequently it is not surprising that temperature affects the absorption features seen in the near infrared.

The implications of this temperature effect on mafic mineral infrared spectra may have profound effects on interpretation of remote sensing data of asteroids and moons because it may confuse of be mistaken for changes in silicate chemistry. However, any attempt to quantify the influence of the temperature effect using the Roush and Singer spectra will be in doubt due to uncertainties in the original data quality. In particular, the pyroxene Band1/Band2 areal ratio analysis of Cloutis and Gaffey[6] may be sensitive to the temperature effect. Current work in the field of remote sensing of planetary surfaces dominated by mafic minerals has reached the point now with the Galileo and NEAR-Shoemaker missions that these subtle details begin to be important. Telescopic NIR remote sensing analysis has also advanced since the days of the original Roush and Singer work with new instruments such as SPEX at the IRTF such that temperature differences may now be detectable. Any analysis of mineral spectra using band area or the location of pyroxene band minima will be in question if the temperature effect demonstrated by Roush and Singer is not accounted for. It is important at this point to better quantify the effects reported by Roush and Singer.

To see where the Roush and Singer data may be improved it is important to review how their data were collected. Figure 1.2 shows the apparatus used by Ted Roush for his experiments. A powdered sample was placed in the sample cup inside an evacuated chamber immersed in liquid nitrogen. The sample was heated from below and a temperature probe embedded in the powdered sample monitored the

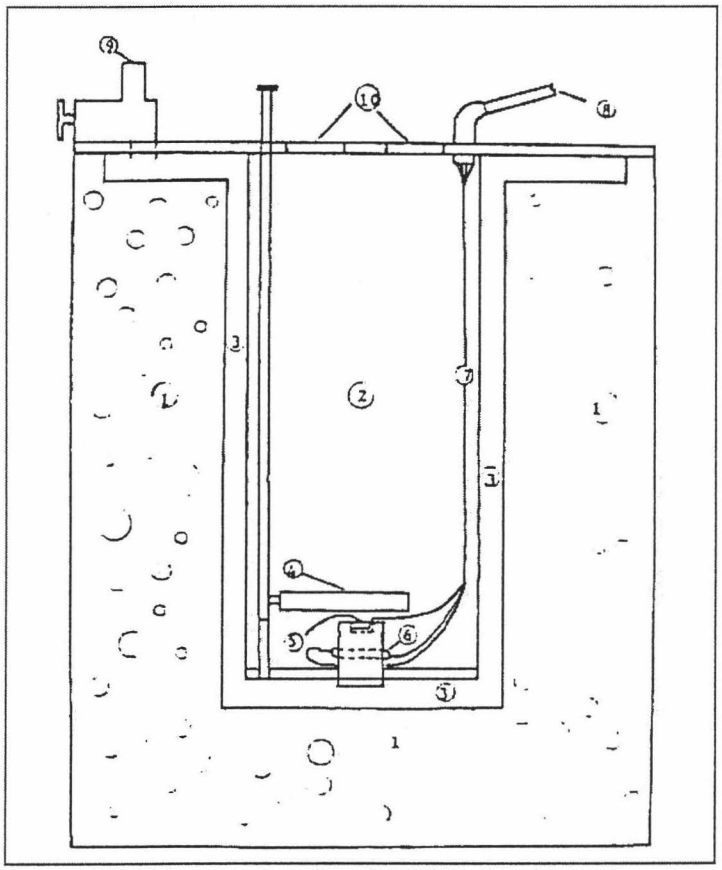

Figure 1.2. Schematic from Roush (1984) of the his environment chamber. Note that the LN_2 level is unconstrained and the top surface is not isolated from ambient temperatures.

sample temperature. The sample was illuminated and measurements taken through windows in the cover of the chamber. The cover itself was at close to ambient

temperature and the level of liquid nitrogen bathing the inner chamber walls is variable and unknown for any particular measurement.

Silicate powders in vacuum are notoriously low in thermal conductivity. For example the conductivity of lunar soils is measured to be 1.72×10^{-4}W/cmK as reported in the Lunar Sourcebook[7]. This leads to what may be the greatest uncertainty of the previous measurements: thermal gradients will be produced between the heating element and the temperature sensor; between the optical surface and the heating element; and between the optical surface and the temperature sensor. Heat flow, driven by the existence of temperature gradients is unable to dissipate those gradients in any reasonable time scale for laboratory measurements because of the extraordinarily low thermal conductivity of the silicate powder in vacuum. Temperature gradients on the order of hundreds of kelvins per centimeter are common on the lunar surface. Hence, for the earlier measurements, the *actual* thermodynamic temperature of the optical surface is uncertain.

The implication is that the radiation environment of the sample becomes the primary means of setting the optical surface temperature. This assertion will be tested in this work.

Any new work to improve the measurements made by Roush should address the following points:

- What is the true optical surface temperature of the sample?
- How does the radiation environment affect optical surface temperature?
- Does the act of measurement affect sample temperature – source illumination?

- The need for smaller temperature steps to better characterize sample response
- The need to measure more and varied samples

Planetary Geosciences' New Environment Chamber

At Planetary Geosciences/HIGP we have constructed an environment chamber that enables us to address these points directly. The key to the new system is an inner radiation chamber that acts as a blackbody cavity to control the sample's radiation environment. This concept is the idea of Dr. Paul Lucey who designed the new chamber. Using this chamber we have been able to test the idea that the radiation environment is the primary factor determining sample optical surface temperature. Once the factors controlling the sample optical surface temperature are understood and controlled then we have been able to make many new measurements with this chamber far surpassing the Roush measurements in temperature and wavelength resolution.

Figure 1.3 shows details of the chamber. There is an outside vacuum jacket that keeps humid air from condensing ice or dew onto cold samples and improves the thermal isolation of the sample from the laboratory environment. The vacuum canister is fitted with two BK-7 windows: one to allow sample illumination into the environment chamber and the other as an exit path for the light reflected off the sample to get to the detector. Both windows are situated 10.5° from the normal such that the phase angle of the system is 21°. Just inside the vacuum jacket is the first radiation shield, which protects the inner parts of the chamber from the thermal

radiation emitted by the vacuum canister and provides a constant background of known temperature. This outer radiation shield is physically attached to a large liquid nitrogen reservoir in the base of the vacuum jacket. Its surfaces are raw aluminum on the outer surface - facing the inside of the vacuum jacket - and the inside surface is painted with Krylon flat black primer which is very black and flat in the NIR spectral range. This combination of reflective outside surface and black, highly absorbent to radiation, inside surface helps isolate the radiation shield from the outside environment while acting as a sink for radiation within its confines. Further inside the environment chamber is a cold-plate holding the sample enclosed in another second, inner radiation shield euphemistically called the "doghouse". Like the outer radiation shield the doghouse is reflective aluminum on the outside and painted with Krylon flat black primer on the inside. The doghouse also has two BK-7 windows used for illuminating and measuring the sample. The doghouse is firmly attached to the cold plate, made of brass, to ensure solid thermal contact. A temperature sensor is placed on an upper surface of the doghouse far from the cold plate to determine the temperature at this remote location and ensure it is uniform with the cold plate. The inside of the doghouse is painted with Krylon flat black primer which is the major source/sink of radiation within the cavity and contributes to the cavity's blackbody characteristics. Sitting on the cold-plate inside the dog house is a sample cup typically holding 1.5g of powdered sample at a depth of up to four millimeters and with a 20mm. diameter. The sample cup spatially extends to the inner surface of the dog house and is coated with a special hardened flat black coating from High Performance Coatings of Salt Lake City, Utah. The BK-7 windows of the doghouse

pass NIR but absorb MWIR and LWIR radiation so the doghouse becomes a very effective black body cavity with the sample inside it. Spatially the sample is completely surrounded with surfaces of high emissivity in the IR with the exception of the BK-7 windows. However, in the wavelength domain the windows provide only a small opening into the outer environment in the NIR but act more like a black wall in the MWIR and LWIR so the classic blackbody cavity is approached by this configuration. Attached to the cold-plate is a heater, a temperature probe, and an adjustable cold-finger to a liquid nitrogen reservoir separate from the outer radiation shield's reservoir. By adjusting the cold-finger and the heater any temperature environment from liquid nitrogen temperatures (~77K) to 473K may be maintained in the doghouse and due to the black body nature of the dog house in the radiation environment of the sample.

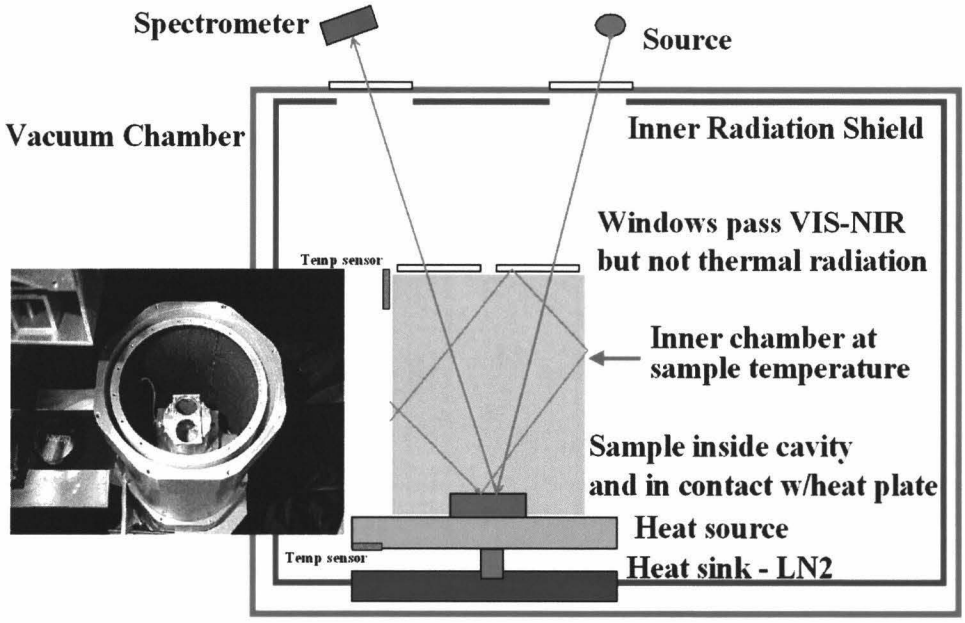

Figure 1.3. The Planetary Geosciences/HIGP environment chamber used for the new measurements. The sample is held in a well constrained radiation environment.

The spectrometer used to acquire data is a Spectral Devices FieldSpec spectro-radiometer. The FieldSpec measures radiance between 350nm and 2499nm with spectral resolution of 3nm or better depending on wavelength[8]. This wide detection range is due to three complementary sets of detectors, VIS, SWIR1 and SWIR2, which span the entire set of wavelengths. However, using three detector ranges to synthesize one spectrum adds complications of instrumental drift and calibrations for each detector range, different dark current rates and readout noise, and temperature stability for each detector range. To minimize these problems the FieldSpec takes instrumental dark current measurements as a regular part of the set-up process and at regular intervals. The instrument also automatically sets and calibrates the various gain and offsets used to make the radiometric measurements using calibration data from Analytical Spectral Devices.

Since reflectance data is the goal of this experimental setup, several calibration uncertainties that may creep into the radiance data are ratioed out in the process of converting the raw radiance data into reflectance data. This process eliminates many of the experimental uncertainties inherent in the raw radiance data. To produce reflectance data from a sample a set of five measurements are made. Before measuring the sample a Spectralon standard is measured in the same place the sample will sit moments later when the environment chamber is moved into place. The optical path between the light source, the Spectralon, and the detector is geometrically the same as when the chamber with sample is in place. The repeatability of moving Spectralon standard and chamber back and forth into the illumination/detector path is ensured by a track with solid detents placed at the two measuring locations. After the

Spectralon is measured the environment chamber is moved into position and a 3 mm thick piece of blackened aluminum is placed between the light source and chamber to block off all external illumination into the chamber. This second measurement gathers information about any residual dark current counts not fully corrected for by the FieldSpec internally, any scattered light from inside the chamber which might exist and, more importantly in practice, measures any radiance emitted by the sample within the chamber. After the "chamber-dark" measurement the aluminum shutter is removed and the sample itself is measured. Another chamber-dark measurement is taken after the sample is measured. Finally the Spectralon is moved back into position and another white reference is taken. The bracketing of sample measurements by darks and white reference data ensures that any temporal drift of the apparatus is compensated for and averaged out. Each of these five measurements is composed of a set of ten separate measurements: to reduce noise, to generate error statistics, and to provide a bit of redundancy in the data. Each of the ten measurements of each set are the result of between 200 and 256 spectra which are co-added and averaged by the FieldSpec internally before an output file, one of the set of ten for each of the five basic radiance measurements is written to disk. A typical output spectrum will be the product of fifty files of between 200 to 256 individual spectral measurements each resulting in 10,000 to 12,800 raw radiance measurements going into each single reflectance spectrum presented here. The fifty output files represent ten white reference, ten measurements of the environment chamber with no outside illumination (a so called "dark"), ten measurements of the sample, ten more measurements of the environment chamber with no illumination, and finally ten white reference

measurements. These fifty radiance spectral files, in five sets of ten, are made by the FieldSpec spectro-radiometer over about 25 minutes.

After the raw radiance data has been collected by the FieldSpec spectro-radiometer it is transferred to the Planetary Geosciences unix network for data reduction and analysis. The data reduction method is done using an IDL program that gathers statistics on each set of 10 files then averages all the reference data, the dark data, and the sample data and then derives a reflectance spectrum from the fifty files. Since an entire data run may be composed of 19 output spectra at different temperature the data analysis routine typically performs this task on all 950 data files, 19 sets of fifty, at one time resulting in an array of reflectance spectra that can be plotted against wavelength or temperature.

Mathematically the IDL routine does this for each temperature data set after averaging the five sets of files into the three radiance spectra:

$$\left[(Srad*Tr)-(D1rad*Tr)\Big/(REFrad*Tr)-(D2rad*Tr)\right]=Sreflect\_raw$$

Where:

- Tr = the data path transfer function, (included to demonstrate how it ratios out of the result) probably close to one but not well known. It is the accumulated error of the data path between measured object to the hard disk. This function is assumed to be a linear function of the true data and that it doesn't change over the 50 file measurement time interval, about 25minutes. The quality of the reduced data indicate that these assumptions are reasonable.

- Srad = the sample radiance
- D1rad=radiance of the chamber at sample temperature, includes sample emission
- REFrad = the reference radiance
- D2rad = radiance of the reference with no illumination at room temperature
- Sreflect_raw = preliminary sample reflectance spectrum

Once a preliminary spectrum is derived several corrections must be applied. The first correction is for the BK-7 glass that is not present in optical path of the Spectralon standard measurement. Measuring the same piece of Spectralon in and outside of the environment chamber derives this correction. A second correction must be applied for the difference between Spectralon and a perfectly reflecting labertian surface. Finally, a third correction for the water vapor in the optical path of the reference spectra which is mostly absent in the optical path of the sample data because a significant fraction of that optical path is in vacuum.

$$Sreflect\_raw * Window * H2O * Spectralon = Sreflect$$

New Results

Using this new chamber we have revisited the original work of Roush. Measuring a green sand beach olivine, Fo88, and a sample of the orthopyroxene measured by Roush, Pyx110, from Edward Cloutis we have collected the data shown in Figure 1.4. These figures, in comparison with the Roush results in figure 1.1, are

early results of the new chamber but clearly demonstrate the increased spectral resolution and temperature resolution that can be achieved using the new chamber.

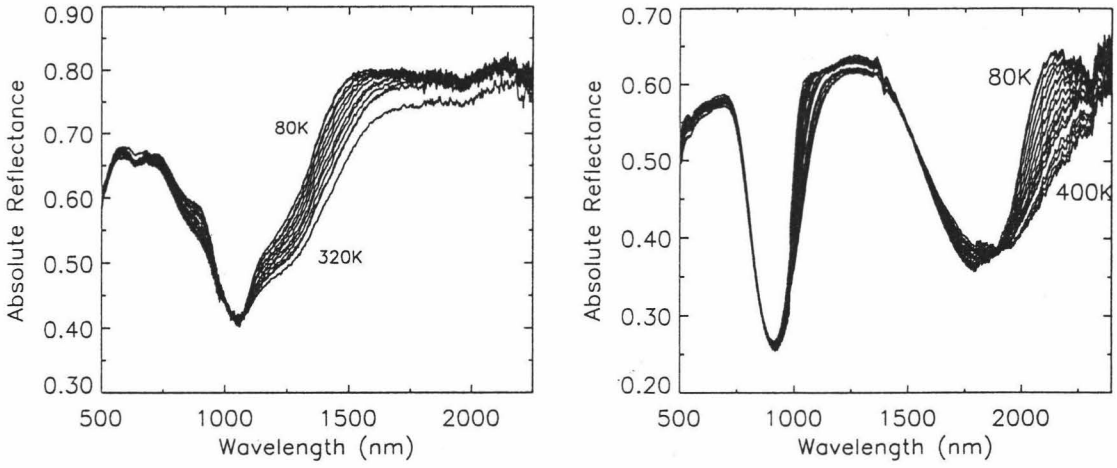

Figure 1.4. Measurements made with the new chamber. At left is a green sand beach olivine, Fo89 , <45 μm grain size, and at right is a bronzite pyroxene 45-90 μm grain size (wet sieved). Both samples are from the same source as the Roush samples and provide a direct comparison to the older data presented in figure 1.1.

how important the radiation environment is for determining the sample optical layer temperature. If the result shows a strong coupling to the radiation environment, as we expect, then all prior measurements, including those of Roush, where the radiation environment has not been well constrained and measured are brought into question.

To test the sample sensitivity to the radiation environment a normal set of data collection is performed three times on the same sample: once with the dog house in place and performing its function to keep the radiation environment as close to sample temperature as possible; once with the dog house removed and outer radiation shield held at ~77K to keep the radiation environment of the sample cold; once with the doghouse removed and the outer radiation shield held warm to keep the radiation environment of the sample hot. Differences between the resulting three data sets

should be due entirely to the differences in radiation environment since the only differences between the runs is the radiation environment of the sample (and the absence of the BK7 doghouse windows for the two runs without the doghouse – which is easily corrected by taking reference Spectralon data without the doghouse in place). A forsteritic olivine ground from whole crystals by Natalie Domergue-Schmidt was used as the reference sample. The olivine was wet sieved by Ms. Domergue-Schmidt to a grain size of 20-63μm and the sample has a measured Mg# of 86. As a measure of the radiation temperature inside the chamber another temperature probe is attached to the very top inside surface of the outer radiation shield between the illumination and measurement apertures. Due to some thermal and radiative coupling between the temperature varying components of the chamber, the hot and cold temperatures of the outer radiation shield had small variation from the optimum. In the case where the outer radiation shield was held cold via its coupling to a LN_2 reservoir the temperature varied from 87K when the sample plate was at 100K to 103K when the sample plate was 400K. The 16K variation of the outer radiation shield was almost certainly due to radiant flux coming off the sample plate. In the case of holding the outer radiation shield hot by jamming aluminum foil between it and the vacuum casing and simultaneously blowing room temperature N_2 gas through the outer can's LN_2 reservoir, the temperature varied between 286K and 294K while the sample plate varied between 100K and 400K The results of the radiation environment experiment are shown in figure 1.5.

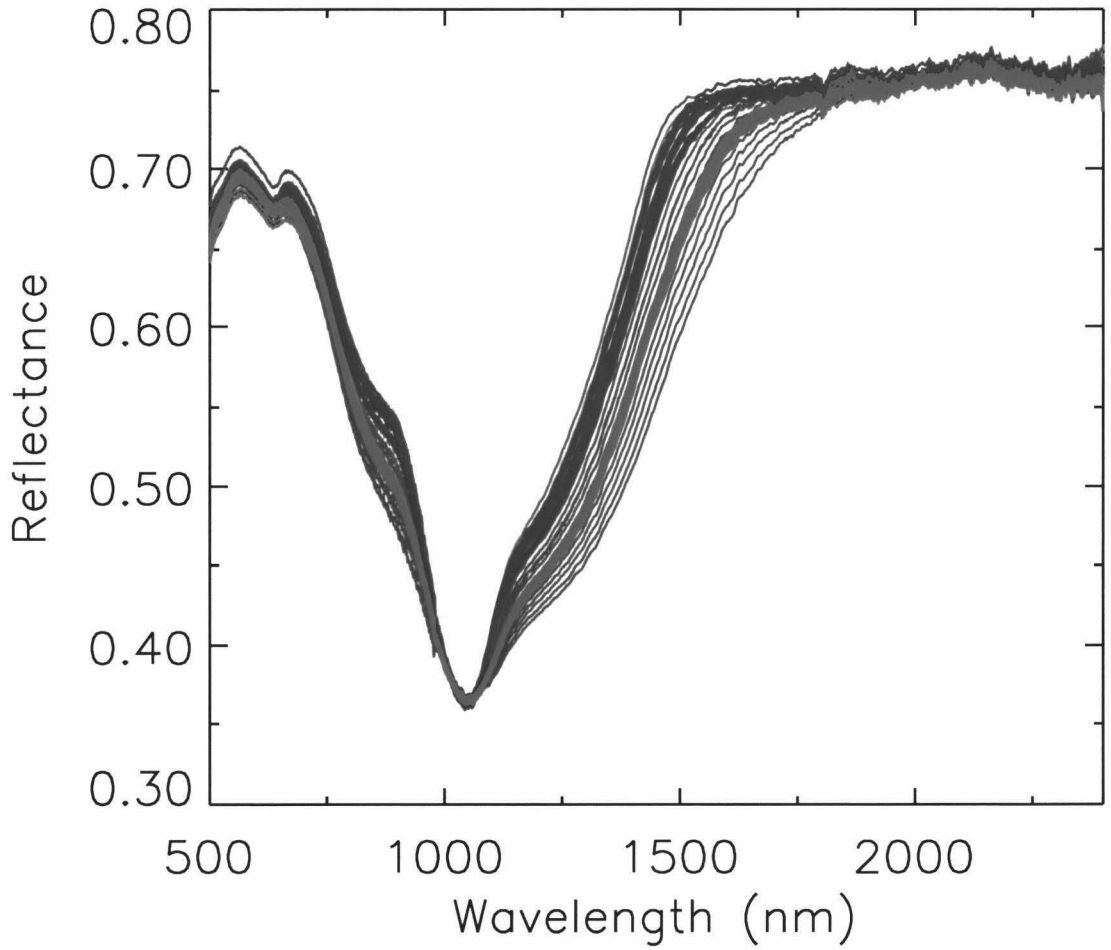

Figure 1.5 Measurements of Fo86 olivine (20-63μm grain size) made with the inner chamber at sample temperature are in green. Measurements without the inner chamber but warm background are red and cold background are blue. Hot plate temperatures cycle from 100K to 400K in all cases and measurements are in 20K increments.

These results clearly demonstrate a strong coupling between the optical surface and the radiation environment. Any heat flow from the base of the sample cup, through the ~3mm of powdered sample, to the optical surface must be negligible when compared to the radiant flux incident to the surface. In fact, this coupling is so strong and the relative effect of sample cup temperature so small that by plotting reflectance at 1.4μm vs. temperature it may be possible to use this effect as a thermometer to determine the optical surface temperature. Note that in figure 1.6 the crossing points

are very near the outer radiation shield temperatures of ~95K and 290K for the cold and hot runs respectively.

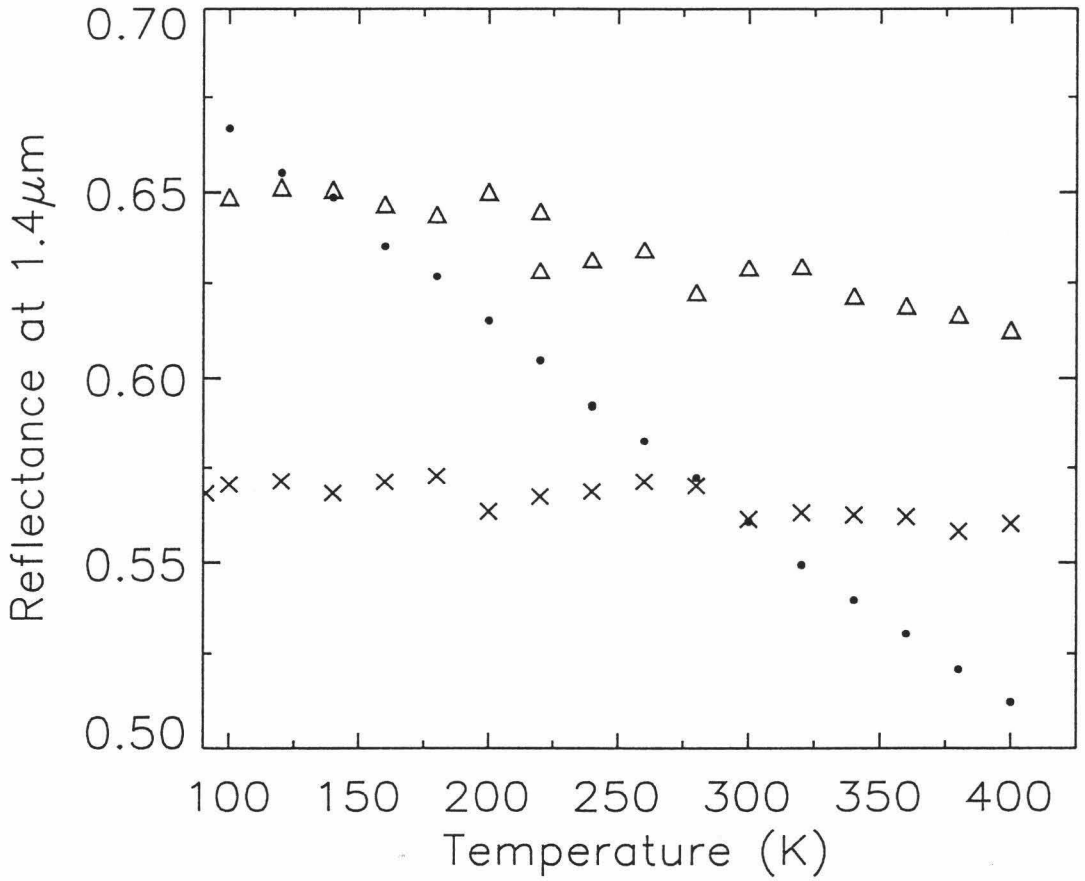

Figure 1.6 Measurements of Fo86 olivine (20-63μm grainsize) Dots are measurements with the inner chamber at sample temperature. Measurements without the inner chamber but ~95K background are triangles and ~290K background are crosses. Sample plate temperatures cycle from 100K to 400K in all cases and measurements are in 20K increments. Note the proximity of the crossing points to the background temperatures.

Because the sample is primarily sensitive to the radiation environment the issue of sample heating by the illumination source becomes important. The illumination for the laboratory setup is provided by a 12 volt DC, 100 watt, quartz-halogen bulb and a collimating mirror is used that directs the sample illumination onto

the sample. To measure the flux of this irradiance on the sample, the FieldSpec spectroradiometer was used in absolute radiance mode. First, the absorption of the BK-7 glass windows between the sample and the detector and the glass in the detector foreoptic was measured. Then a Spectralon reference was placed in the chamber and

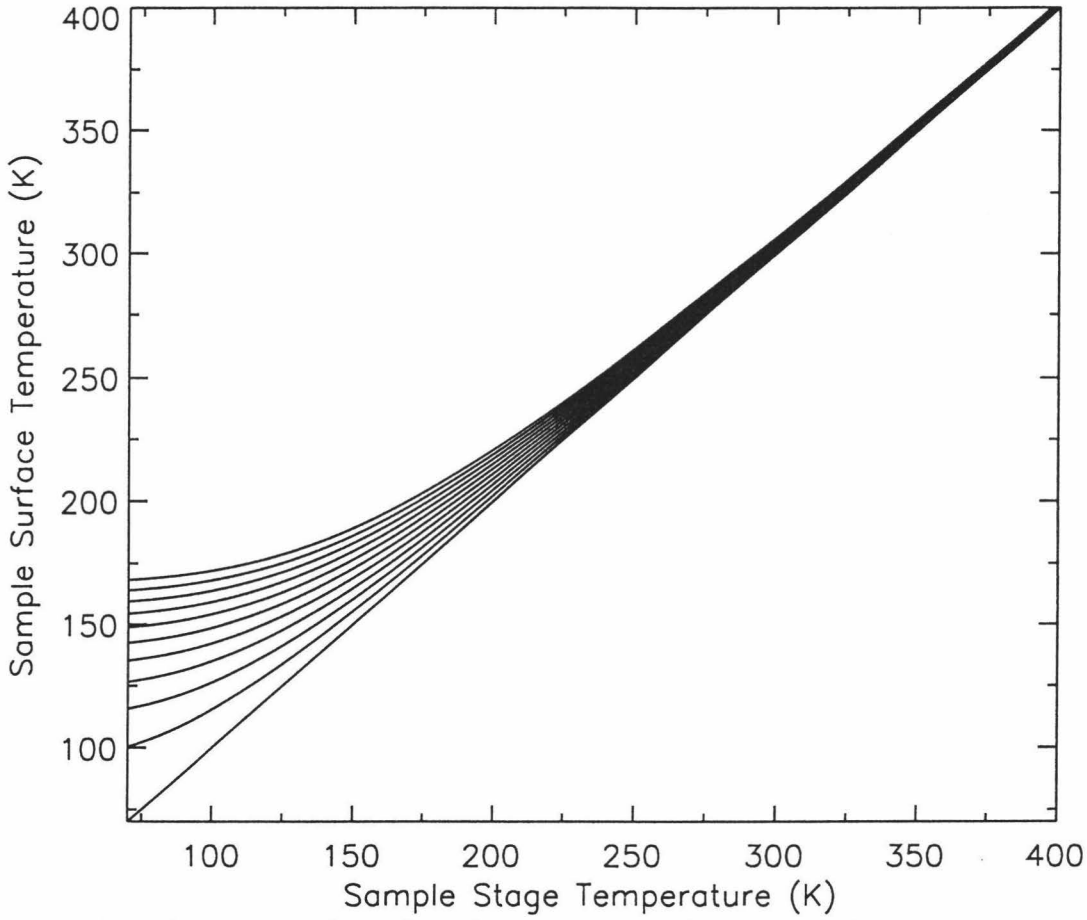

Figure 1.7. The increase of sample surface temperature due to sample heating by the illumination at 44 w/m^2 may be approximated using this family of curves generated from a worst case scenario of zero sample thermal conductivity. The curves range from 0% albedo at top to 100% albedo at the bottom in 10% albedo increments.

the radiance coming off the sample under typical lighting was measured. The corrections for the two BK-7 windows and the detector fore optic were applied and the result integrated over wavelength and multiplied by the solid angle factor (2π

steradians times 0.5 for a lambertian reflector) of π. The irradiance was thus measured to be ~44 watts/m^2 for the samples. Using this information and an assumption that the sample has zero thermal conductivity a set of worst-case sample surface temperature curves can be derived based on the sample surface being in radiative equilibrium with its environment. Essentially these curves show the extra temperature the surface must achieve to re-radiate the illumination source irradiance and the black-body radiation from the doghouse. The resulting family of curves based on sample albedo is shown in figure 7. The result shows that the illumination, less than 1/30 the solar constant of 1,353 w/m^2 has an appreciable effect on sample surface temperature at low sample temperature. The implication is that temperature probe measurements made from any location on the cold stage or on the interior of the doghouse are systematically in error and that the optical surface is warmer than the reported temperatures. Bearing this in mind it is evident that the reported sensitivity to temperatures are *lower bounds* to the true sensitivities since whatever spectral change occurs is actually due to a smaller range of temperatures than that reported from the temperature probe. It is also evident that measurements made without knowledge of the sample illumination flux are of questionable value.

In the future more accurate sample surface temperatures may be determined that the use of radiometric measurements of the sample but that is beyond the scope of our abilities with the present apparatus. Without a radiometric measurement corrections for sample surface heating due to the illumination are contingent on knowing the sample albedo and the thermal conductivity of the sample. While the albedo is known but varies with temperature, the thermal conductivity is not well

constrained in relative terms between samples and can be affected by grain size, sample packing and settling, temperature, and the quality of the vacuum at any point in the series of measurements. Hence, the temperatures reported here *are the measurements of the cold plate* and reflect the true black body radiation temperature of

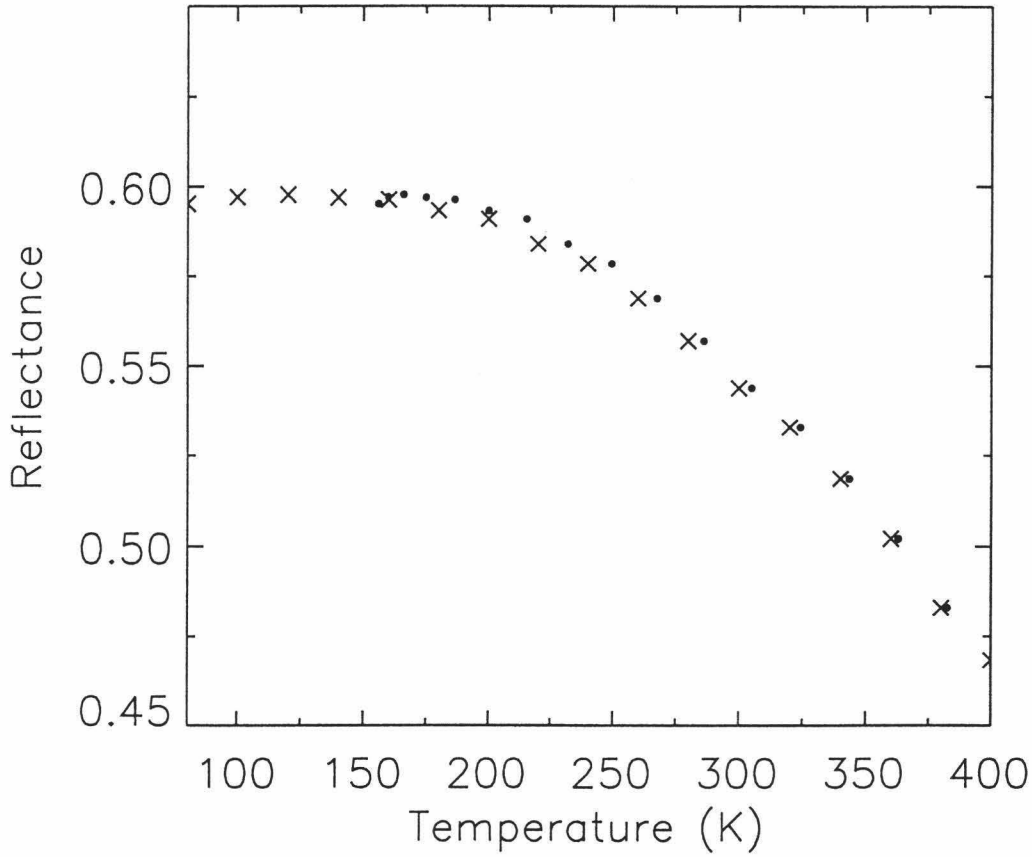

Figure 1.8. Pyroxene data from figure 5 plotted as reflectance vs. temperature at 1.1 μm. The crosses are the uncorrected temperatures, i.e. doghouse temperatures as measured by temperature probes. The dots are the same data with temperatures adjusted to represent sample surface temperature given 30% albedo and sample illumination of 44 w/m^2 and zero sample thermal conductivity. Note the break in slope remains even after the correction.

the doghouse cavity.

A common characteristic of the samples measured is a break in slope observed at colder temperatures in reflectance vs. T plots. At first inspection this break in slope

at colder temperatures might be attributed to the effects of illumination heating. To test this hypothesis the data from the pyroxene sample was plotted as reflectance against temperature at 1.1μm and then replotted with the temperatures adjusted for 30% albedo in our experimental setup. The result demonstrates that this turnover is not an artifact caused by illumination heating but instead is a physical characteristic of the sample. In fact, the sample shows very little temperature effect below ~225 K regardless of a temperature correction.

Now that the utility of the new environment chamber has been demonstrated we have revisited the fundamental measurements of Roush in greater detail. In particular we have made measurements of three different olivines including the previously mentioned green sand beach olivine. Also a pyroxene sample from the same batch, provided by Edward Cloutis, has been measured. With these new measurements a new baseline is established based on a more detailed understanding of the issues surrounding these type of measurements and which replaces the prior measurements in detail, accuracy and precision. The new measurements also provide us with a reference point to look back at the measurements of Roush so as to determine the extent to which the uncertainties in his measurements affected the accuracy of his results. As has been demonstrated here, the two major factors, which he did not account for, are the radiation environment of the sample due to the interior of the measurement chamber and the heating of the sample by the external illumination.

Green Sand Beach Olivine

This sample was collected from the green sand beach near South Point, Hawaii. As this was the first data run using the new environment chamber the data range is only between 80-320K and there is noticeably more noise in the long wave end than in later measurements. Data quality shows great promise for subsequent

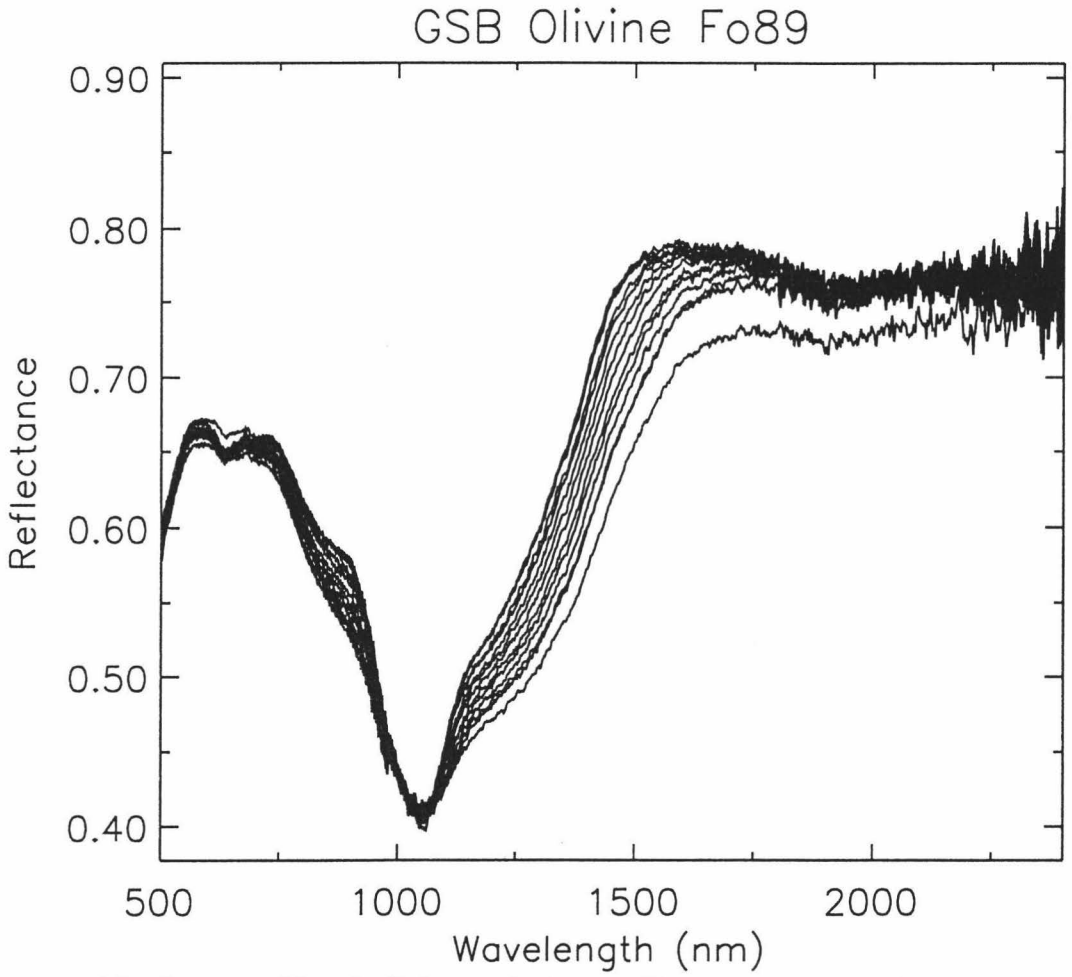

Figure 1.9. Green sand beach olivine, grainsize is <45 μm grainsize. Doghouse temperatures range from 80 K (top curve) to 320 K (bottom curve) in 20 K increments.

measurements and is easily sufficient for comparison with the earlier work of Roush. As with the Roush data the 1 μm feature widens and the overall reflectance decreases with temperature.

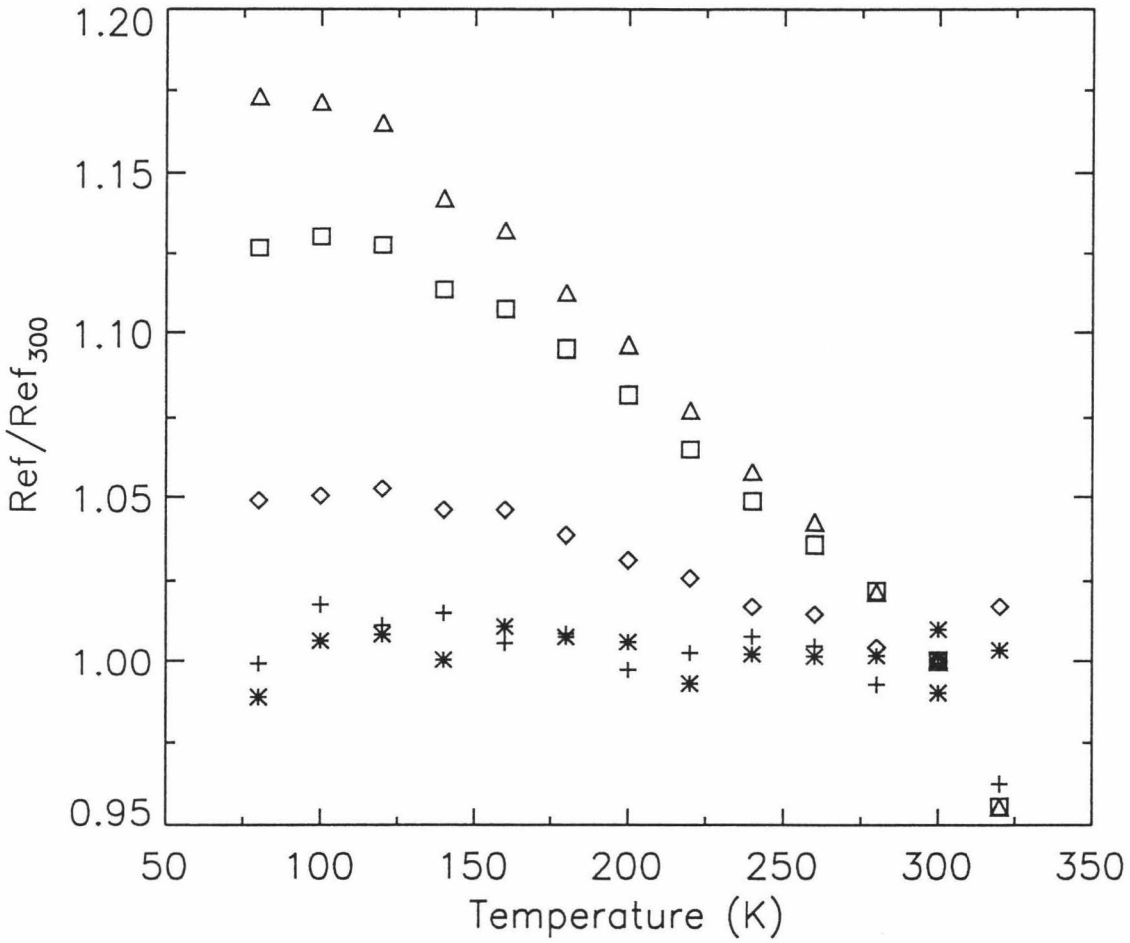

Figure 1.10. Green sand beach olivine reflectance relative to 300 K spectra. Diamonds are 0.8μm, asterisks are 1.0 μm, triangles are 1.4μm, squares are 1.5μm, and plus signs are 2.0 μm.

After data reduction the resulting spectra may be plotted against temperature. The low temperature roll-off, discussed previously, is clearly obvious in figure 1.10. Both the 1 μm data and the 2 μm data are essentially flat while data on either side of the band minimum show the temperature effect with a maximum effect around 1.5 μm. The slopes of these lines (in the linear region) are used to determine a sensitivity spectrum as shown in figure 1.11. The value at the 1.4 μm point in figure 1.11 is the same as the slope presented here except that the slope is measured in % change relative to the 300K value (at 1.4 μm in this example) *per 100 K temperature change.*

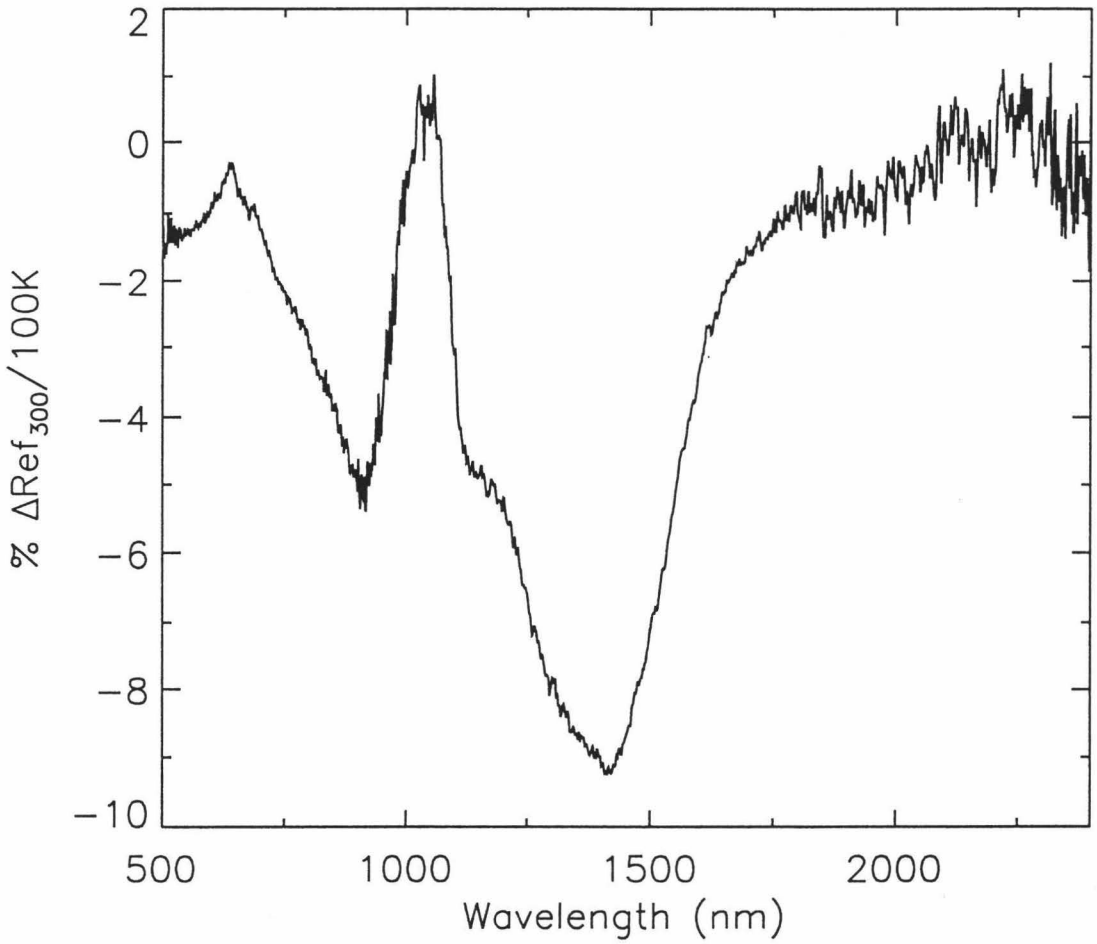

Figure 1.11. Temperature sensitivity plot for green sand beach olivine sample derived from 180K to 300K spectral data. This data represents the slope of data points shown in figure 1.10 in units of percent change vs. the 300K reflectance per 100 K change in temperature.

Fo 88 olivine

Lubja Moroz of DLR Germany provided this olivine sample. These data show improved quality compared to the earlier green sand beach measurements. These data were provided to Jessica Sunshine[9] and she wrote back that she suspected some contamination with a pyroxene component. Comparison of figure 1.13 with figures 1.15 and 1.17 supports this suspicion. Not only does each material have a characteristic NIR spectrum but its sensitivity spectrum can also be used as a tool to determine composition.

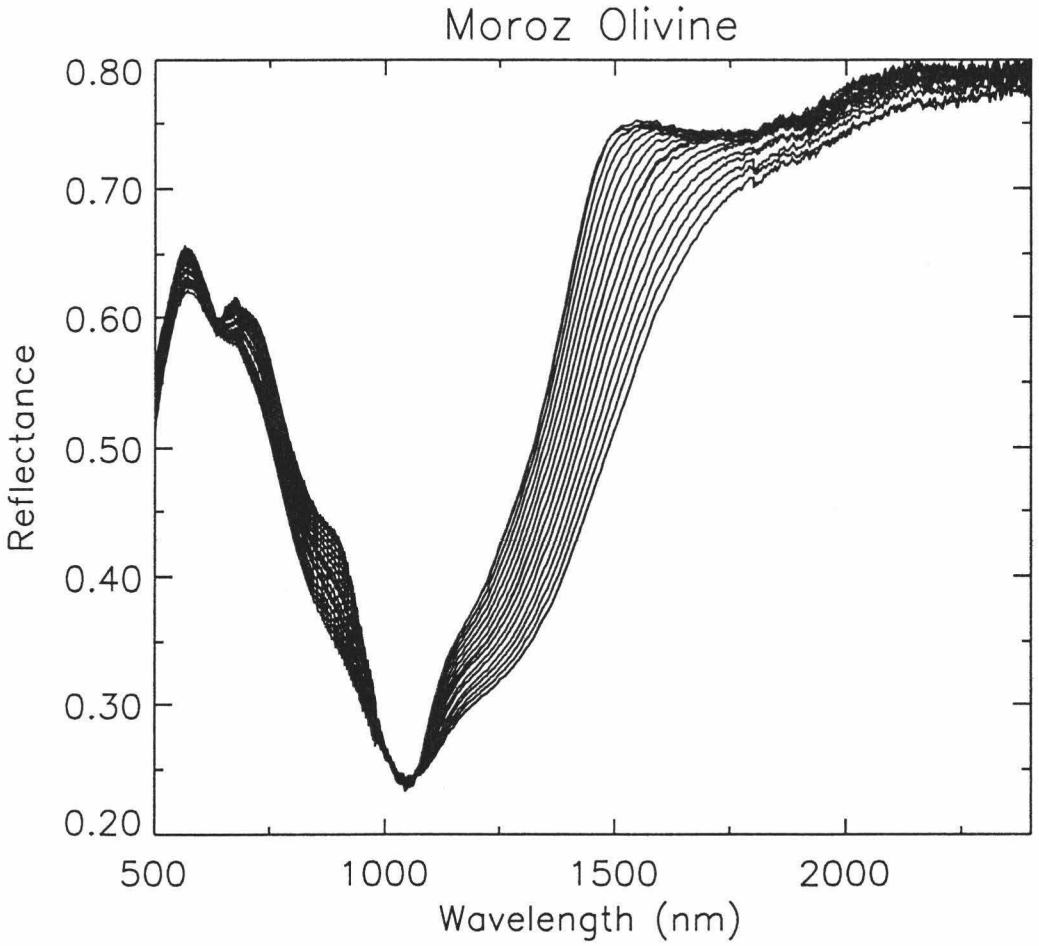

Figure 1.12. This sample of Fo 88 olivine, 32-63 μm wet sieved, demonstrates the same effects seen with the green sand beach olivine Data collected from 80 K to 400 K in 20 K increments.

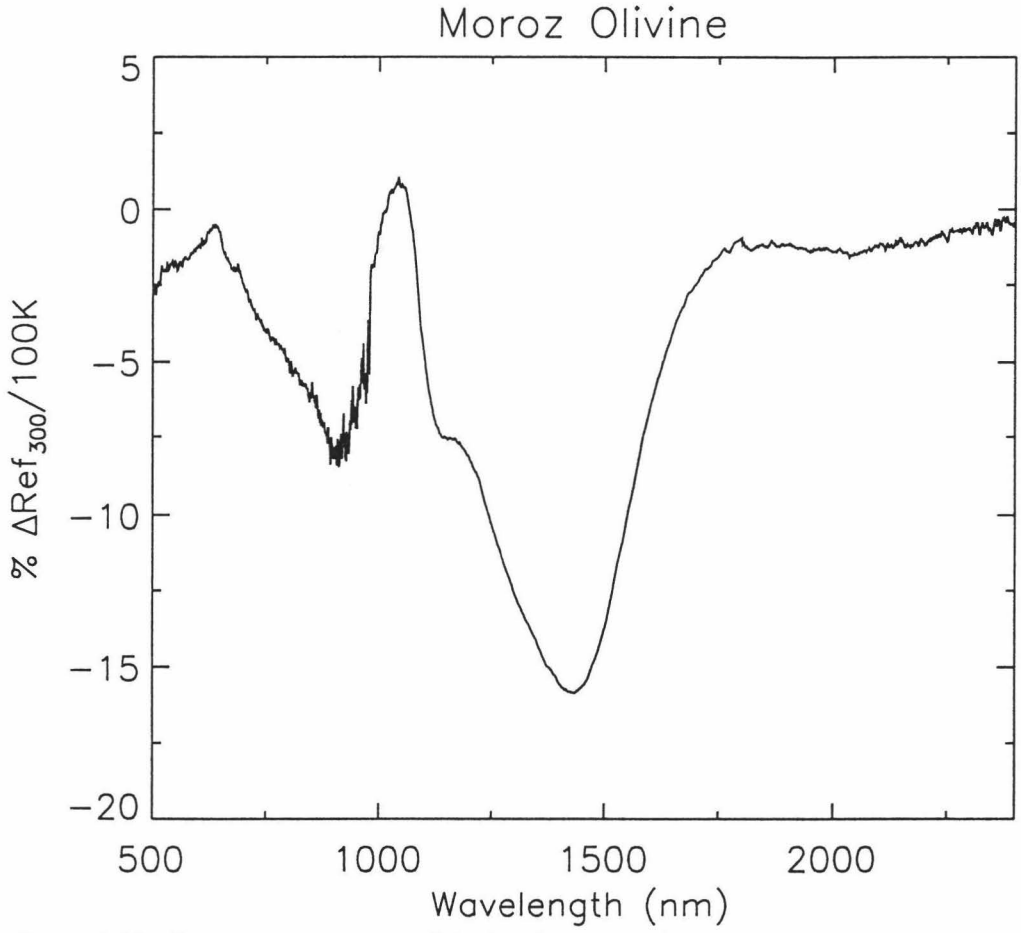

Figure 1.13. Sensitivity spectrum of Fo 88 olivine, 32-63 μm grain size sample. Note the negative valued sensitivity dip around 2.0μm. This, when compared to the other olivine samples may imply contamination of the sample by an unknown pyroxene component.

Fo 86 Olivine

This sample was derived from single large olivine crystals sold as jewelry and prepared for analysis by Ms. Domergue-Schmidt. The spectra are the best in terms of all around data quality and sample quality. The sample was wet sieved to 20-63 μm grain size.

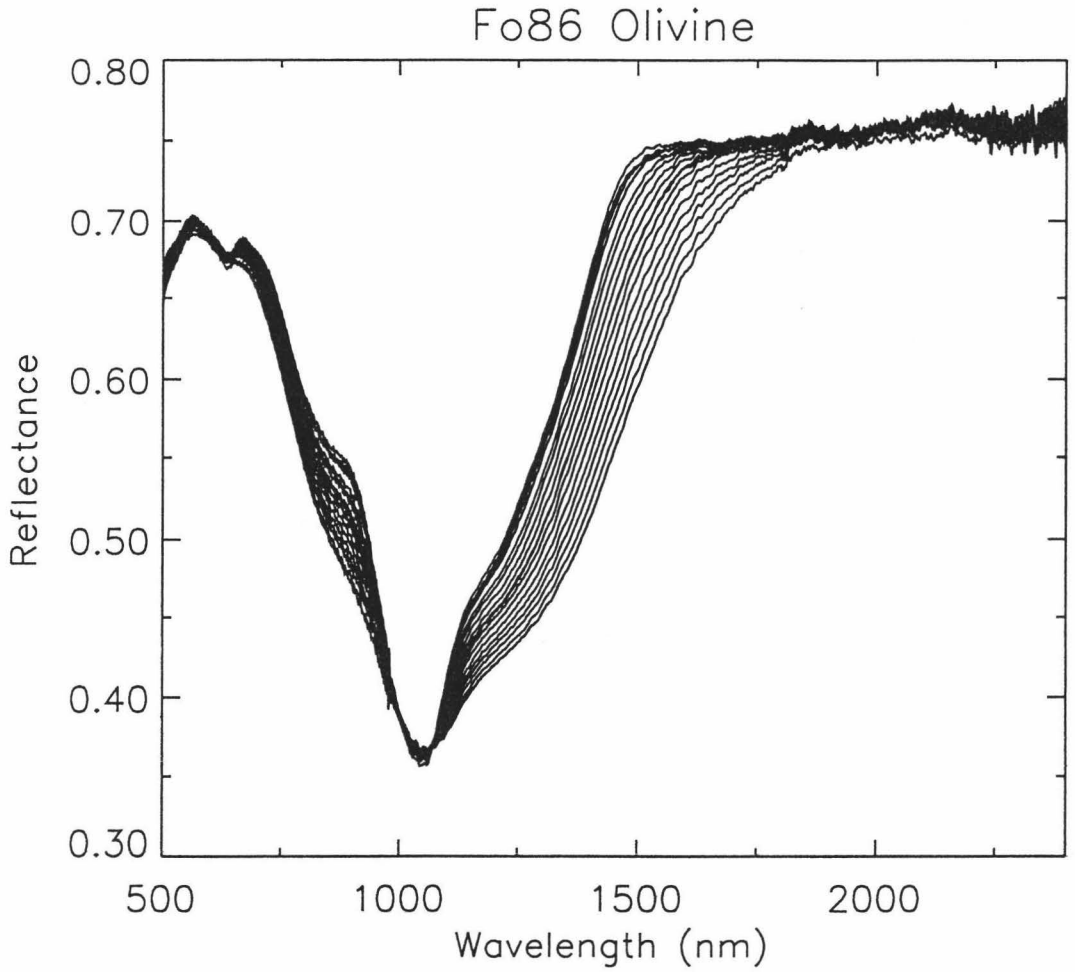

Figure 1.14. Fo 86 olivine derived from single whole crystals of peridot. Grain size is 20-63 μm. Note the differences past 1,500 nm in comparison with figure 1.12.

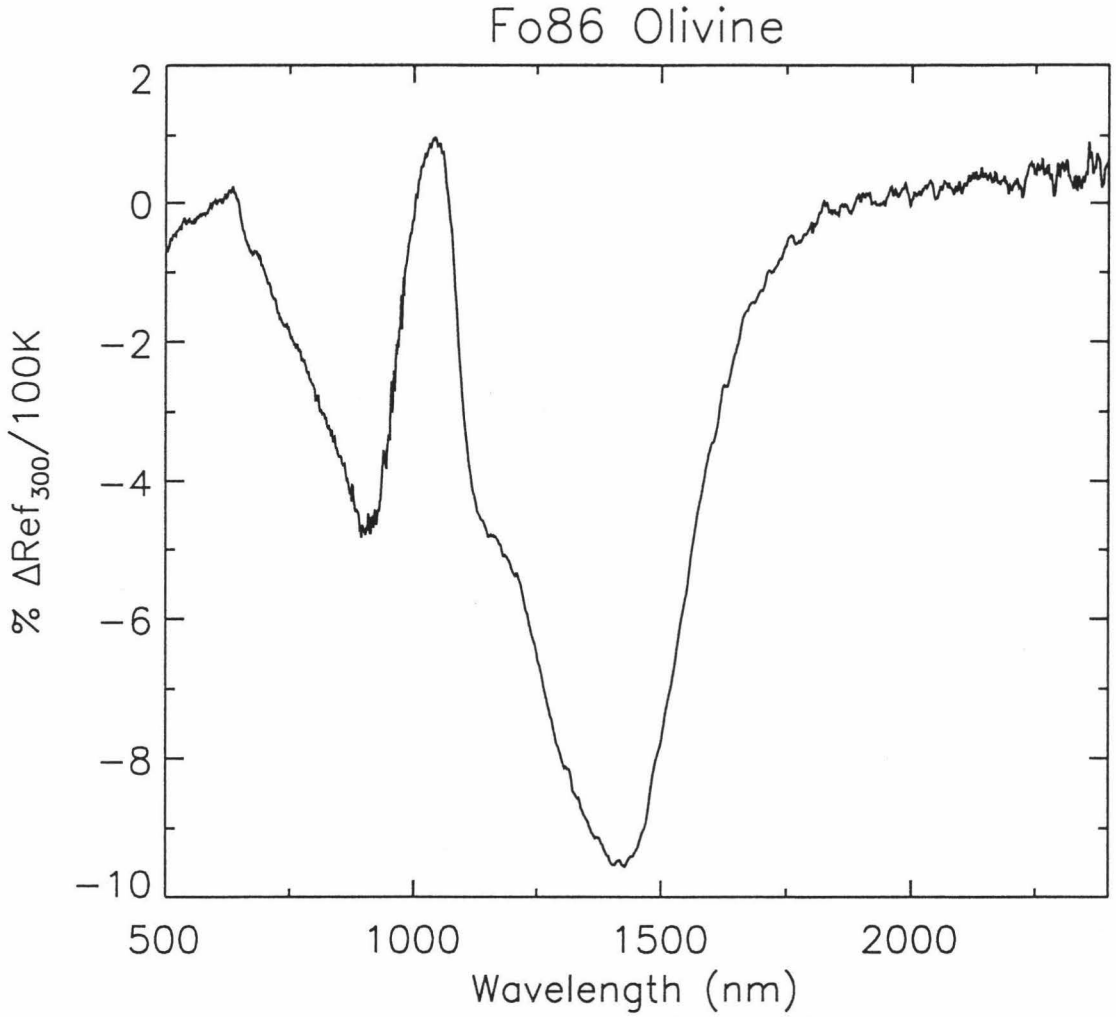

Figure 1.15. Temperature sensitivity spectrum of Fo 86 olivine. This sample was prepared from large crystals by Ms. Domergue-Schmidt.

The sensitivity spectrum of the Fo 86 lacks any features similar to a pyroxene around 2.0 microns in comparison to that of the Fo 88 olivine (figure 1.13).

Pyroxene 110

This sample, provided by Dr. Edward Cloutis, is from the same batch as Roush's bronzite sample.

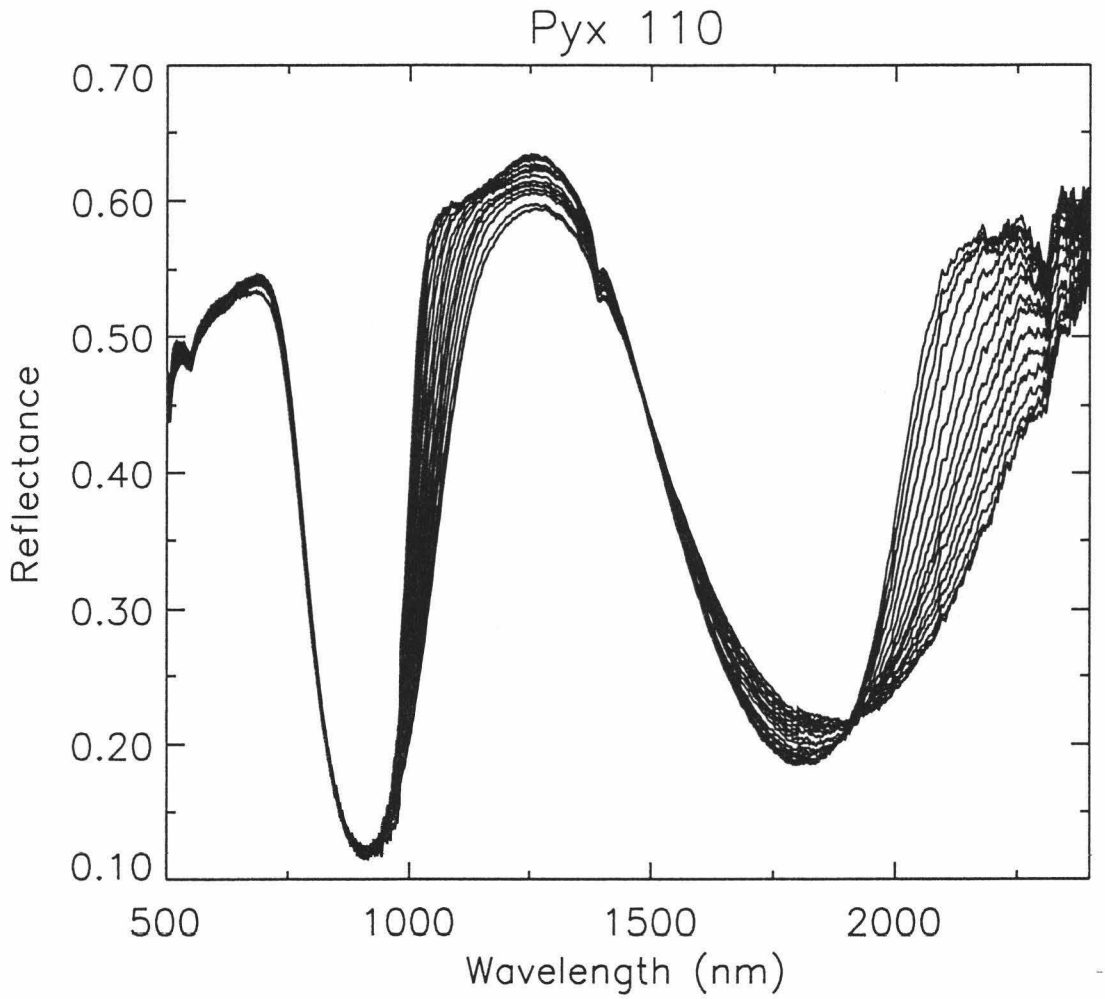

Figure 1.16. Pyroxene 110 from Dr. Edward Cloutis, bronzite En 86, 45-90 μm grain size wet sieved. Note the region at 1.75 μm wavelength which exhibits increasing reflectance at higher temperatures due to the 2 μm band shifting to longer wavelengths.

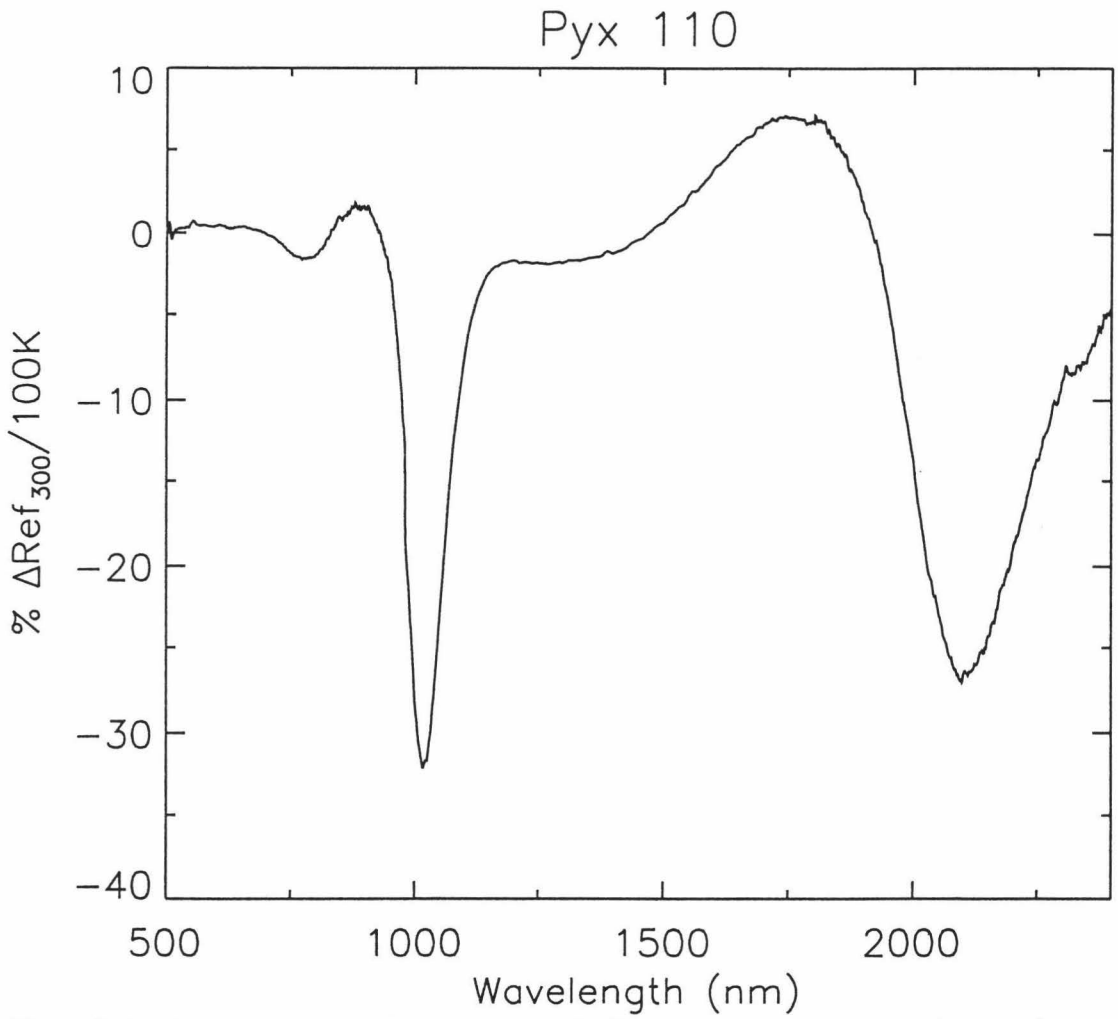

Figure 1.17. Temperature sensitivity spectrum for Pyroxene 100 in figure 1.16. Note the positive values around 1.75 μm. These are due to the 2 μm band shift to longer wavelengths causing dR/DT to go positive in the short wavelength wing of that absorption feature.

Comparisons to Roush's Earlier Rsults

A comparison can now be made between the earlier data of Roush and the new data acquired with the new environment chamber. Because there is no record of the inner can temperature in Roush's experiment, or for that matter the strength of the illumination source, there is no way to predict how well his data will stand up to the new measurements.

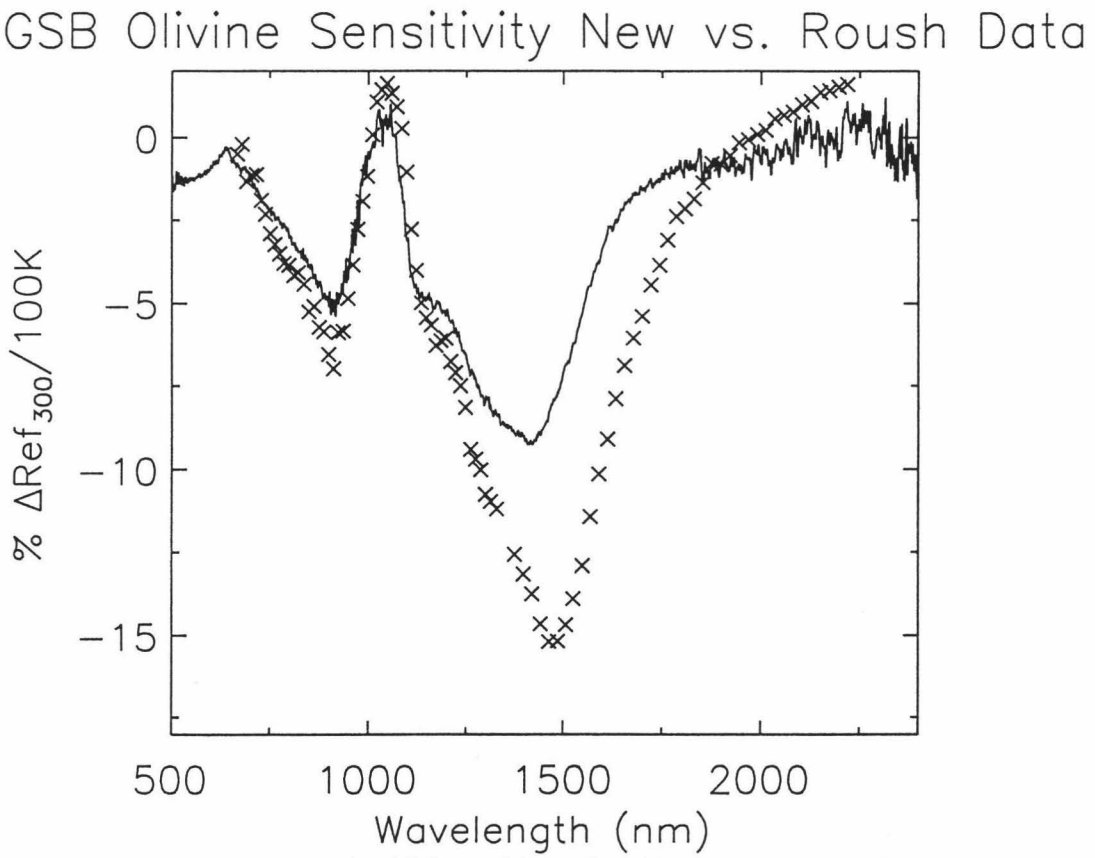

Figure 1.18. Comparison of dR/dT derived from Roush's measurements of the green sand beach olivine (crosses) versus the new data (solid line). The Roush data overestimates the sample sensitivity to temperature change by over 50% in some places. There are also major discrepancies in the location of greatest spectral sensitivity to temperature change near 1.5 μm.

However, we would expect that the radiation environment did not follow the sample temperature and *probably* varied less than the sample temperature. Therefore, a good *guess* would be that the radiation environment buffered the sensitivity to temperature change his samples showed. A likely outcome would be an underestimate of the temperature sensitivity of the samples' NIR spectra.

The data from the green sand beach olivine do not bear this out. There are major discrepancies in the other direction since the earlier data show a greater

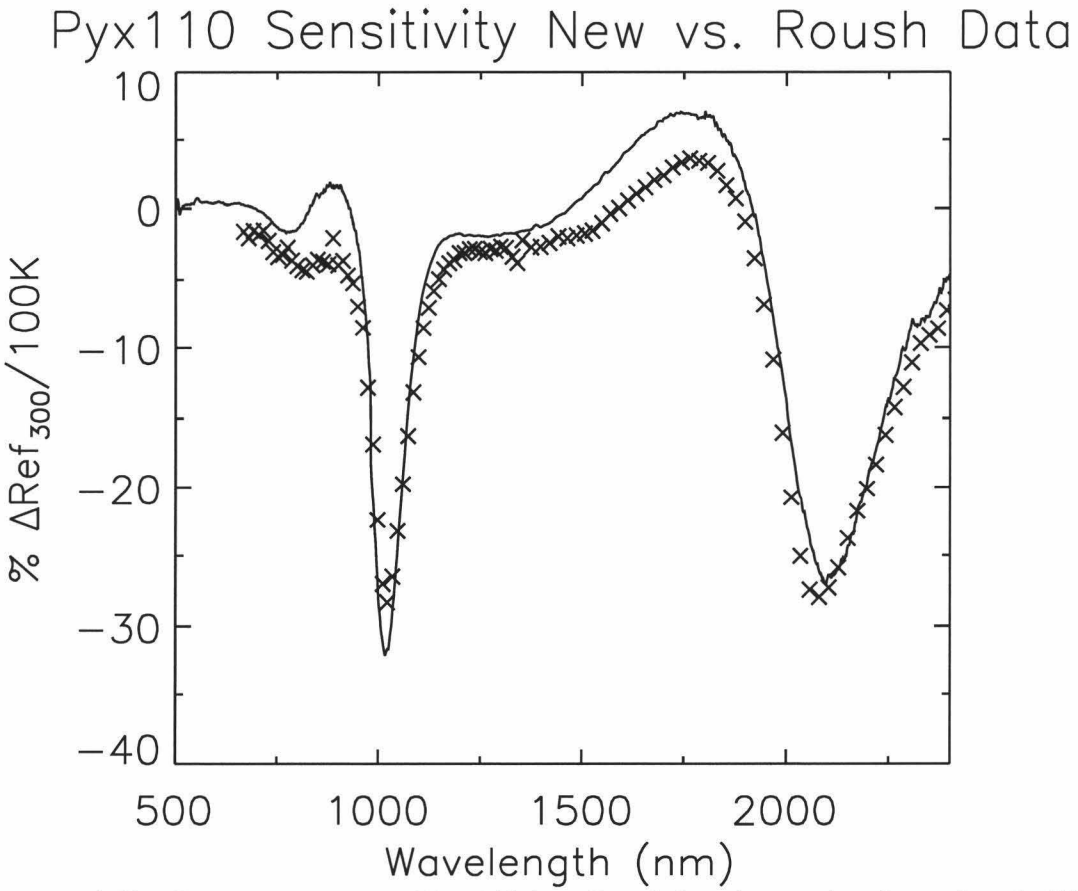

Figure 1.19. Sensitivity spectra of Pyx 110 from Roush data (crosses) and new data (solid line). Clearly any analysis of the earlier data would greatly underestimate the sensitivity to temperature change the NIR spectra of this sample would exhibit.

sensitivity to temperature than the new measurements. There is also a major difference between sensitivity maximum, in absolute terms, between the two sets of data. This difference may be caused by variation in sample compositions or by experimental error.

The data from the pyroxene data sets show remarkable agreement in sample sensitivity between the two sets of measurements.

Conclusions

The new environment chamber is a major improvement to earlier means of making measurements of NIR spectral sensitivity to temperature change. The bulk of this improvement is due to carefully constraining and understanding the sample's radiation environment. Measurements can now be made of a variety of planetary surface materials to determine the extent to which they may be affected by the temperature effect on their near-infrared spectral response.

Experiments detailing the importance of the radiation environment on sample surface temperature for finely powdered silicate minerals in vacuum show a strong coupling to the radiation environment. For this reason the energy added to the sample surface due to illumination used for the measurements is non-negligible and must be considered especially in the low range of temperature measurements.

Comparison to earlier measurements of olivine and pyroxene show some large differences and some agreement with the earlier measurements. Because the earlier measurements have unknown radiation environments for the sample measurements any definitive answer for the results of the comparison can not be made.

CHAPTER 2

Meteorites as Asteroid Proxies

Near-infrared spectroscopy is widely used for remote sensing analysis of asteroids and other mineral-bearing surfaces throughout the Solar System. To what degree the effects of temperature variation on the spectra of these surfaces introduce error into our mineralogical interpretations has, with few exceptions, been neglected. In the same University of Hawaii Masters Thesis[10] where Ted Roush detailed how the infrared spectra of mafic minerals change with changing temperature, he noted that these effects might affect our interpretation of asteroid spectra unless they are taken into account. Later, Roush and Singer touched on these matters in an Icarus follow-up article[11]. Recently, in 1998 Lucey, Keil and Whiteley produced an analysis of A-asteroid spectra, spectra dominated by the mineral olivine[12], which demonstrated that the spectra are consistent with Roush's measurements of olivine at cold temperatures and inconsistent with any room temperature olivine of variable Mg/Fe solid solution composition[13]. This last evidence for detection of the temperature effect is strong motivation for improved laboratory studies with samples of complex mineral mixtures representative of the asteroids.

Olivine and pyroxene dominate the spectra of the S-asteroids[14] so they may be particularly susceptible to the temperature effect with resulting remote sensing errors in compositional analysis. Lately the Near Earth Asteroid Rendezvous mission has attained low orbit around the S-asteroid 433 Eros and a determination of potential errors due to the temperature effect on spatially resolved spectra may be timely. However, until now the direct observation of the temperature effect on asteroidal

material had not been observed, either in the laboratory or in telescopic observations, and remained an unproved logical deduction based on the mineral and basalt data of Roush.

Any discussion of the importance of the temperature effect seen in the spectra of mafic minerals on remote sensing analysis of asteroids must address three main points:

- Is the effect seen in complex mineral mixtures representative of asteroidal surfaces (*e.g.* meteorites)?
- If there is an effect, is it large with respect to the difference in temperature between the asteroid belt and terrestrial ambient temperatures (i.e. temperatures under which meteorites spectra are commonly measured)?
- If there is an effect, is it large with respect to temperatures a spacecraft may find in resolved observations across an asteroid surface?

A simple thermal model of asteroid temperatures:

First, the question of what temperatures to expect in the asteroid belt must be understood. This is necessary to assess the importance of any temperature effect detected in all the meteorite samples. A simple model of asteroid temperatures will give us a rough idea of the temperatures to expect as a function of asteroid albedo and heliocentric distance, and as a function of albedo and insolation angle. This model will simply balance radiative input and output.

In the case of unresolved asteroids the whole-integrated disk is modeled. Two end-member cases of the fast and slow rotator models will be necessary. In actuality, real asteroids will fall somewhere between these two extreme cases and other secondary effects may influence the results slightly. However, the results of these models will give us a good idea of the temperatures and temperature changes to expect for spectra of unresolved asteroids. In the fast rotator model the thermal inertia of the surface has a much longer characteristic decay time than the rotational period so the surface re-radiates into 4π steradians. In the slow rotator case the thermal inertia of the asteroid surface has a characteristic decay time constant much faster than the rotational period so the asteroid can only re-radiate into 2π steradians. In both these cases the asteroid is effectively treated as a whole with re-radiation occurring as a true black body with a model emissivity of unity. The result is an average whole disk integrated brightness temperature.

In the following equations:

S_c= Solar Constant at 1 AU = 1,353watts/m^2

R = Heliocentric distance ratio of asteroid in AU (dimensionless)

r = radius of the asteroid

A = Bond Albedo of the asteroid, an asteroid dependent variable

X = geometric factor, 4 for fast rotator, 2 for slow rotator

σ = Stefan-Boltzman constant = 5.6703×10^{-8} watts/m^2K^4

T = Temperature of asteroid in Kelvins

Balancing the incoming absorbed radiant flux to the re-radiated thermal flux give us:

$$(S_c/R^2)(\pi r^2)(1-A)=(X\pi r^2)\sigma T^4$$

Which reduces to a whole disk integrated temperature of:

$$T = \sqrt[4]{\frac{S_c(1-A)}{XR^2\sigma}}$$

The resulting plot can be seen in figure 2.1.

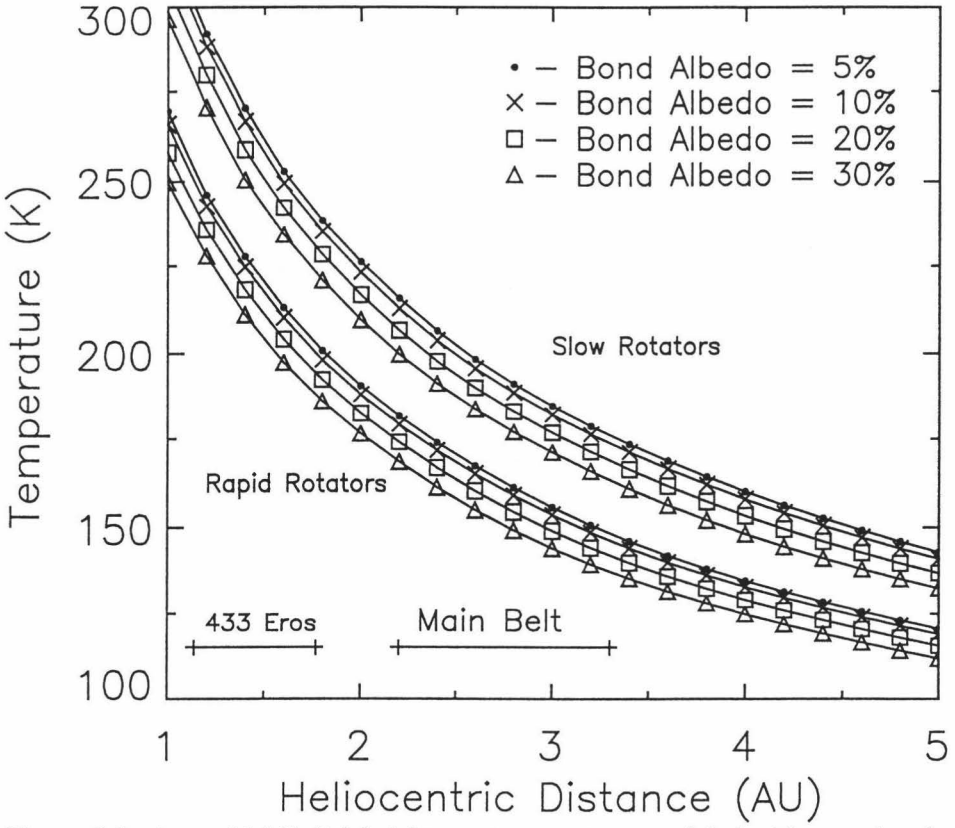

Figure 2.1. Asteroid full disk brightness temperature modeled with equation 1 as temperature vs. heliocentric distance. Four Bond albedos: 5% (dots), 10% (crosses), 20% (boxes), and 30% (triangles); are plotted in both cases of slow rotators (top set of curves) and fast rotators (lower set of curves).

From figure 2.1 two points become clear:

1. The Main Belt temperatures can be expected to be from between 100 K to 150 K colder than ambient laboratory temperatures.
2. Temperature variations of tens of kelvins may be expected between perihelion and aphelion of asteroids of moderate orbital eccentricity

In the case of resolved observations of an asteroid, the local solar insulation angle, a function of topography, latitude, longitude, and rotational phase will become an important factor. In this case the surface element of interest receives and re-radiates with the same effective area but the incoming radiation is modified by the cosine of the local solar insolation angle, θ_z, and low thermal inertia (*i.e.* instantaneous radiative balance) is assumed. The radiative balance equation becomes:

$$(S_c/R^2)(\cos\theta_z)(\pi r^2)(1-A)=(\pi r^2)\sigma T^4$$

Which reduces to an instantaneous local temperature as a function of local solar insulation angle, Bond albedo, and heliocentric distance of:

$$T = \sqrt[4]{\frac{S_c(\cos\theta_z)(1-A)}{R^2\sigma}}$$

The resulting plot, for the cases of 433 Eros aphelion and perihelion can be seen in figure 2.2.

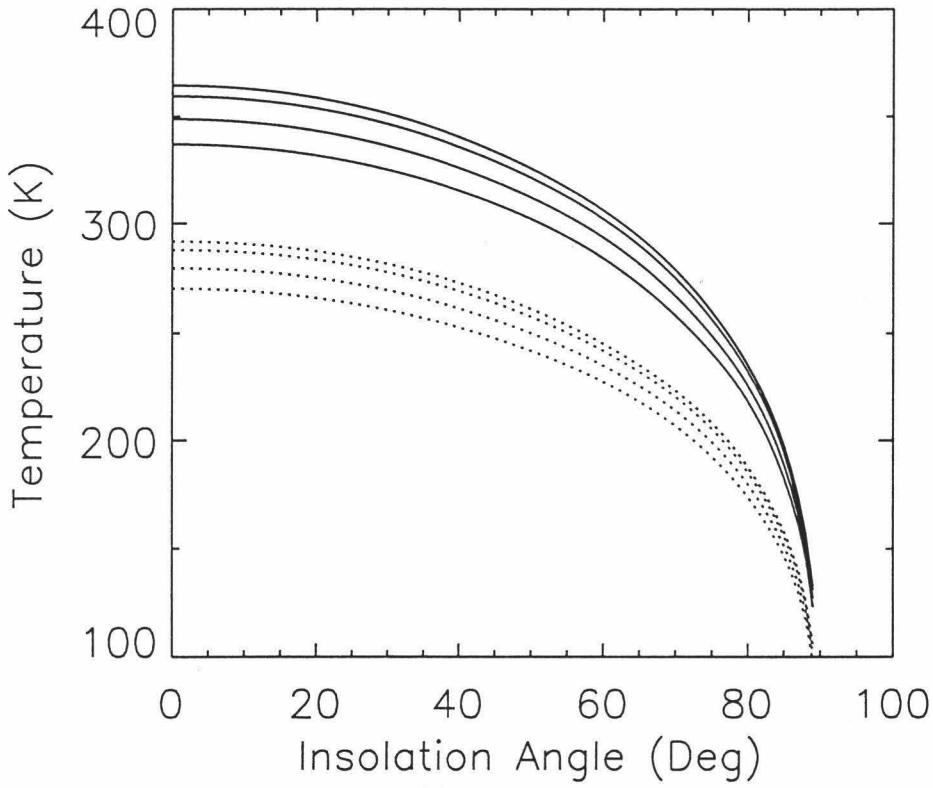

Figure 2.2. Asteroid 433 Eros model asteroid surface temperatures as a function of solar insolation angle at perihelion (upper curves) and aphelion (lower curves). Each set of four curves represent the same Bond albedos as in figure 2.1.

Figure 2.2 demonstrates that it is not unrealistic to see temperature differences of hundreds of Kelvins across the lit hemisphere of an asteroid with low surface thermal inertia. Local topography with slopes as little as 20° may also cause temperature variations of 50 K or more.

Measurements:

The availability of our new environment chamber at Planetary Geosciences – University of Hawaii has enabled us to test the NIR spectral sensitivity to temperature of actual meteorite samples - which act as a proxy for asteroidal surfaces from which they were derived[15]. Ordinary chondrite meteorites show systematic olivine and pyroxene spectral featuresand these meteorites provide a natural starting place for an examination of the temperature effect on asteroidal materials. While a *prima facie* expectation would be to see the temperature effect in the spectra of these meteorites, these real-world samples contain significant amounts of spectrally neutral components and metal that may have an overwhelming and non-linear damping effect[16] on their spectral sensitivity to temperature. Actual measurements of meteorites will tell us if the effect is strong enough to be a concern when conducting spectral based compositional analysis of asteroids with similar spectra.

Ordinary Chondrites:

We looked at the following ordinary chondrites:

Allegan (H5)

Allegan spectra show a significant temperature sensitivity as demonstrated in figure 2.3. All meteorite samples were acquired through the assistance of Dr. Anders Meibom at Planetary Geosciences/U of HI. The Allegan sample was dry sieved to a grain size of between 45-150μm. Dry sieving was used instead of wet sieving because of worries of leaching components from the mixture.

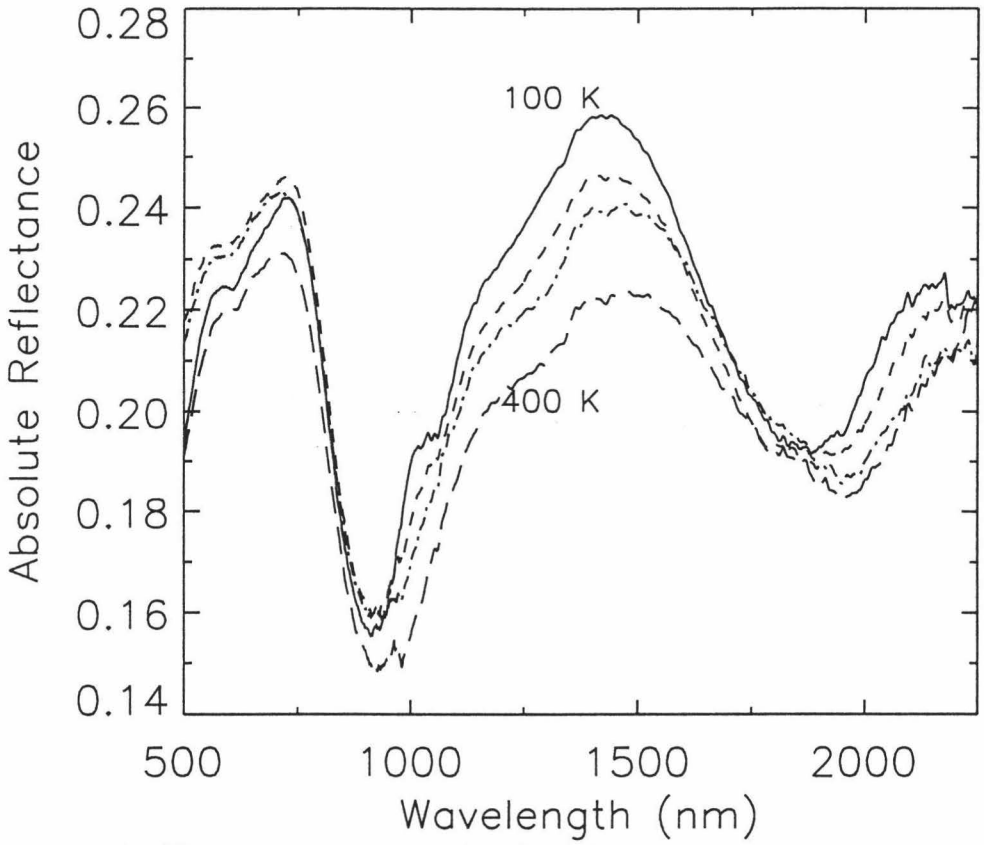

Figure 2.3. Allegan, an H5 ordinary chondrite, showing significant temperature effect on the NIR spectra. For clarity only spectra at 100K (solid line), 200K (short dash line), 300K (dot-dash), and 400 K (long dashed line) are presented. The sample was dry sieved to 45-100μm grain size.

The temperature response of the meteorite spectra can be understood as a combination of olivine and pyroxene spectral effects. The overlapping olivine and pyroxene bands become narrower and begin to separate as the temperature goes down. This process is particularly notable in the 100 K spectrum and produces a shoulder near 1.1 μm. As the temperature drops the effect of the pyroxene band shift to shorter wavelengths is also apparent. The temperature sensitivity of the meteorite spectra as a

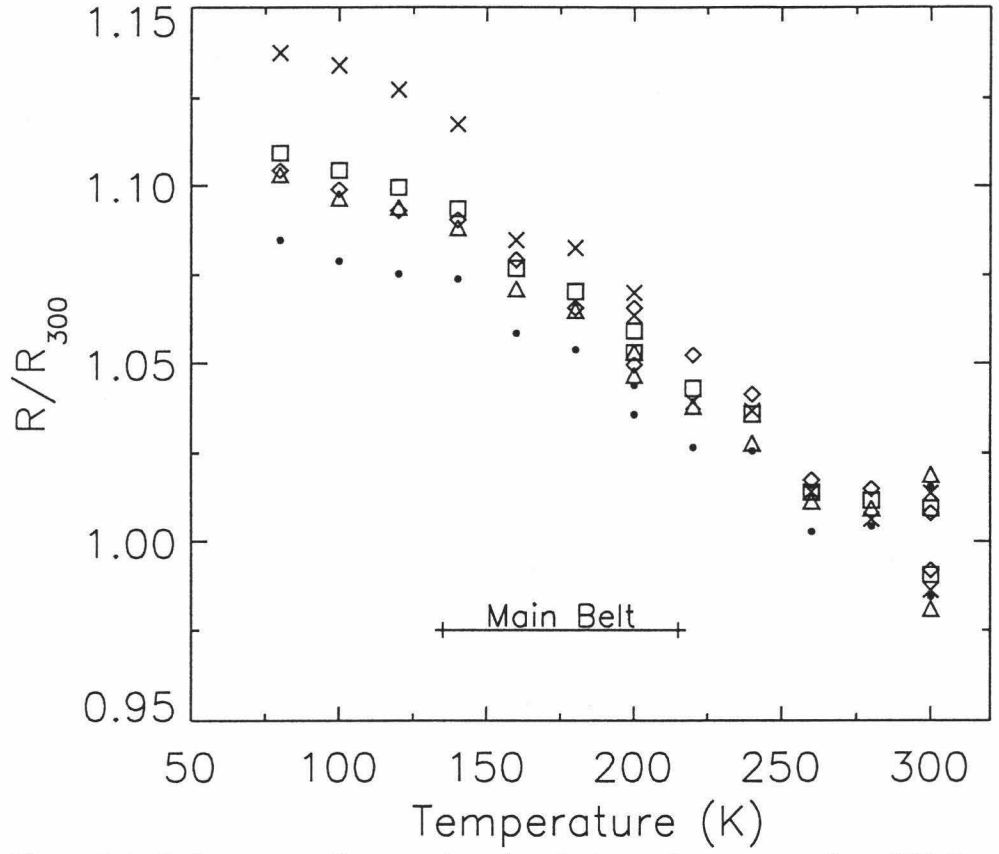

Figure 2.4. Reflectance at five wavelengths relative to the average of two 300 K spectra. The wavelengths of 1.0μm (crosses), 1.3μm (squares), 1.4μm (triangles), 1.5μm (dots) and 2.1μm (diamonds) are represented. Range of temperatures expected in the main asteroid belt is indicated.

fractional change from the 300 K spectrum is shown in figure 4 for five different wavelengths.

Figure 2.4 demonstrates that the spectra of main-belt asteroids may be over 5% different than the same materials in the laboratory at several important diagnostic wavelengths. The figure also shows spectral variation of several percent can be produced by variations of heliocentric distance within the belt and this holds the possibility of being misconstrued as a compositional trend with respect to heliocentric distance especially in conjunction to the 2 μm band minimum shift.

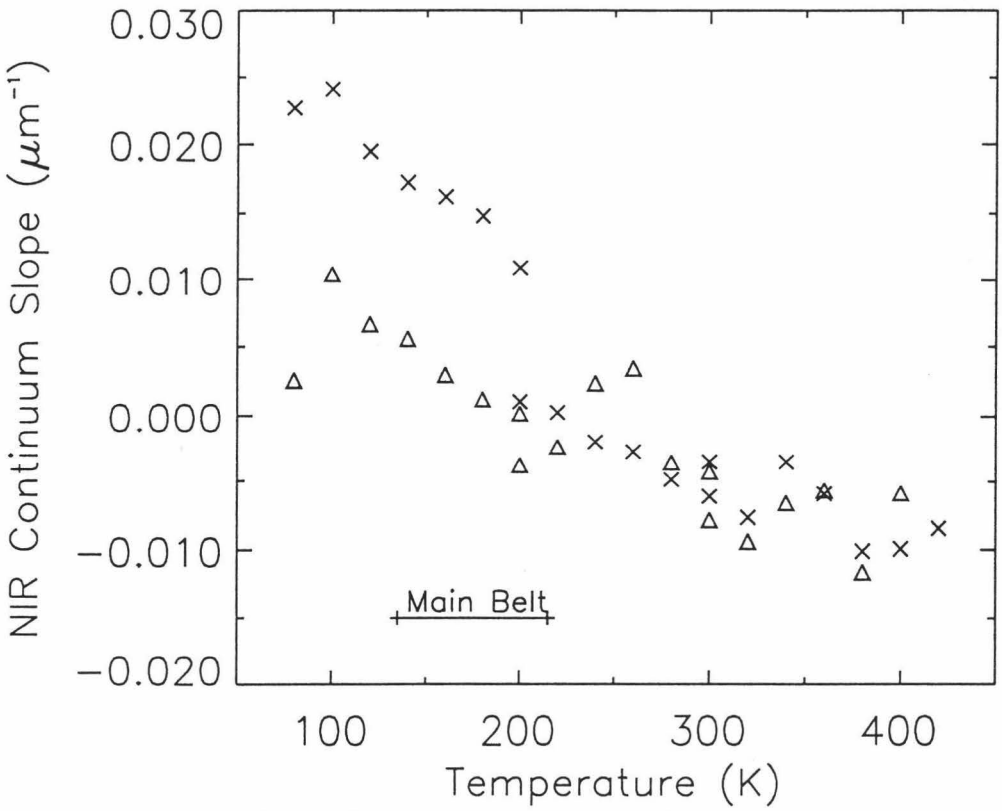

Figure 2.5. NIR continuum slope between ~700nm maximum and ~1500nm maximum of two H5 ordinary chondrites Allegan (triangles) and El Hammami (crosses) as a functon of temperature. Slope is measured as $\Delta R/\Delta\lambda$ between the two maxima where R is reflectance and λ is measured in μm for spectra which have been normalized such that 0.56μm =1.0, e.g. Cloutis et al. 1990.

Because the olivine and pyroxene absorption bands narrow at lower temperatures the 1.5μm continuum is also markedly affected by the temperature change resulting in a change of NIR continuum slope. Figure 2.5 shows the continuum slope[17] change as a function of temperature for both the H5 ordinary chondrites measured.

Figure 2.5 also demonstrates the change in sign from a negatively valued slope at terrestrial ambient temperatures to a reddened, positively valued slope, at colder temperatures. This slope change may contribute to systematic errors in compositional analysis based on NIR reflection spectra of asteroids.

El Hammami (H5)

The results from this H5 ordinary chondrite are virtually identical to those of Allegan. The major difference between the results being the presence of weathering products, iron oxides, in the spectra of El Hammami which was a visibly rusty sample before preparation. The weathering products are noticeable in the visible region of the spectra of this meteorite as seen in figure 2.6.

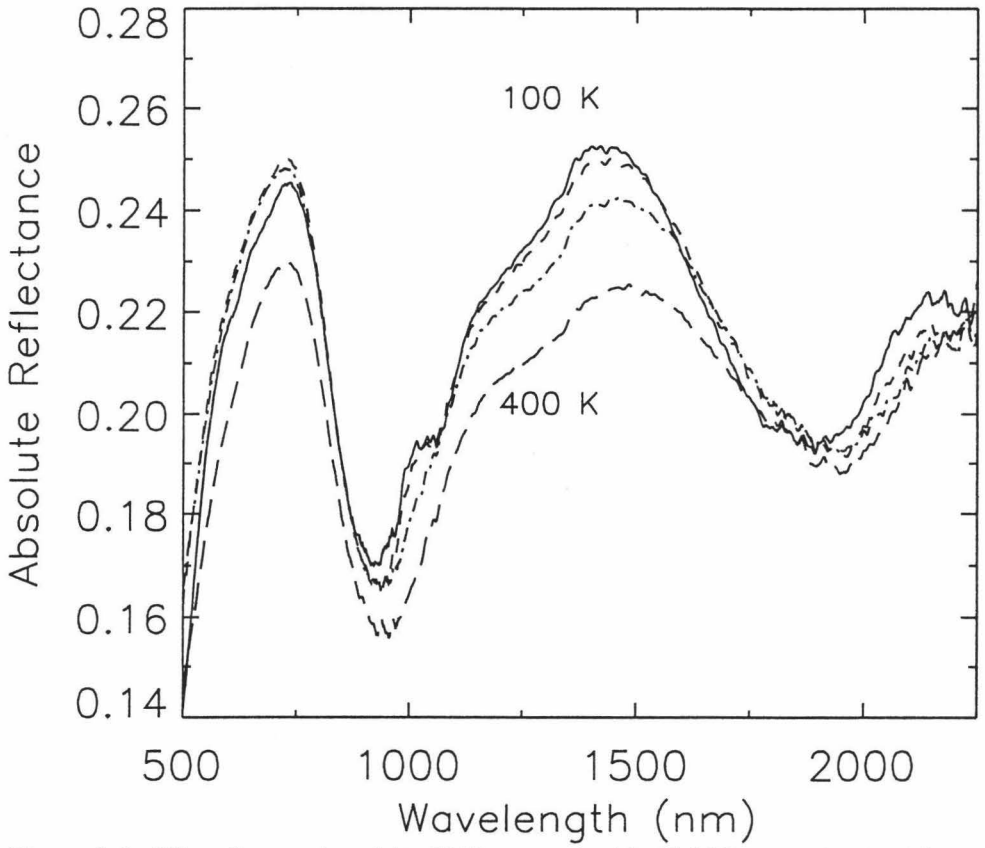

Figure 2.6. H5 ordinary chondrite El Hammami with 45-150μm grain size (dry sieved). The spectra are almost identical with those of Allegan in figure 5 except for the presence of weathering products, i.e. rust, noticeable by the sharp drop in reflectance at shorter wavelengths in the visible region.

Manbhoom (LL6)

The measurements of Manboom were compromised by a vacuum leak so the many intermediate temperatures were skipped in order to sample as full a range of temperatures before the vacuum leak presented a problem.

The results for temperatures of 100, 200, and 400 K are seen in figure 2.7. Figure 2.7 shows the same trends seen in the H5 ordinary chondrites Allegan and El Hammami. In all these cases there is a significant broadening of the 1 and 2 μm

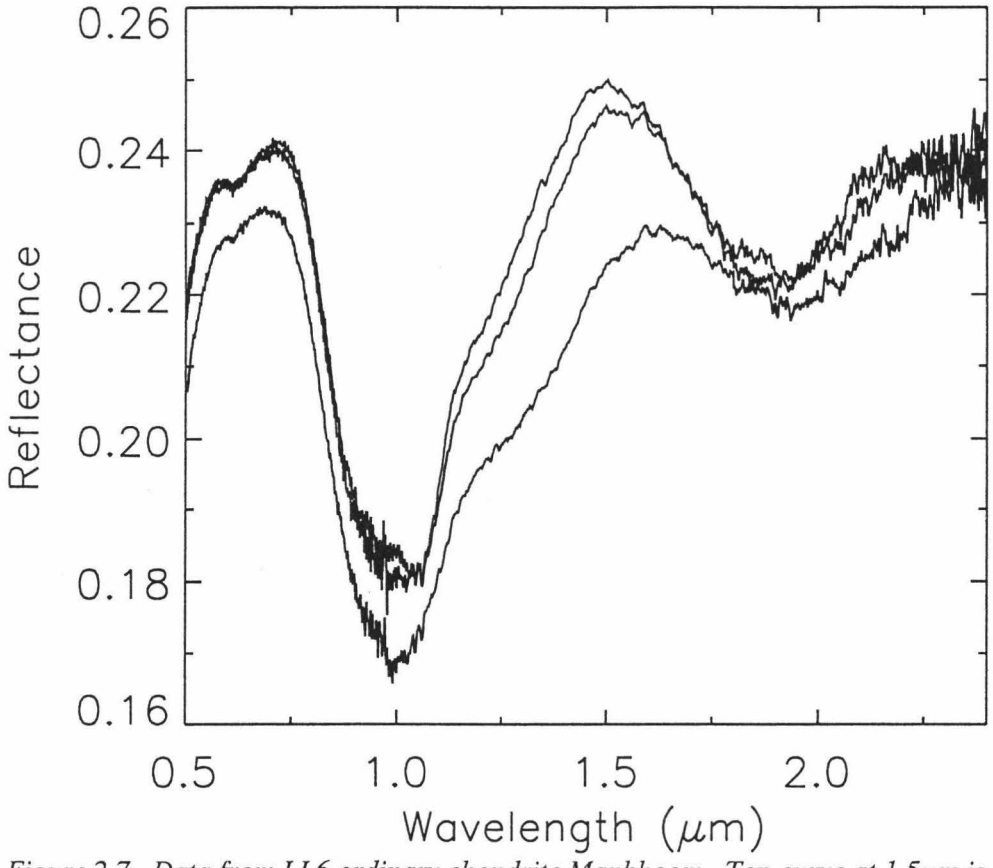

Figure 2.7. Data from LL6 ordinary chondrite Manbhoom. Top curve at 1.5μm is for 100 K, middle curve is 200 K and bottom curve is 400K. Grain size is < 63μm dry sieved.

bands, a reddening of the continuum slope and shifts in the 2 μm band center with increasing temperature.

HED Meteorites

The Howardite/Eucrite/Diogenite meteorites are a unique class of basaltic achondrite meteorites conjectured to have originated from the asteroid 4 Vesta[18]. Two HED meteorites have been measured with the new environment chamber in support of work by Tom Binzel at the Massachusetts Institute of Technology attempting to locate

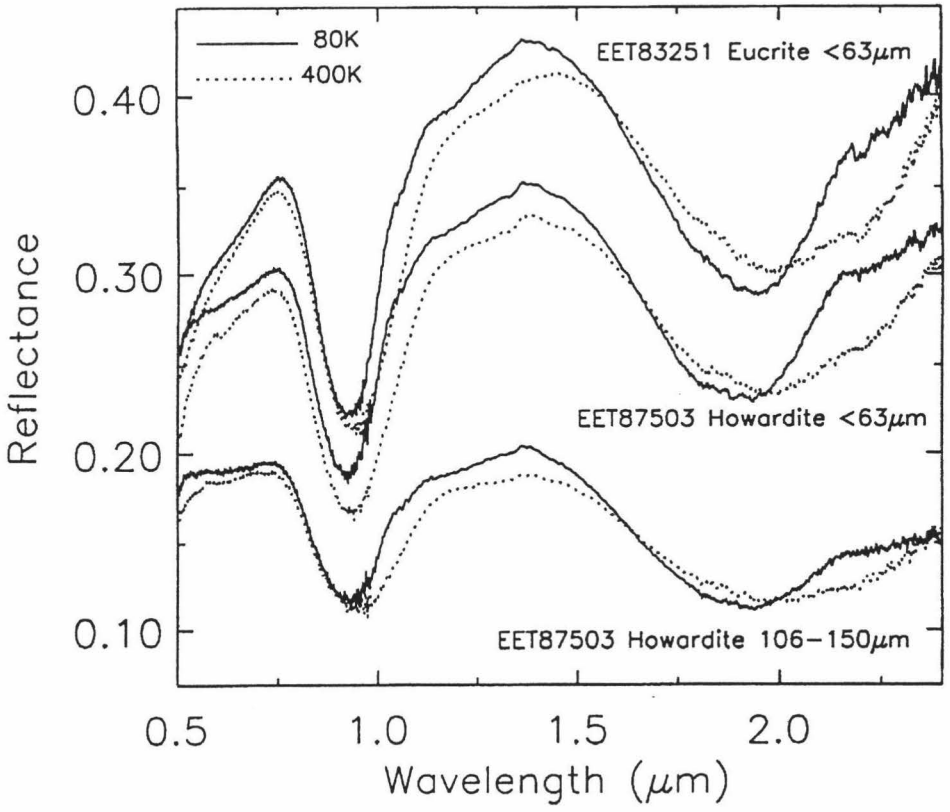

Figure 2.8. Two temperature data for HED meteorites EET83251 and two grain size splits of EET87503. Note the larger grainsize split of EET87503 is darker as expected but the absolute temperature sensitivity is also proportionally smaller.

the asteroid source and mechanism of delivery of these meteorites. We have measured a eucrite, EET83251, which contains low-Ca pyroxene and plagioclase feldspar. The other HED meteorite measured is EET87503, a howardite: a brecciated meteorite composed of varying degrees of eucritic material and dioginitic, magnesian orthopyroxene, material. One key issue is whether or not the increased reddening at colder temperatures seen in the ordinary chondrite meteorites might explain the spectral differences between the HED meteorites and the smaller "vestoids" which may or may not be the means of delivery of Vesta material to the Earth[19].

The HED meteorites showed a similar magnitude of sensitivity (also see the appendix of sensitivity vs. wavelength plots) to temperature change as the ordinary chondrite samples but there are important differences of wavelengths affected. Figure 2.8 shows the HED data with two runs for two different grain size splits of howardite EET87503. The NIR continuum slope of these samples also reddened with decreasing temperature as indicated by two different runs with the same particle size of EET83251 as seen in figure 2.9.

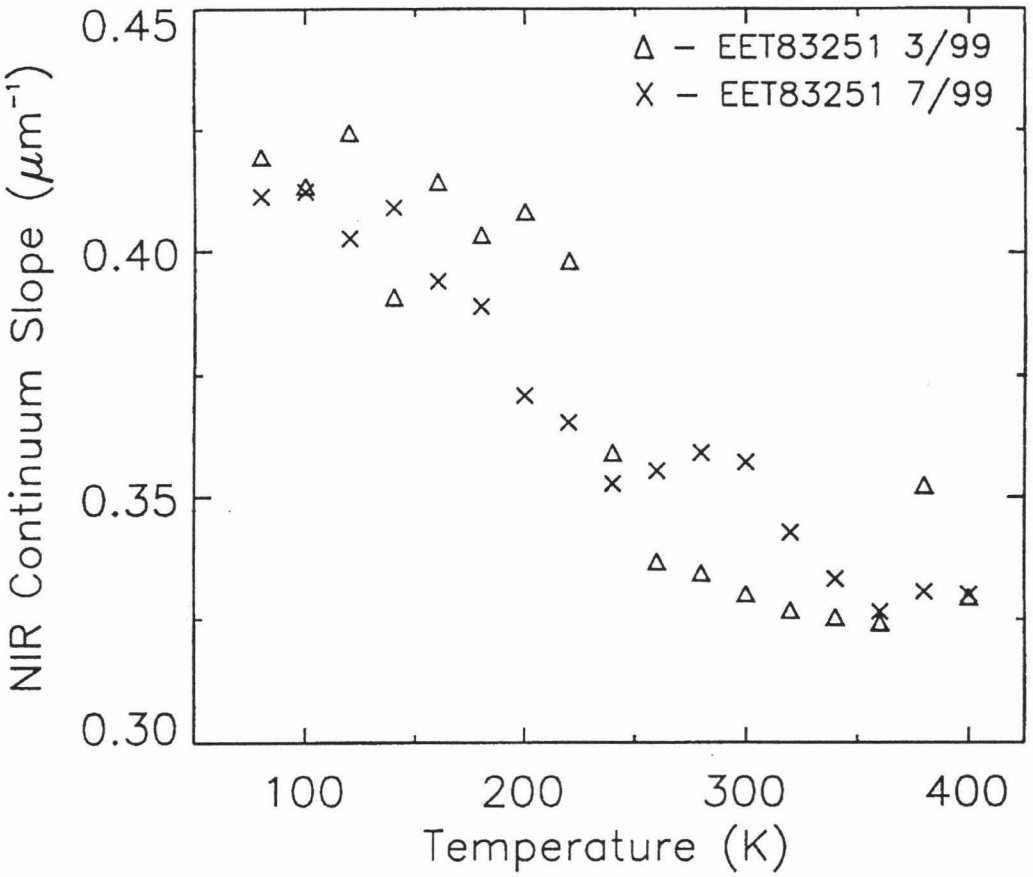

Figure 2.9. NIR continuum slope as a function of temperature for eucrite EET83251 derived from spectra normalized to 0.56μm=1 as previously described. Grain size is a <63 μm split. The second run was done to confirm the earlier results and demonstrates the stability of the new environment chamber system.

With the results of figure 2.9 in mind the results of the two grain size splits for howardite EET87503 are plotted with the figure 2.9 eucrite data in figure 2.10.

Figure 2.10 again reminds us that grain size will have a strong effect on continuum reddening while temperature effects are secondary. However, that is not to discount the contribution temperature effects may make towards the sum of reddening effects. Figure 2.10 also demonstrates that the two different HED meteorites behave somewhat differently in the <63 μm splits as temperature decreases. This may be due to the differing behavior of the two meteorite samples' ~0.75μm maximum – the howardite shows much more change with respect to temperature there than does the

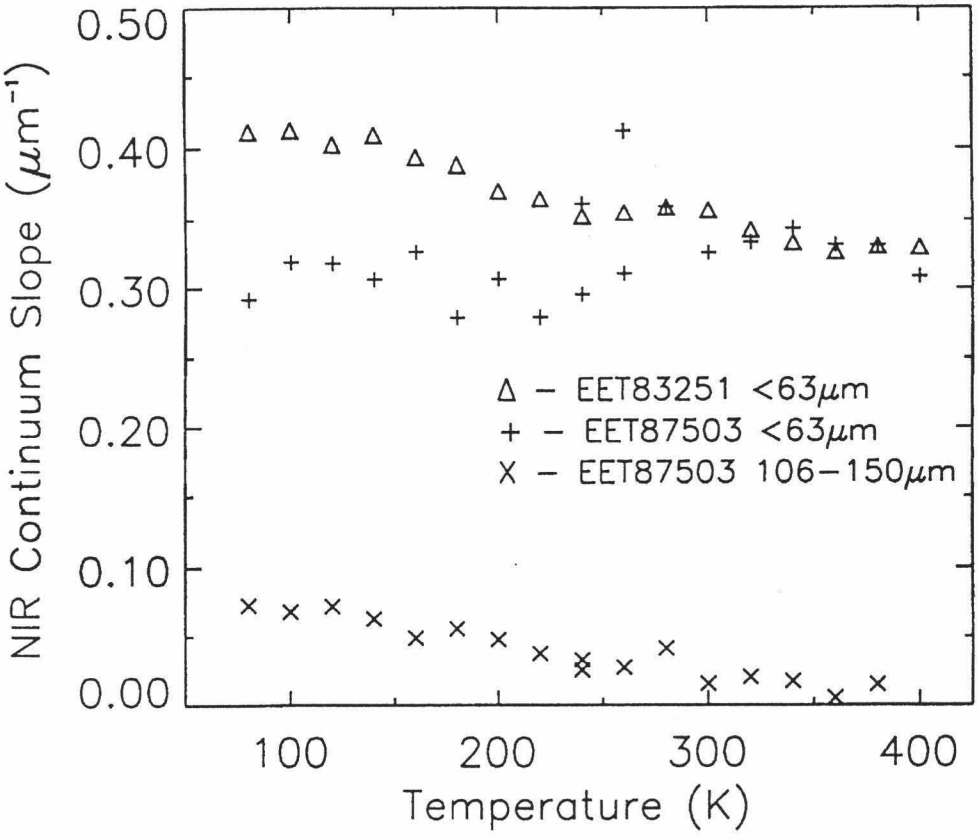

Figure 2.10. Continuum slope for HED meteorite samples eucrite EET83251 and howardite EET87503 at two different grain size splits. The data serve as a reminder that grain size dominates temperature in affecting NIR continuum slope.

eucrite while both have similar response to temperature change at the ~1.5μm maximum, as demonstrated in figure 2.8.

Thus, the pyroxene band 1 and 2 narrowing as well as the large band center shift due to decreasing temperatures have been demonstrated in HED meteorite samples. There is further evidence for a small band 1 shift to shorter wavelengths at colder temperatures as well as some cold temperature reddening of the meteorite spectra. These measurements may help identify the delivery sources of the HED meteorites from the asteroid belt.

Carbonaceous Chondrites:

Two carbonaceous chondrites have been measured: Warranton (CO3) and Murchison (CM2). Both meteorites are rich in spectrally neutral components and both yielded the same almost null result. Because of the samples very low reflectance the measurements are noisy and even more so in the 0.98μm end of the VIS detector array. Even with the difficulties of making these measurements some systematic sensitivity to temperature change was observed but at a level so small as to be meaningless for any useful application. This is demonstrated by the reflectance at 1.5μm vs. T plot for Warranton shown in figure 2.11. The trend is clear but a closer inspection of the abscissa shows the small amplitude of the variation. A similar but even smaller amplitude of spectral response to temperature change is demonstrated by Murchison. The spectra of Warranton at 100K, 200K, 300K and 400K are plotted in figure 2.12 while the complete data set for Murchison is plotted in figure 2.13. The data are so noisy and the effect so subtle that it is essentially a null result.

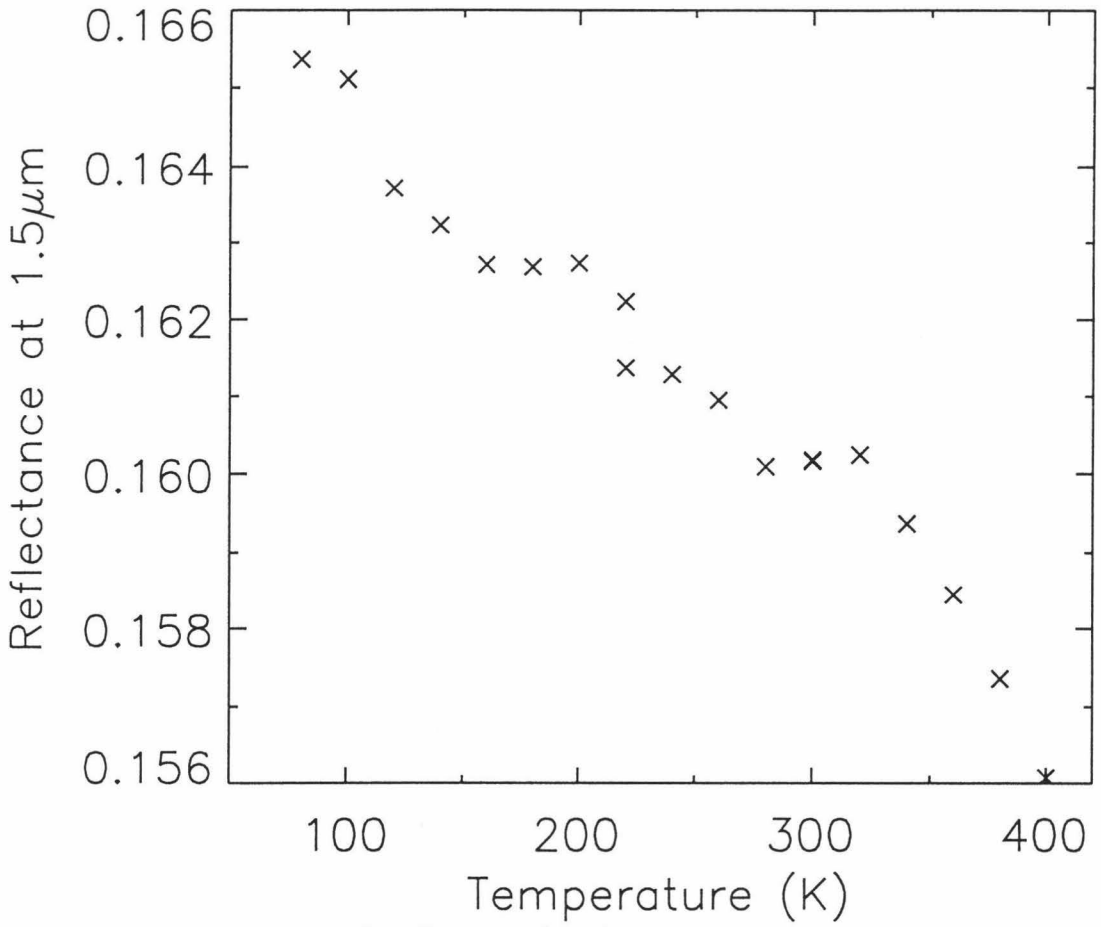

Figure 2.11. Warranton (CO3) reflectance plotted against temperature at the relatively low noise wavelength of 1.5μm. Note the double measurements at 200K and 300K. This trend looks like a clear result until the realization that over 420 kelvins the reflectance changes less than 1% in absolute terms.

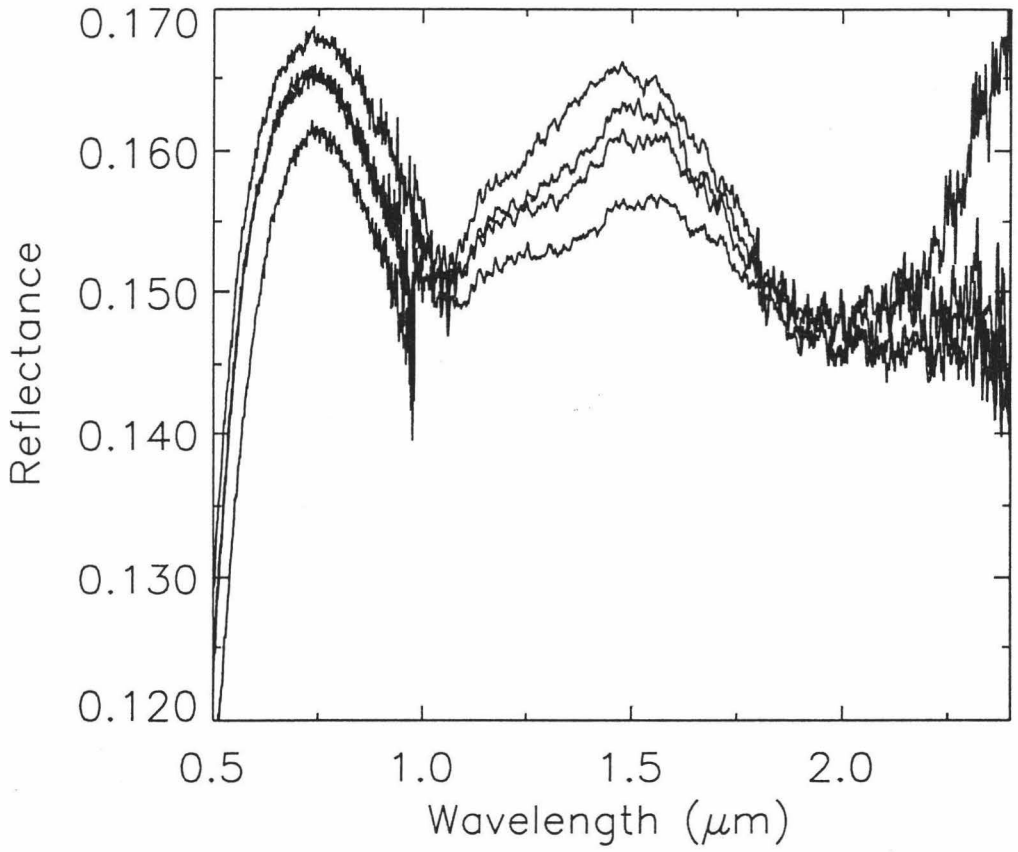

Figure 2.12. Warranton (CO3) plotted with temperatures of 100K (top), 200K, 300K and 400K (bottom).

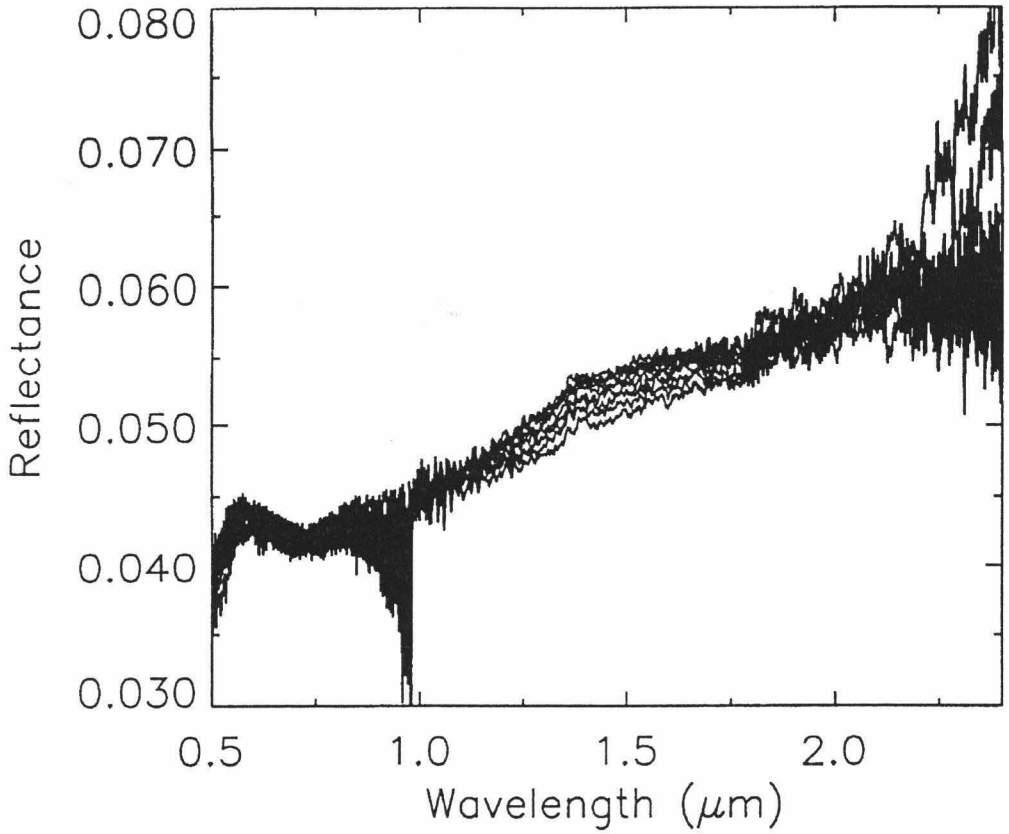

Figure 2.13. Complete set of Murchison (CM2) spectra from 80K to 400K. Even with spectra so overwhelmed by dark, spectrally neutral components there is still a small detectable trace of temperature sensitivity but so small as to be meaningless.

Conclusions

- The original admonition by Roush and Singer (Icarus 1987) is supported by new NIR spectral measurements of meteorites samples at different temperatures. Their warning that quantitative analysis and detailed interpretation of asteroid spectra using meteorite spectra obtained at room

temperature may be in error unless temperature effects are taken into account still stands.

- The albedo may be a strong function of temperature in some wavelength ranges (Roush and Singer, 1987). The photometric phase function may therefore include a temperature dependent factor particularly in the NIR region and this is not a consideration in standard Hapke-based photometric analysis (Hinrichs et al, 1999).
- Comparisons of the spectra of different regions of an asteroid by spatially resolved spacecraft observations must include consideration of temperature effects (Roush and Singer 1987). Unit maps derived from spectral information may be systematically in error due to temperature effects if these considerations are neglected (Hinrichs et al, 1999)
- Topography may give rise to spectral differences due to solar insulation angle heating differences. Variations of slope of 20-30 degrees may potentially produce temperature differences as great as 50K. Conclusions of compositional differences may result in misinterpretation of the spectral data Hinrichs et al., 1999)
- The temperature effect may give us a handle on thermal inertia. Regions which are less susceptible to the temperature effect may have greater thermal inertia (Hinrichs et al, 1999).

APPENDIX TO CHAPTER 2.

The following plots come in a pair for each meteorite that underwent a full data run. The first plot of the pair is the reduced data from the entire run. The second plot is the sensitivity of the spectra to temperature change as a function of wavelength. It is the slope of a best-fit line to the data, after normalizing it to the 300K spectrum, between 200K and 300K for every wavelength. The 200-300K region is chosen because it is typically the best quality data and typically the most linear in all cases. The result is a sensitivity spectrum as a function of wavelength scaled so that the units represent *percent change relative to the 300K reflectance value per 100 Kelvin of temperature change.* Hence, a negative value, the most common observed, indicates that reflectance decreases with an increase of temperature. If the value at a particular wavelength is –10 for example then at that wavelength the 200K reflectance should be 10% greater than the 300K reflectance.

The red sensitivity spectrum is for the sample in question. There is an olivine spectrum in green and a pyroxene spectrum in yellow plotted as references with which to compare the sample spectrum.

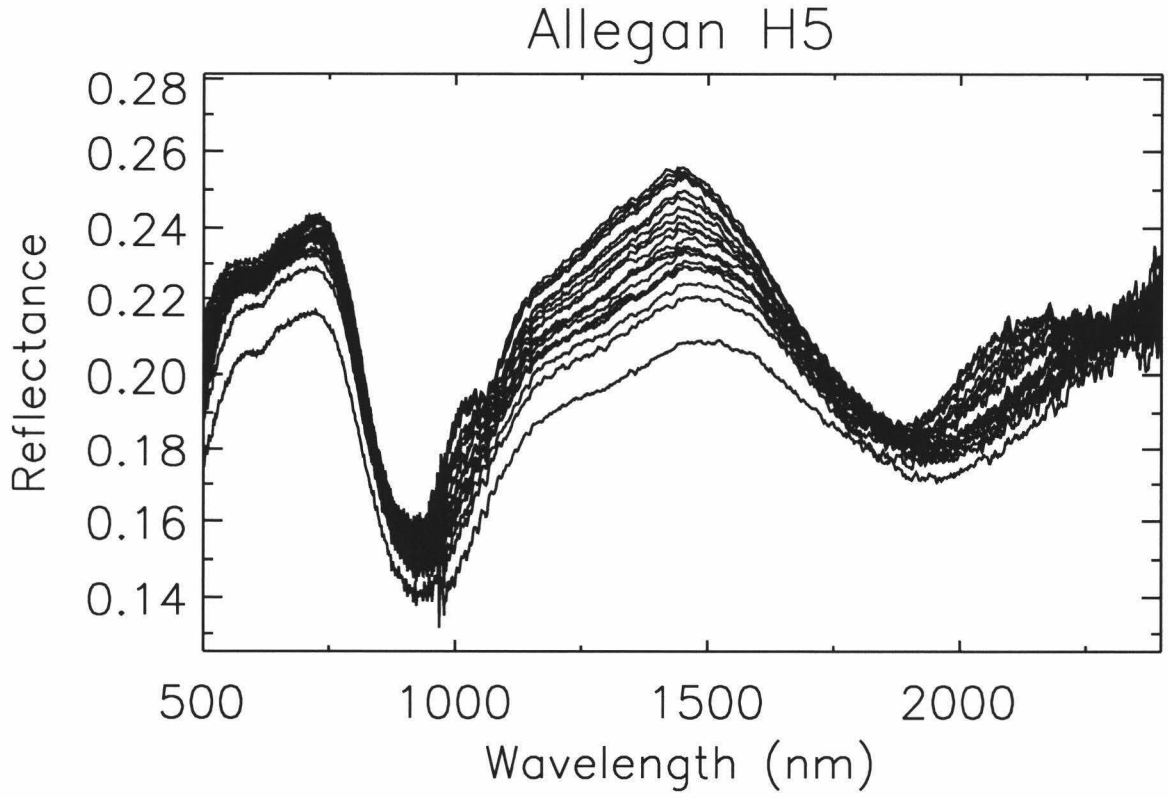
Allegan H5
Reflectance
0.28
0.26
0.24
0.22
0.20
0.18
0.16
0.14
500
1000
1500
2000
Wavelength (nm)

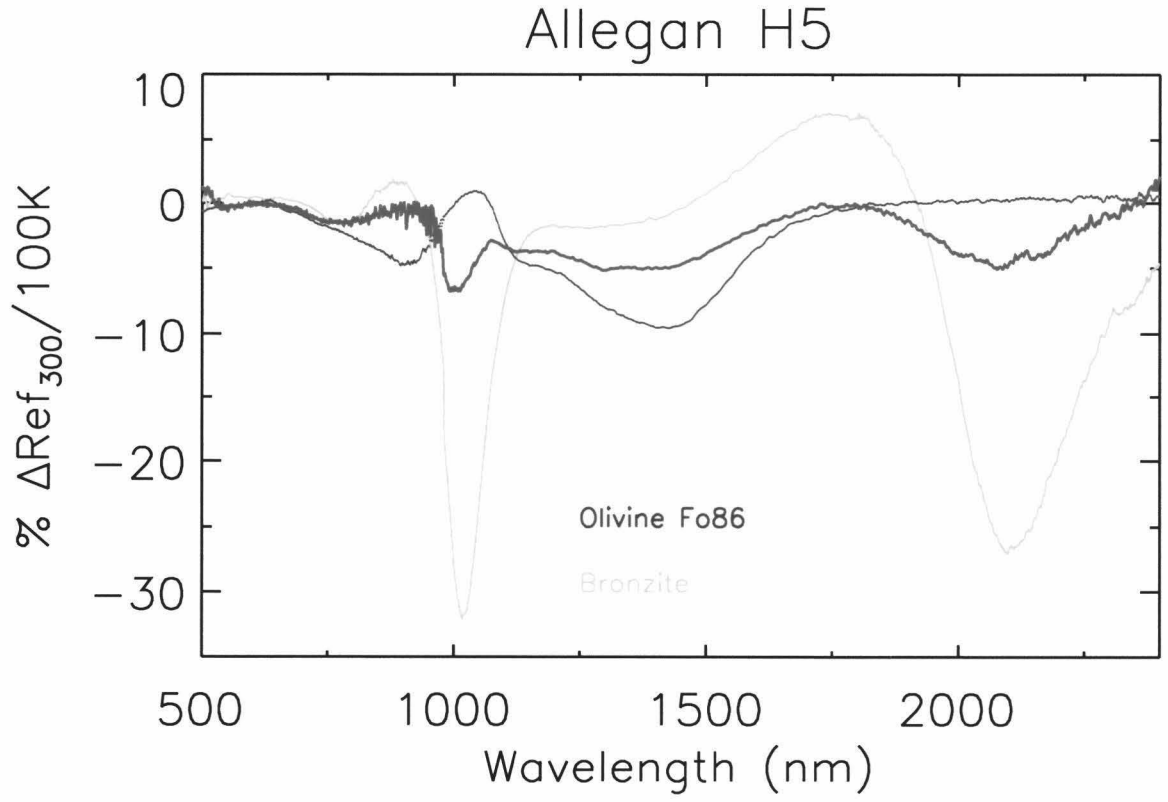
Allegan H5
% ΔRef300/100K
10
0
−10
−20
−30
Olivine Fo86
Bronzite
500
1000
1500
2000
Wavelength (nm)

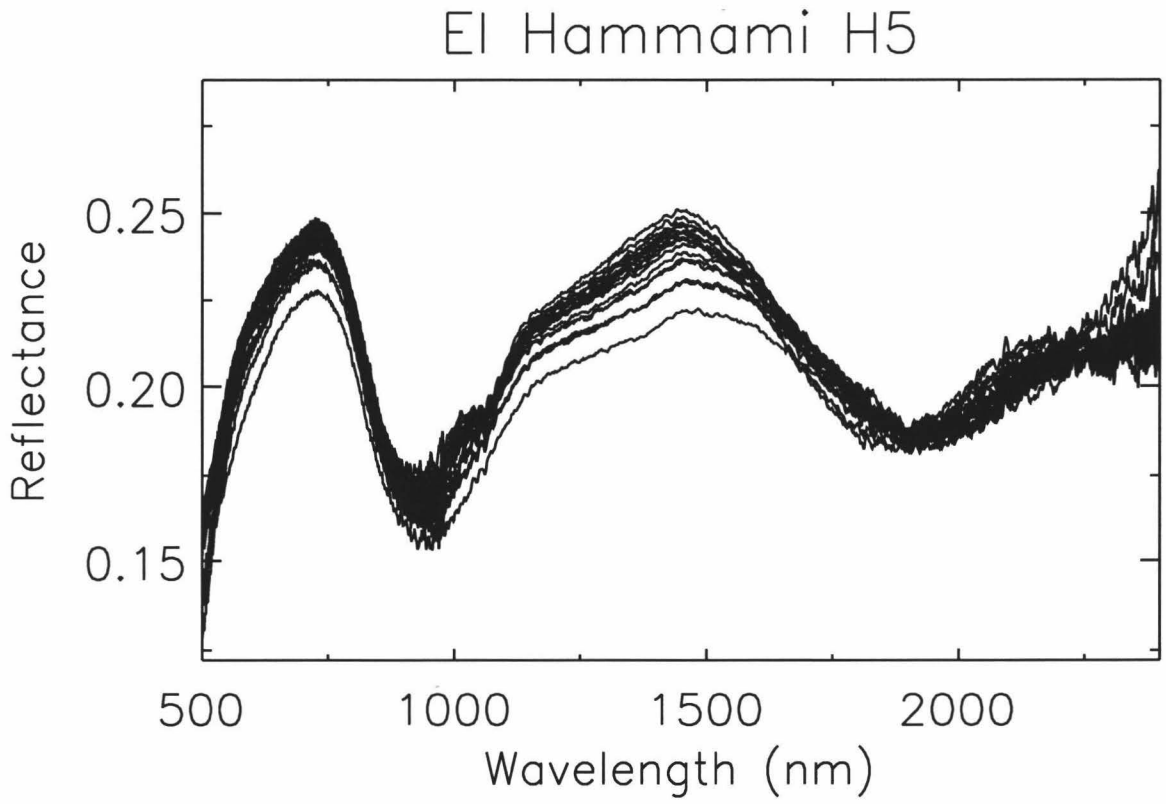
El Hammami H5
Reflectance
0.25
0.20
0.15
500
1000
1500
2000
Wavelength (nm)

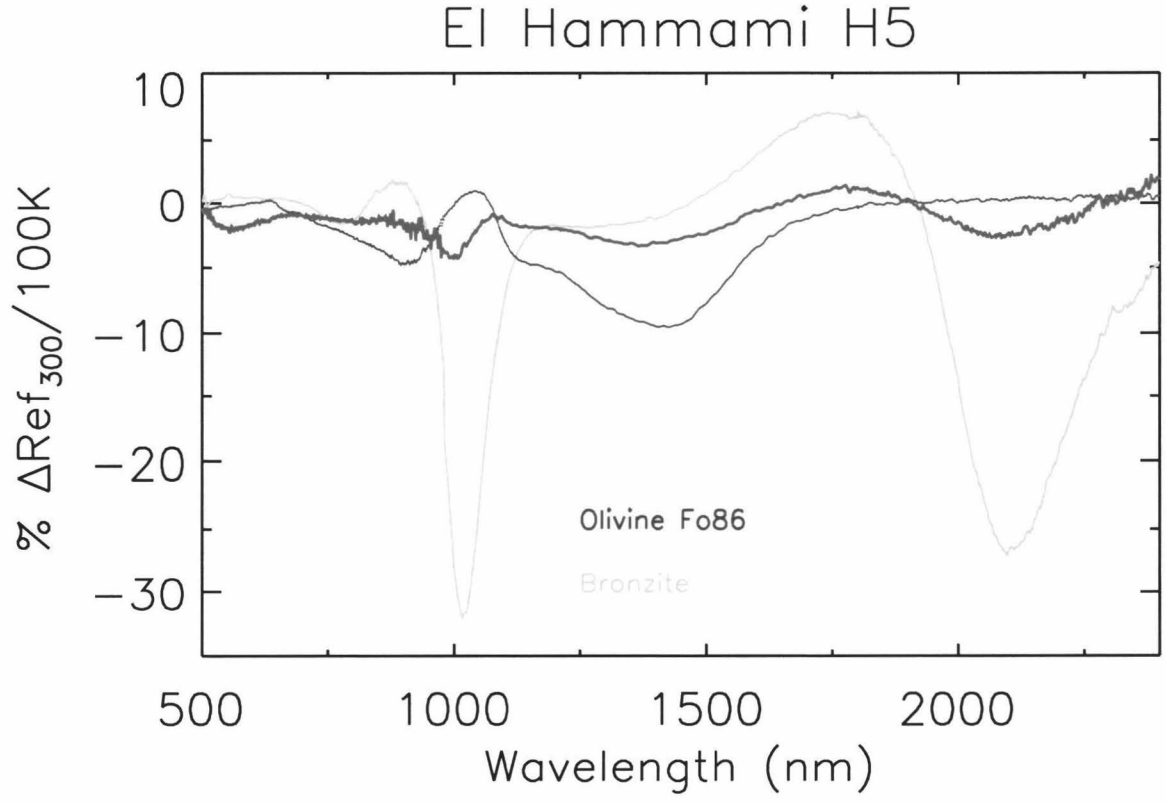
El Hammami H5
% ΔRef300/100K
10
0
−10
−20
−30
Olivine Fo86
Bronzite
500
1000
1500
2000
Wavelength (nm)

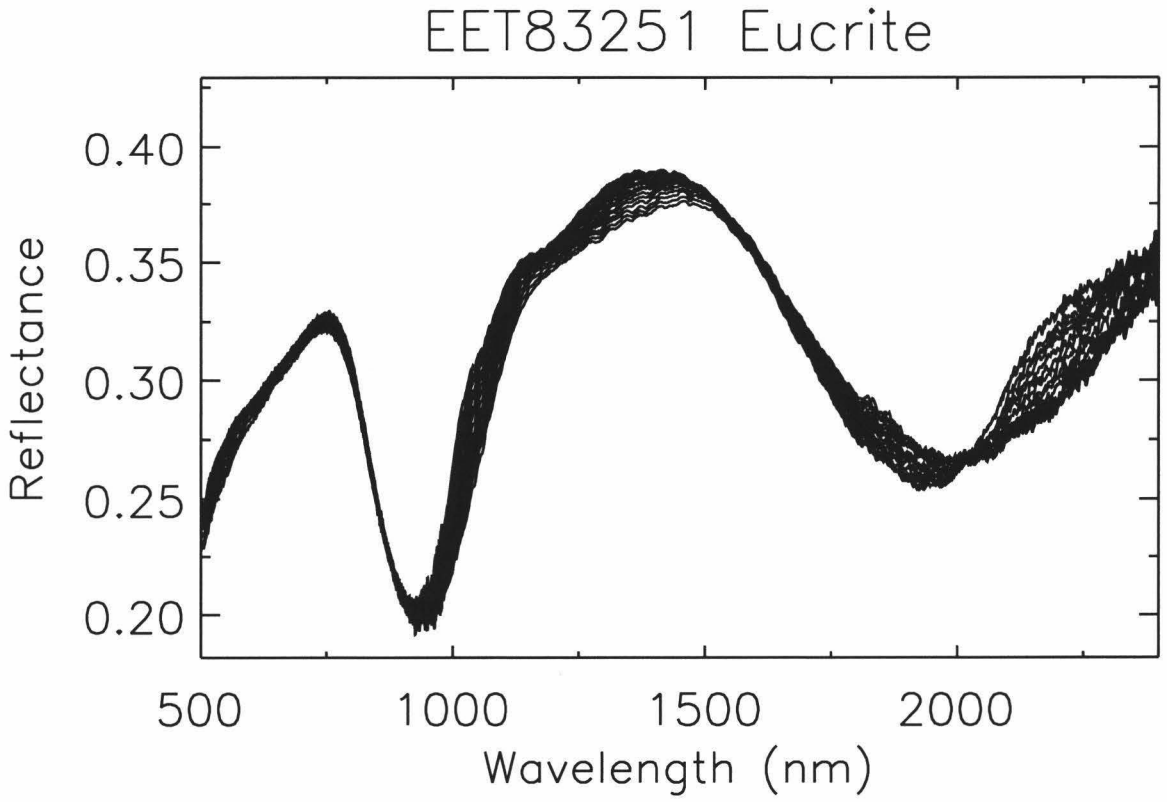
EET83251 Eucrite
Reflectance
0.40
0.35
0.30
0.25
0.20
500
1000
1500
2000
Wavelength (nm)

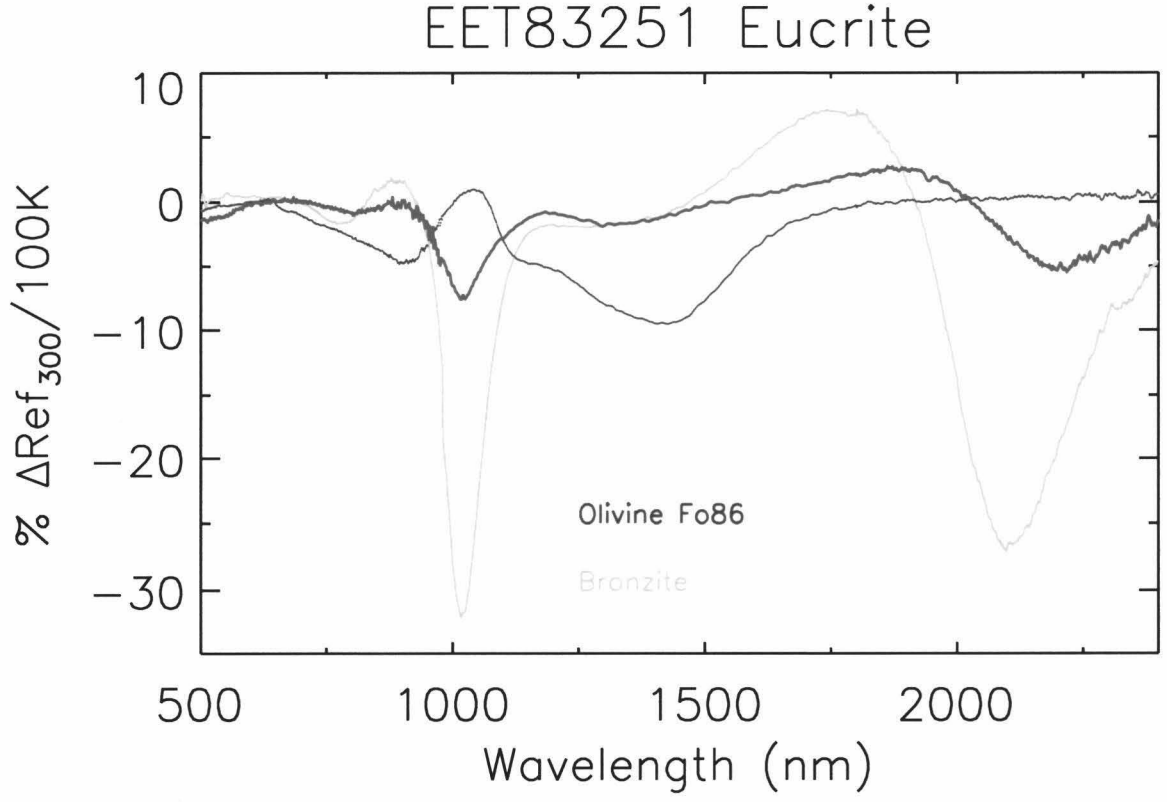
EET83251 Eucrite
% ΔRef300/100K
10
0
−10
−20
−30
Olivine Fo86
Bronzite
500
1000
1500
2000
Wavelength (nm)

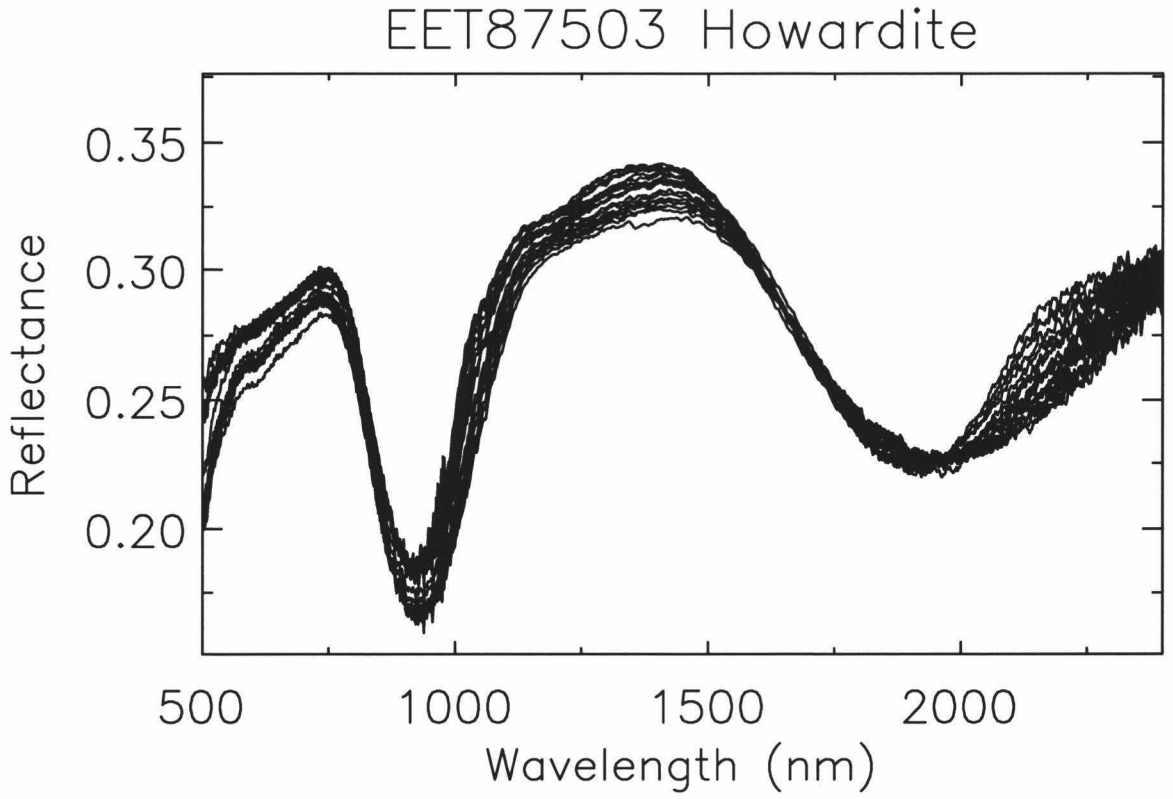
EET87503 Howardite
Reflectance
0.35
0.30
0.25
0.20
500
1000
1500
2000
Wavelength (nm)

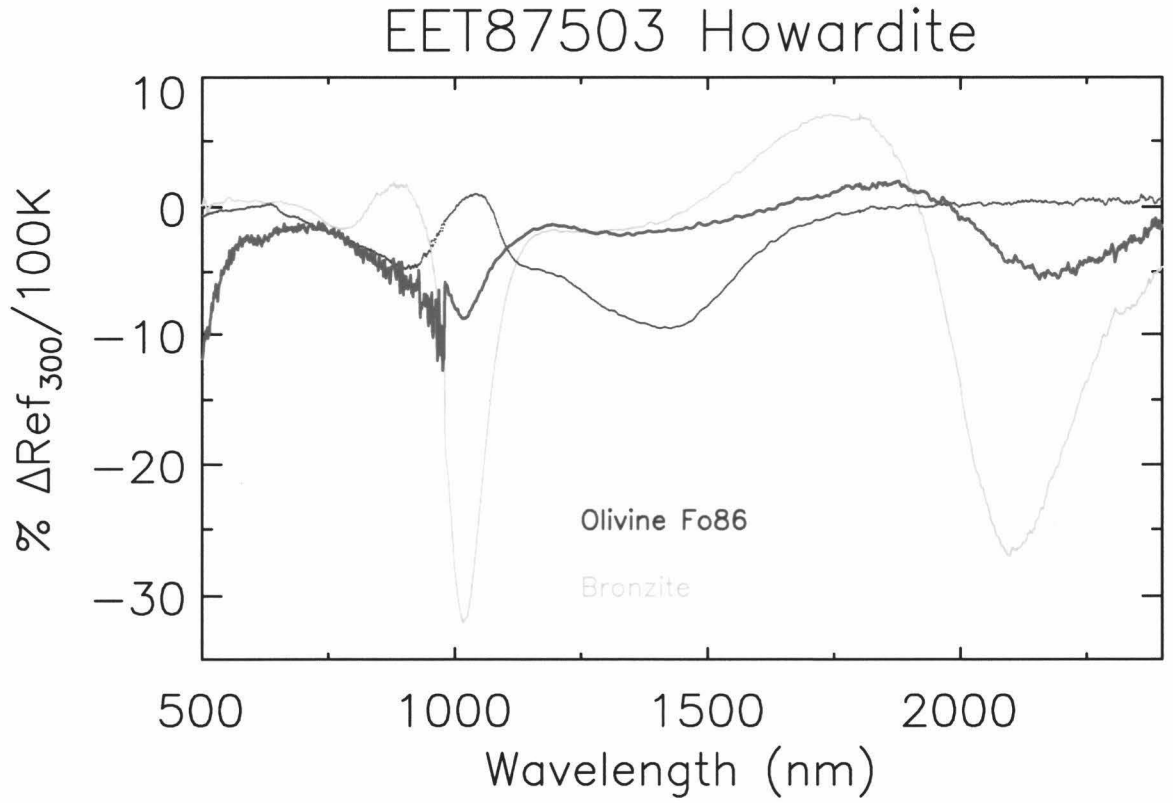
EET87503 Howardite
% ΔRef300/100K
10
0
−10
−20
−30
Olivine Fo86
Bronzite
500
1000
1500
2000
Wavelength (nm)

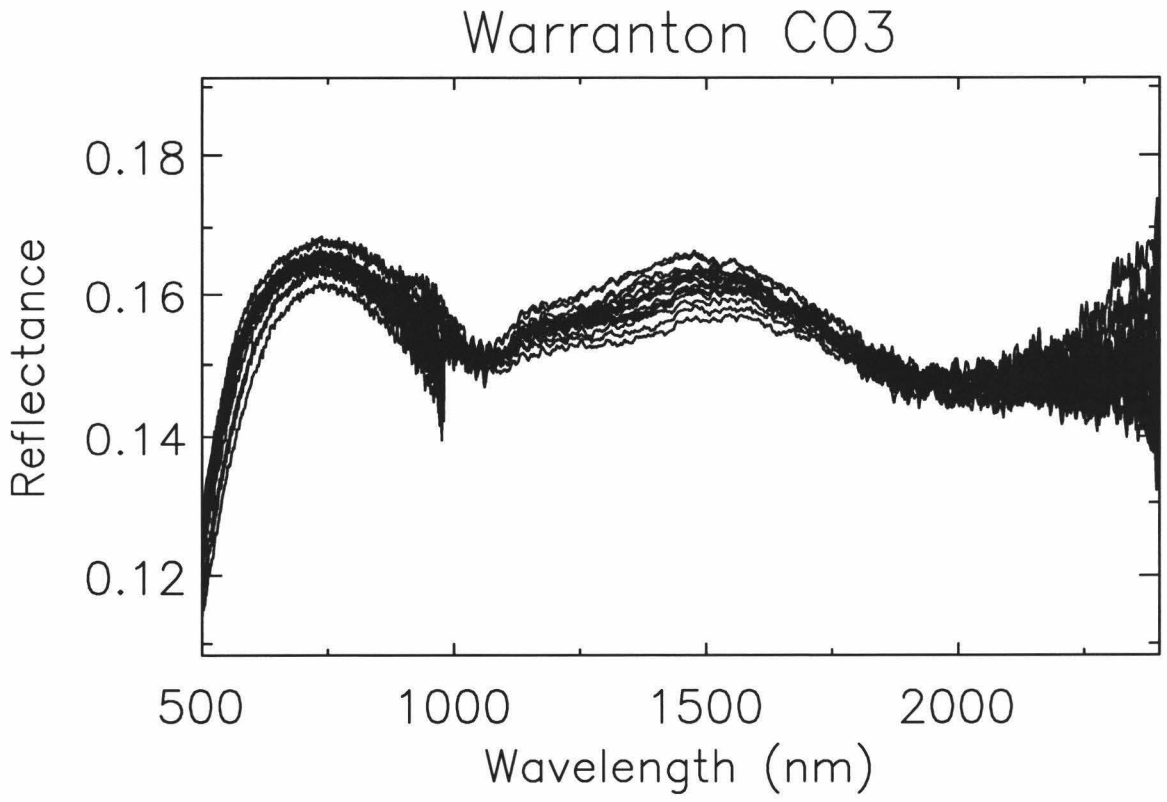
Warranton CO3
Reflectance
0.18
0.16
0.14
0.12
500
1000
1500
2000
Wavelength (nm)

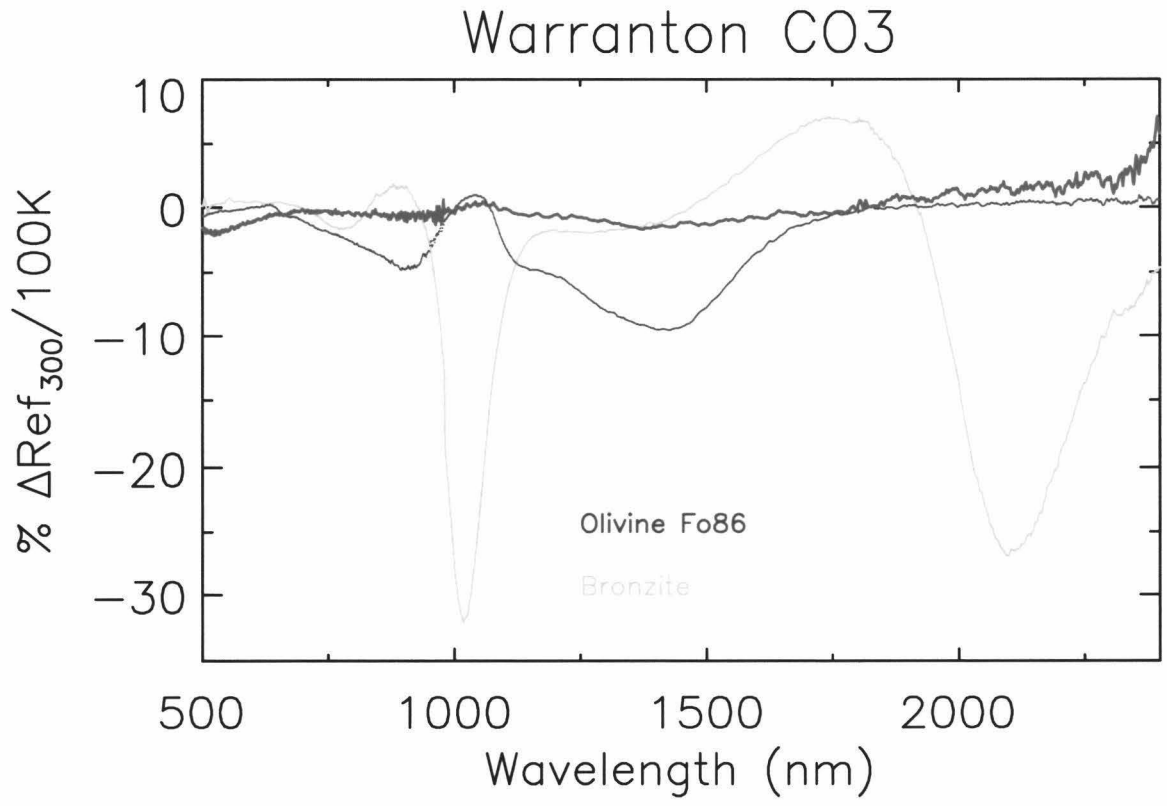
Warranton CO3
% ΔRef300/100K
10
0
−10
−20
−30
Olivine Fo86
Bronzite
500
1000
1500
2000
Wavelength (nm)

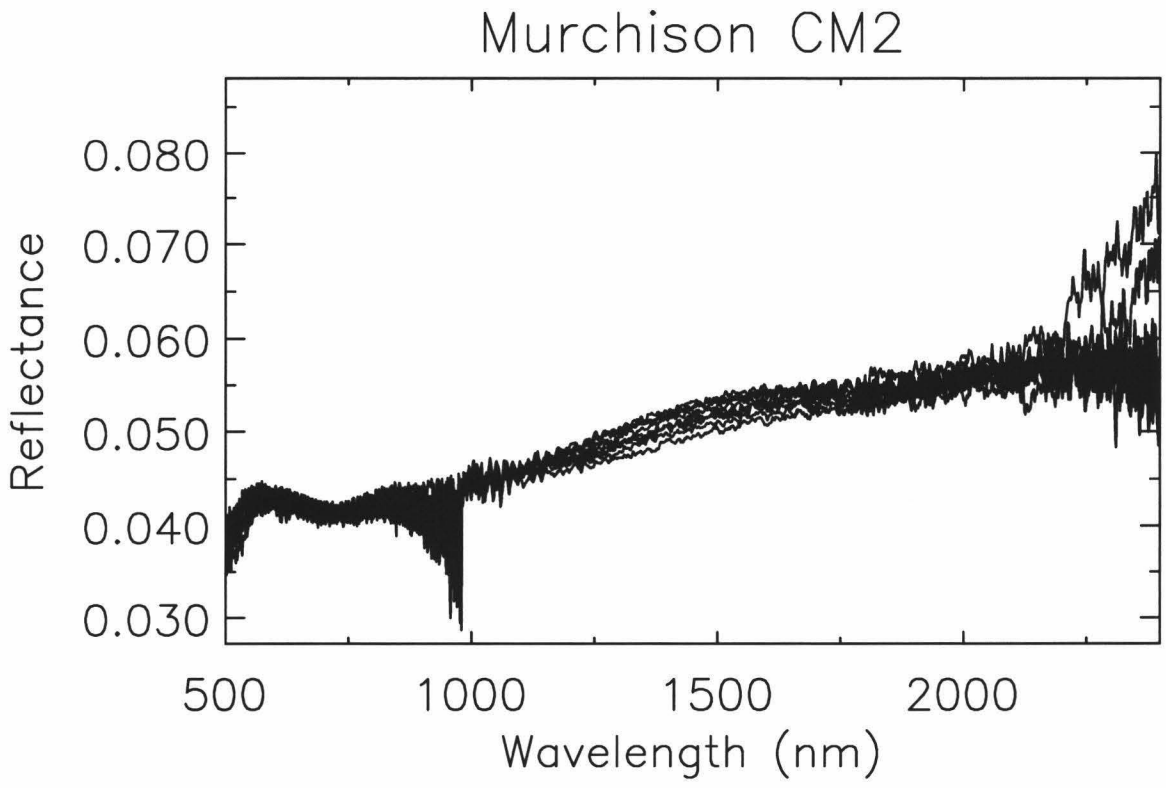
Murchison CM2
Reflectance
0.080
0.070
0.060
0.050
0.040
0.030
500
1000
1500
2000
Wavelength (nm)

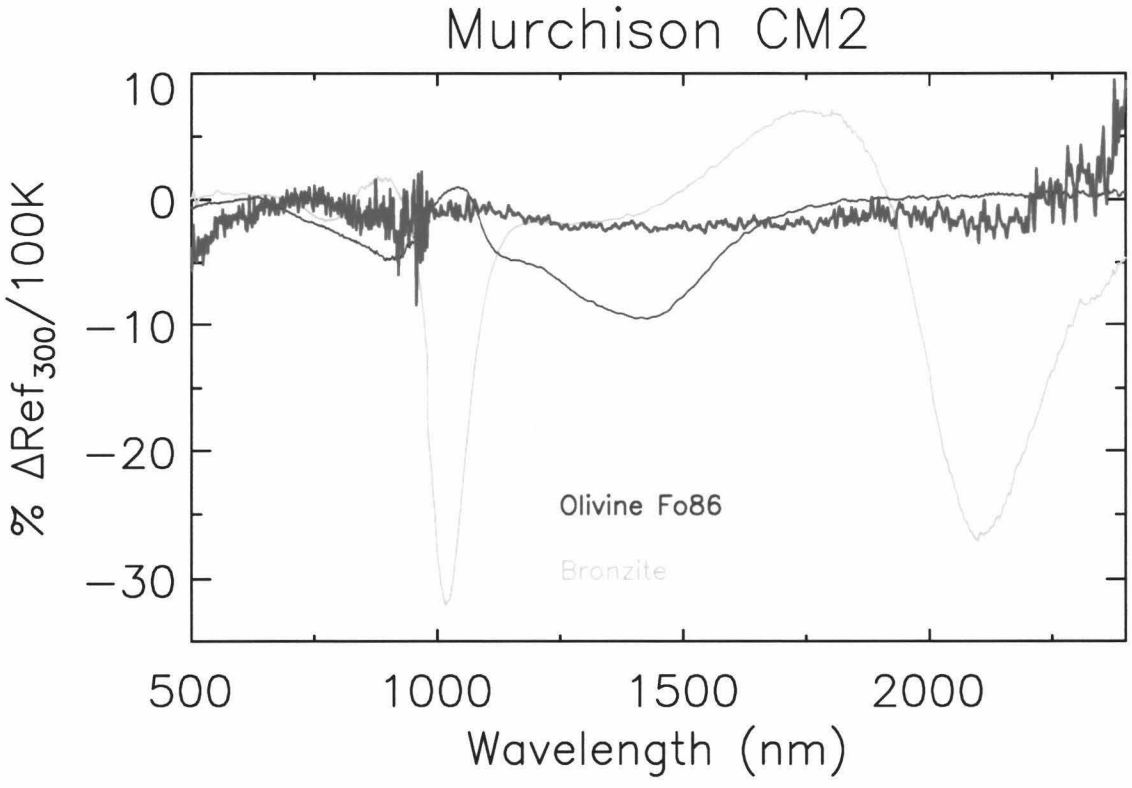
Murchison CM2
% ΔRef300/100K
10
0
−10
−20
−30
Olivine Fo86
Bronzite
500
1000
1500
2000
Wavelength (nm)

CHAPTER 3

It has been demonstrated that meteorites, serving as proxy for asteroid surfaces, show systematic and detectable variations of near-infrared spectra over a temperature range important to asteroid science. These effects in meteorites casts doubts on NIR spectral analyses of asteroids based on meteorite spectra taken at laboratory temperature. The question arises of whether or not the temperature effect will be important in spectral analysis of the lunar surface too. Lunar rocks and soils, particularly in the mare, typically contain a large fraction of pyroxene - a mineral shown to have a strong temperature dependence of its NIR spectrum over the range of temperatures, 105 K to 390 K, seen on the lunar surface[20]. Pyroxene, it should be remembered, is a major constituent of the ordinary chondrite and HED meteorite samples which exibit important temperature effects.

If a strong temperature effect is measured in lunar samples over a range of temperatures representative of the temperature differences between terrestrial laboratory and the lunar surface then many previous remote spectral analyses will need adjustments for the effect. A further complication would exist for remote sensing analysis if the temperature effect were sufficiently strong to be important with respect to temperature variations across the disk of the Moon. However, if measurements of lunar samples show little or no effect, possibly due to the many spectrally neutral components; ilmenite, sub-micron reduced Fe, and probably agglutinate glasses; in the lunar soils, then no adjustments will need to be made to previous work.

In order to definitively answer these questions eleven lunar soil samples have been acquired from the Lunar Sample Curator at Johnson Space Center with the help of Drs. Klaus Keil, Paul G. Lucey, and G. J. Taylor. The samples were chosen to represent the widest possible range of compositions and maturities. Table 1 lists the characteristics of the samples.

Table 1: Measured Lunar Soils (analysis from Handbook of Lunar Soils[21])

Sample	Characterization	Agg/Pyx/Olv/Fel/Glass or petrographic notes	I_s/FeO maturity	SiO_2/TiO_2/Al_2O_3/FeO/MgO/CaO
10084	Hi Ti mature	52% agglutinate 24% mare basalt	78 mature	41/7.3/12.8/16.2/9.2/12.4
12001	Lo Ti submature	40% agglutinate 13% basalt	56 submature	46/2.8/12.5/17.2/10.4/10.9
12023	Lo Ti mature	*	60 mature	*/2.8/13.9/15.4/*/11.2
12032	Lo Ti immature	29/15/13/17/23	12 immature	46.5/2.9/15.2/14.1/9.4/10.7
14163	Lo Ti submature	65% fused soil 14% h-land comp.	57 submature	48/1.8/17.6/10.4/9.2/11.2
60501	Mature highland	*	80 mature	45.6/0.6/27.1/5.4/5.5/15.4
67711	Immat. highland	41% feldspar 43.6% breccia	2.8 immature	44.2/0.26/29.4/3/4/16.3
72131	mature ray material	* mafic ray material	60 mature	*
72501	mature mafic h-land (S.massif)	48% agglutinate 29% breccia	81 mature	45.1/1.56/20.6/8.8/10.1/12.9
73241	immature mafic h-land (lt. mantle)	8.4% agglutinate 62% breccia	18 immature	44.6/1.73/20.2/8.5/11.1/12.9
75061	Hi Ti submature	24% agglutinate 56% Cpx+basalt	33 submature	39.3/10.3/10.4/18.2/9.5/10.7

* missing data

Results for Lunar Soils

In all cases the temperature effect is observed. However, the amplitude of the effect is small and in some of the darker samples almost lost in the noise. The following spectra of the lunar samples demonstrate the quality of the data with ~18 spectra nicely overlaying one another (darker samples often show some detector noise just short of 1μm) in plots of absolute reflectance vs. wavelength. The reflectance at 1.1μm plotted against temperature demonstrate that although a subtle effect is detected the amplitude is so small as to be of no importance in NIR spectral analysis of the Moon.

10084 – High Ti mature, I_s/FeO= 78, Apollo 11 soil.

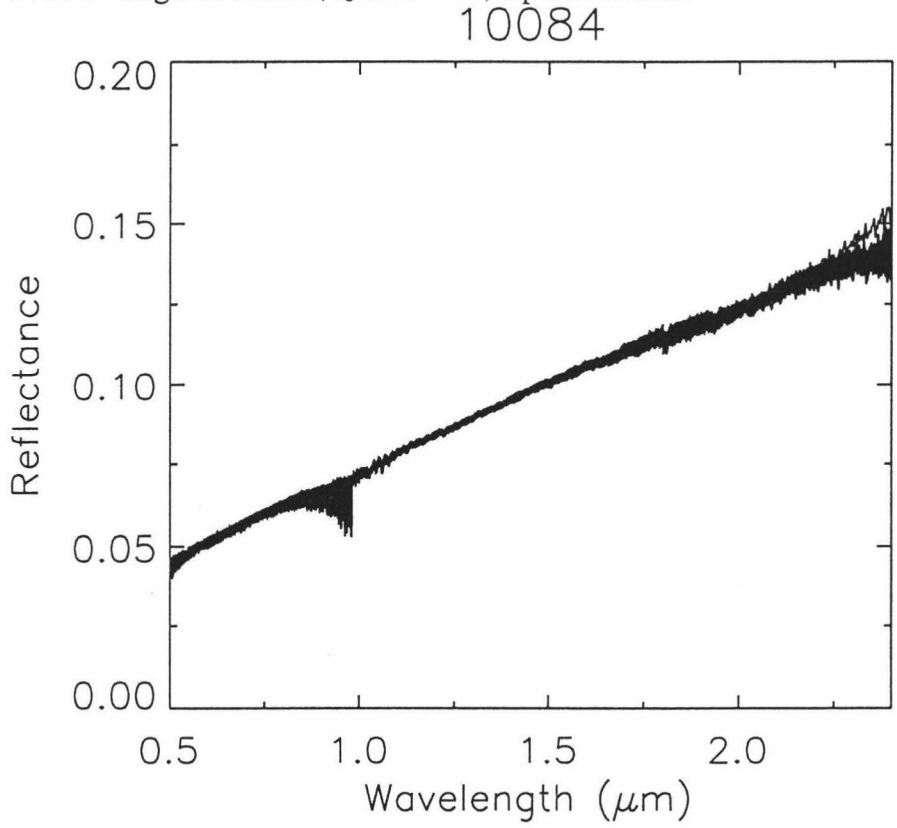

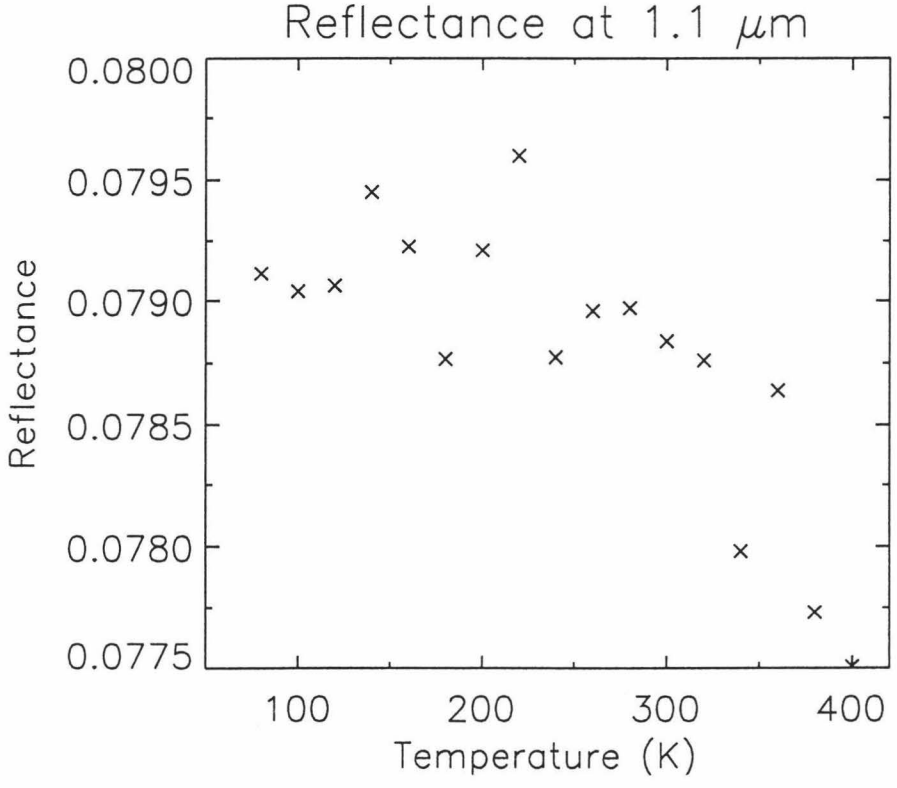

12001 – Low Ti submature, I_s/FeO = 56, Apollo 12 soil.

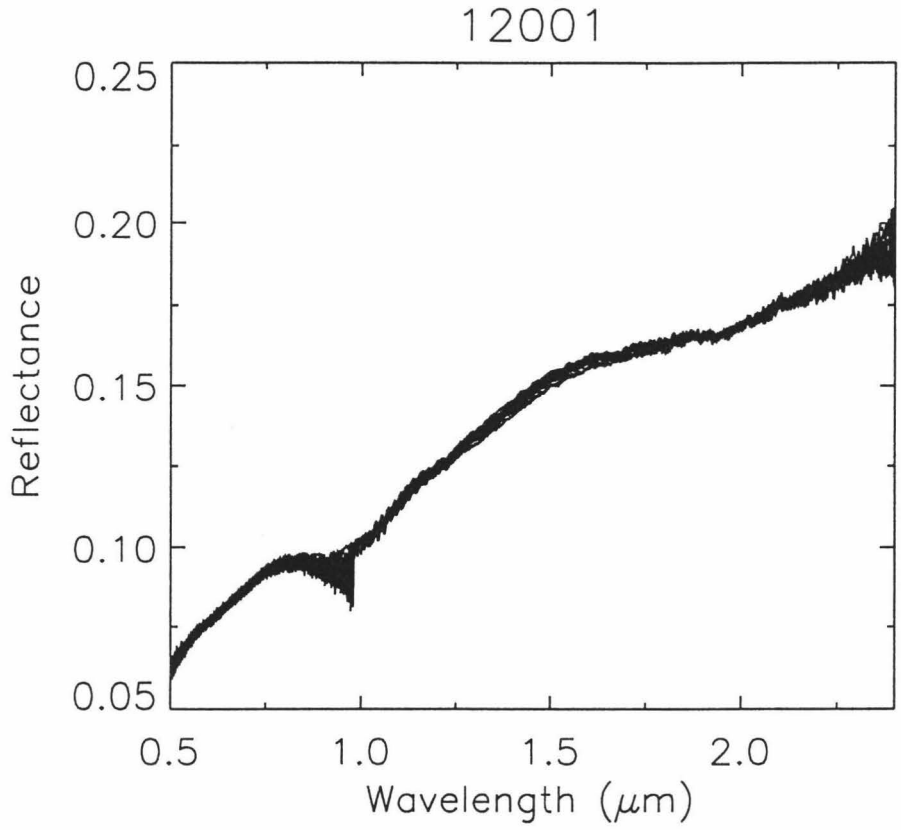

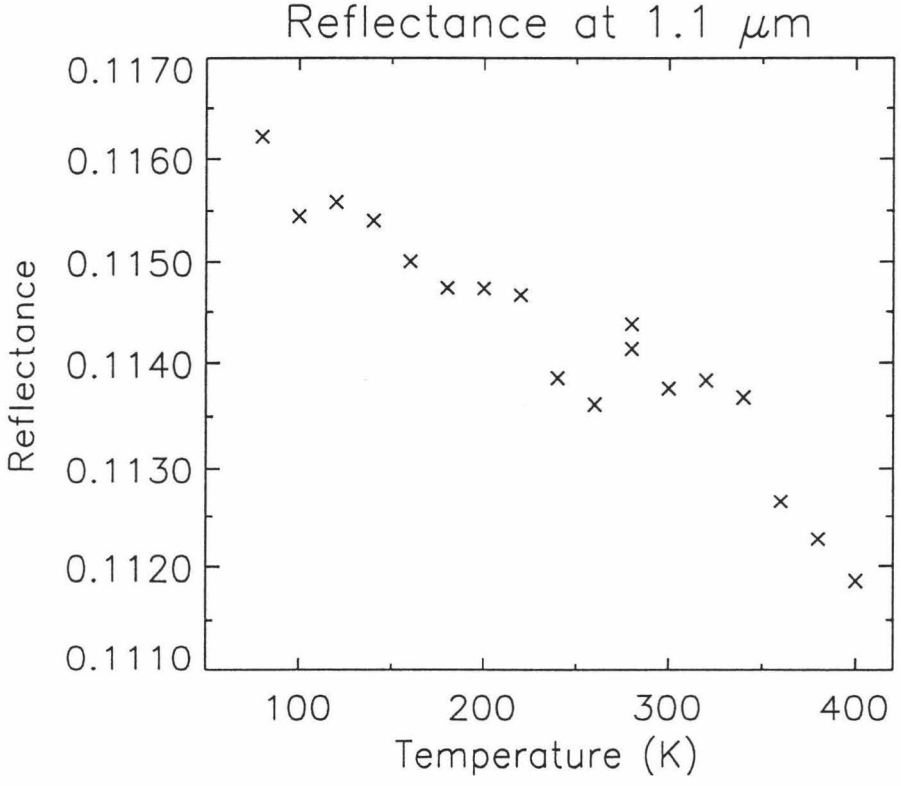

12023 – Low Ti mature, I_s/FeO = 60, Apollo 12 soil.

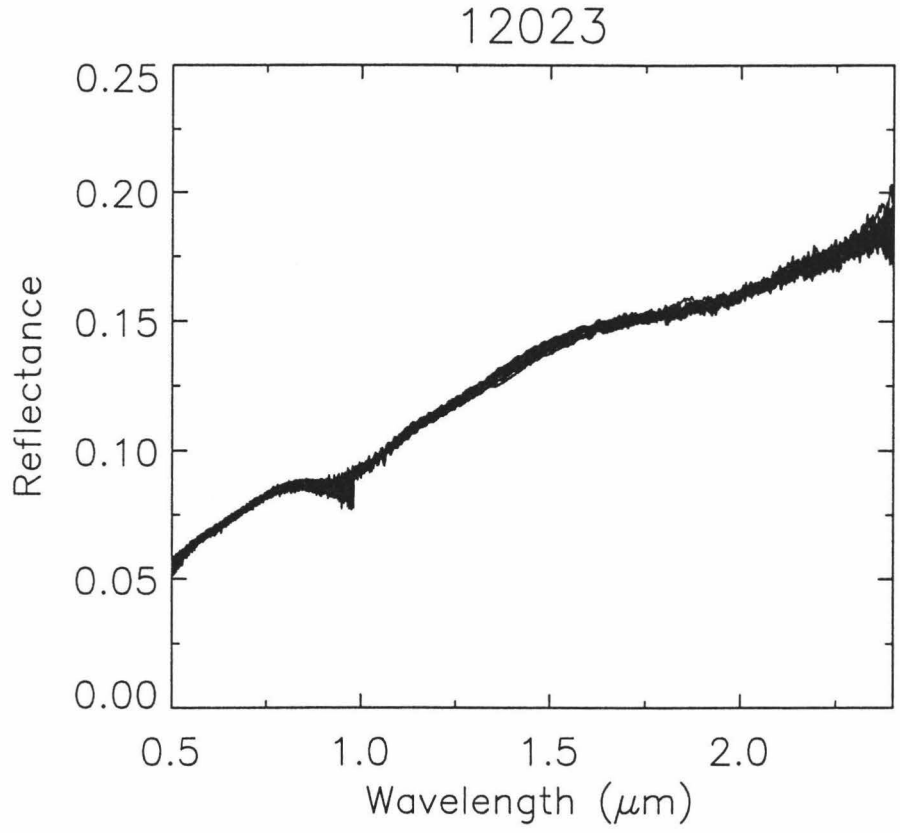

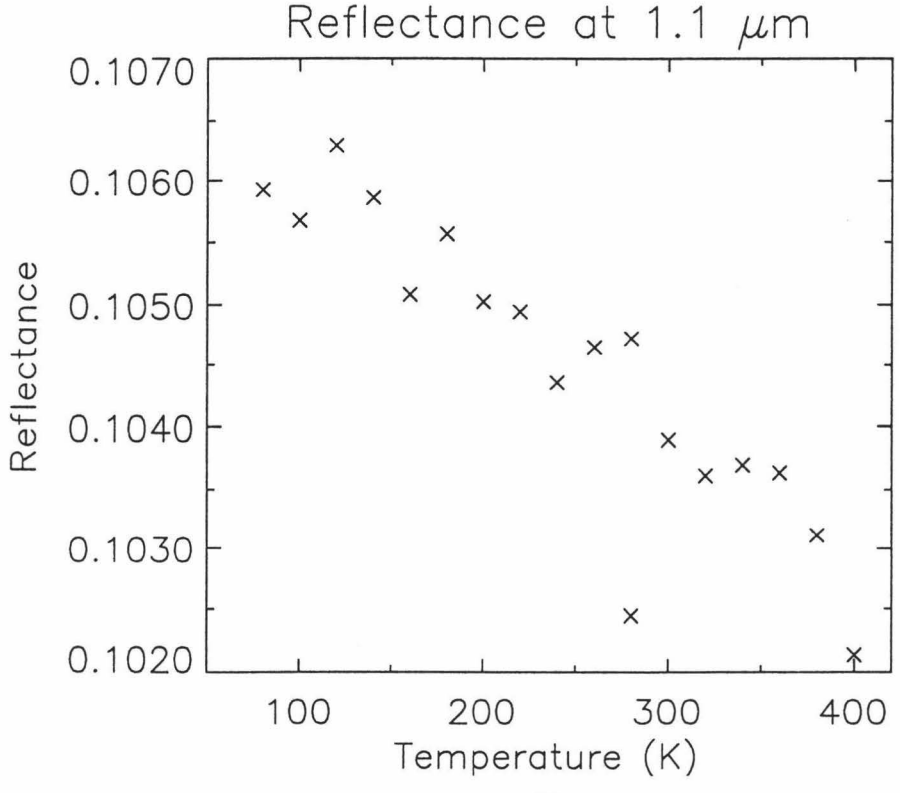

12032 – Low Ti immature, I_s/FeO = 12, Apollo 12 soil.

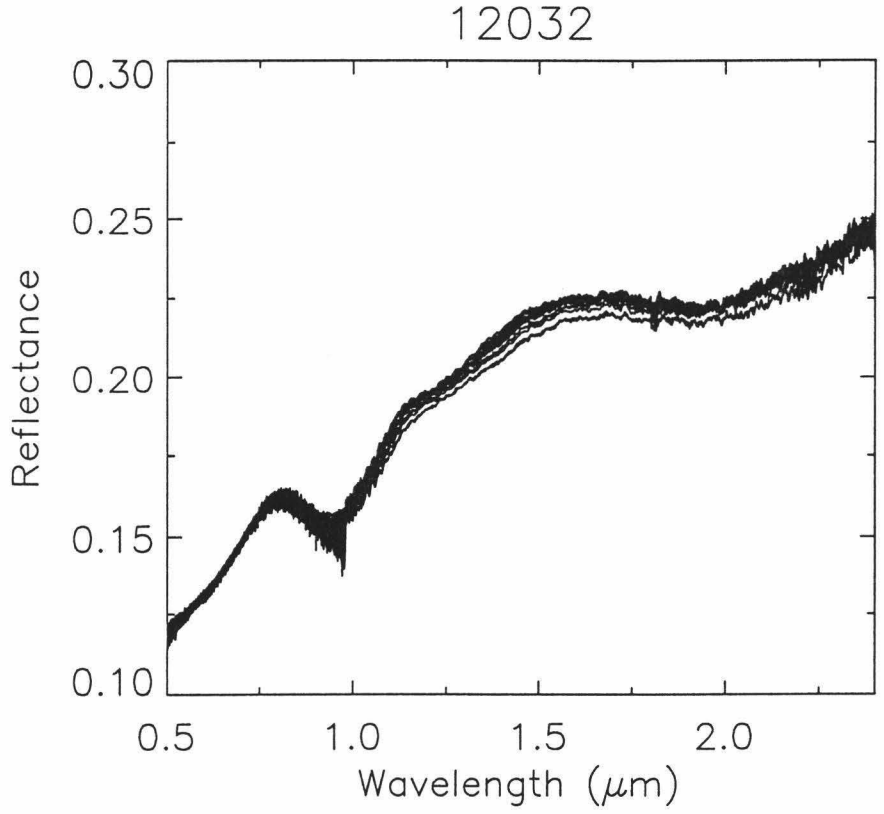

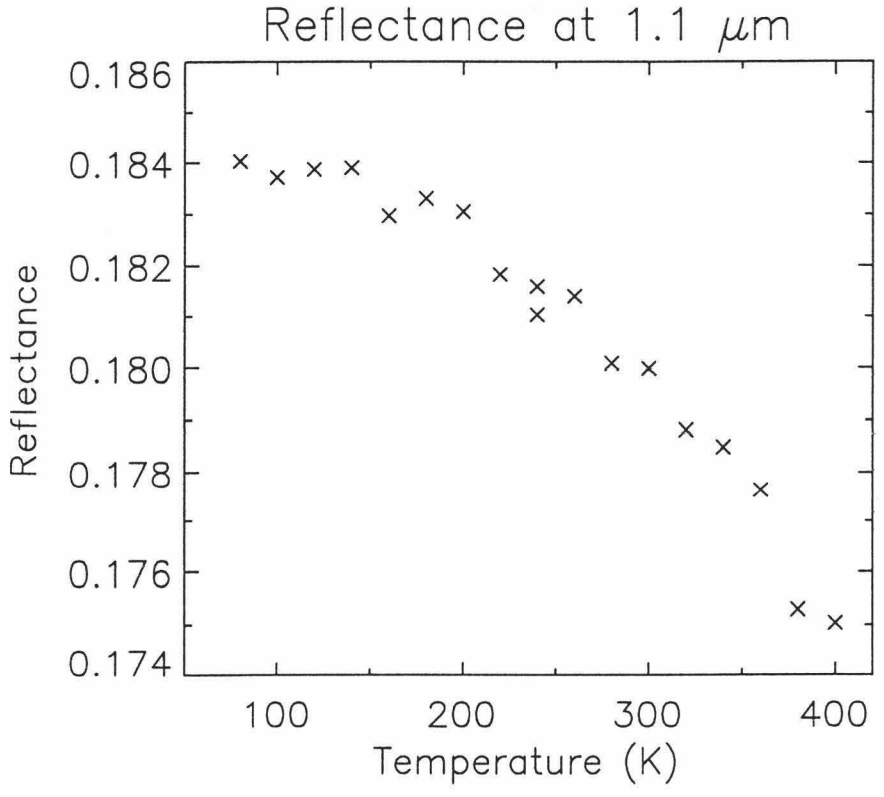

14163 – Low Ti submature, I_s/FeO = 57, Apollo 14 soil.

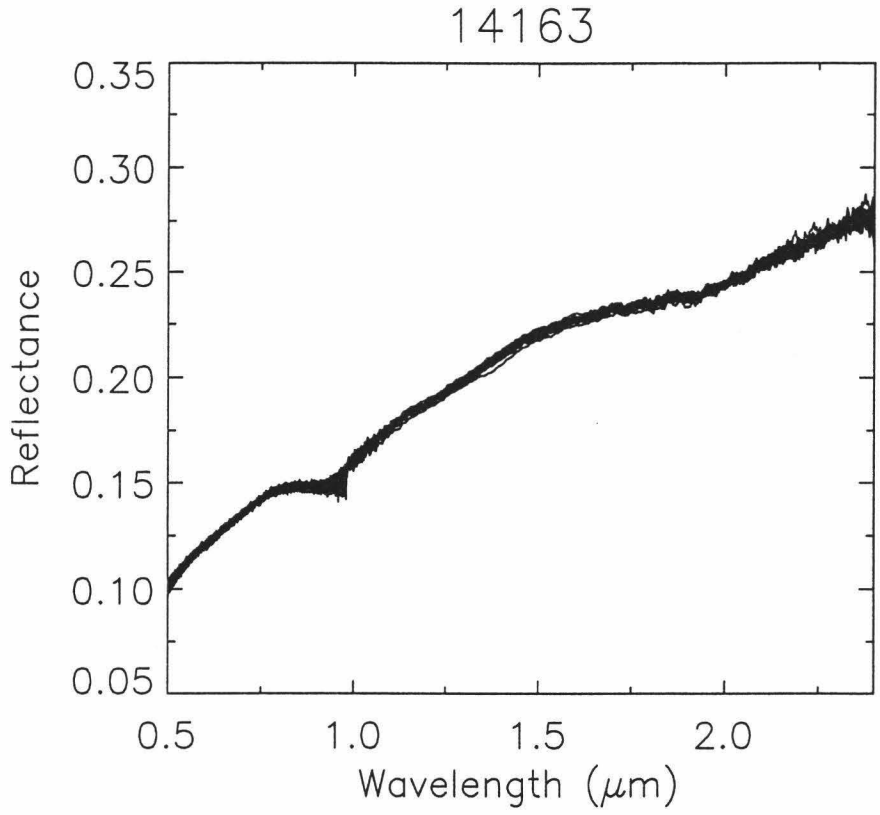

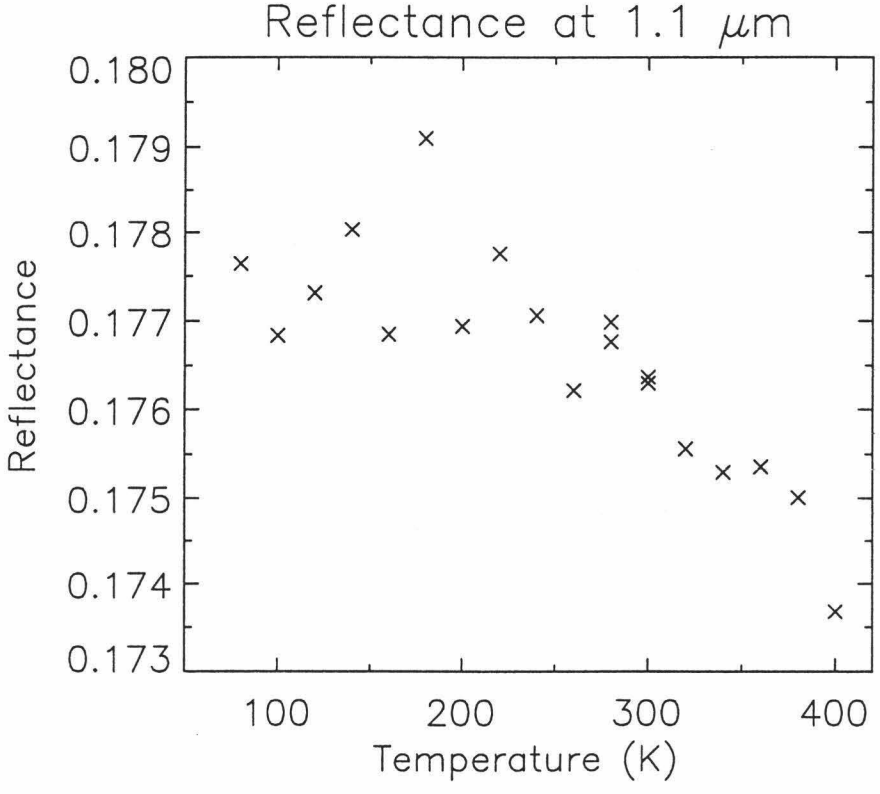

60501 – Mature highland soil, I_s/FeO = 80, Apollo 16.

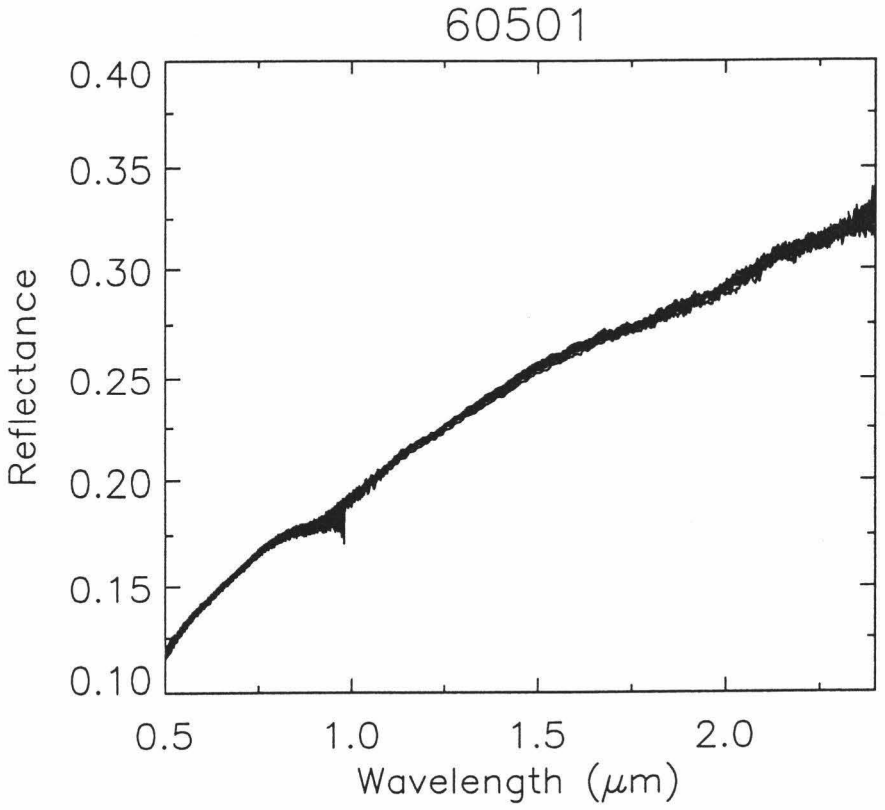

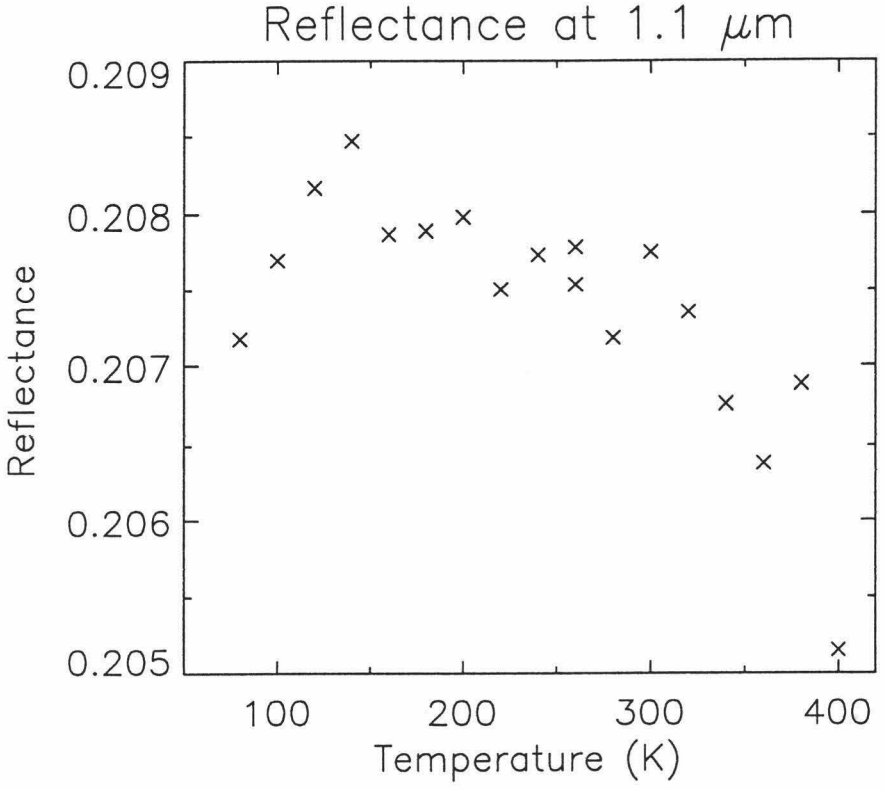

67711 – Immature highland soil, I_s/FeO = 2.8, Apollo 16.

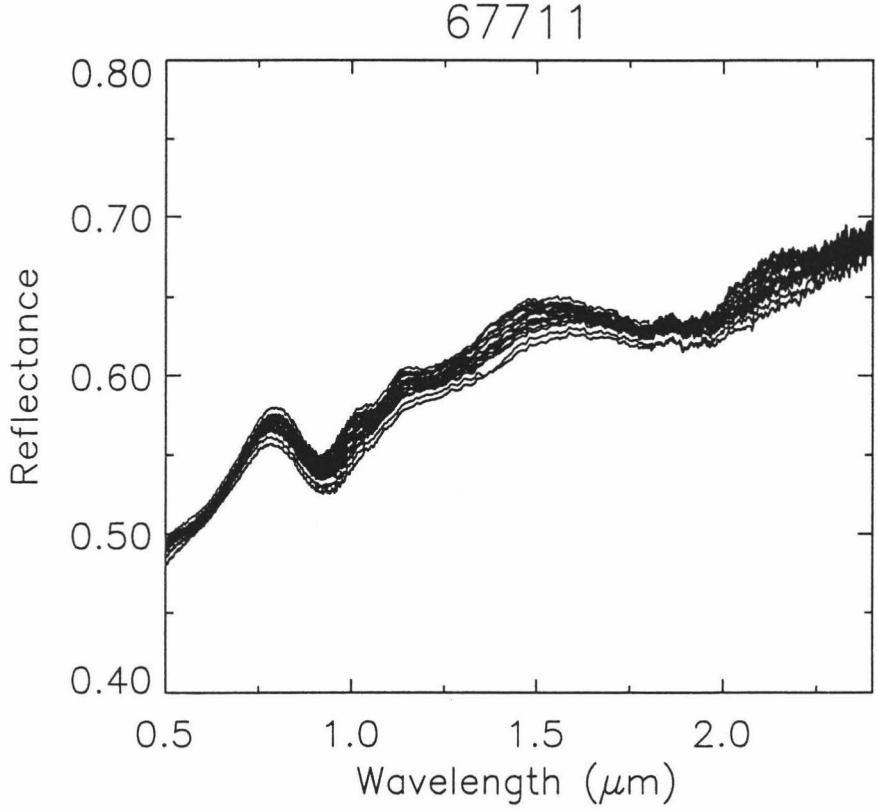

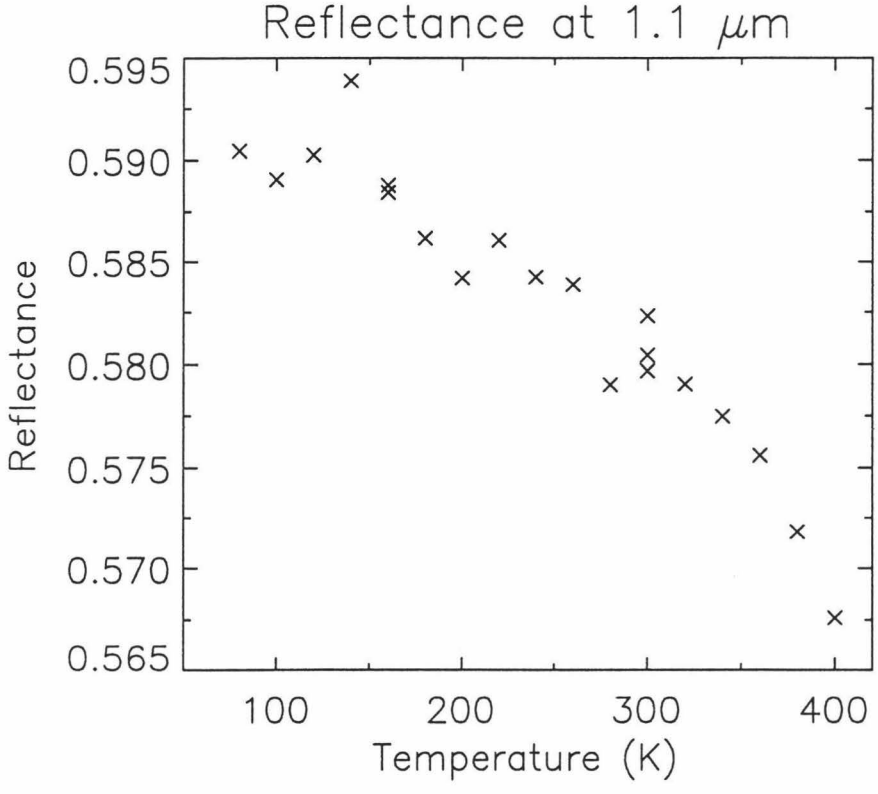

72131 – Mature mafic ray material, I_s/FeO = 60, Apollo 17.

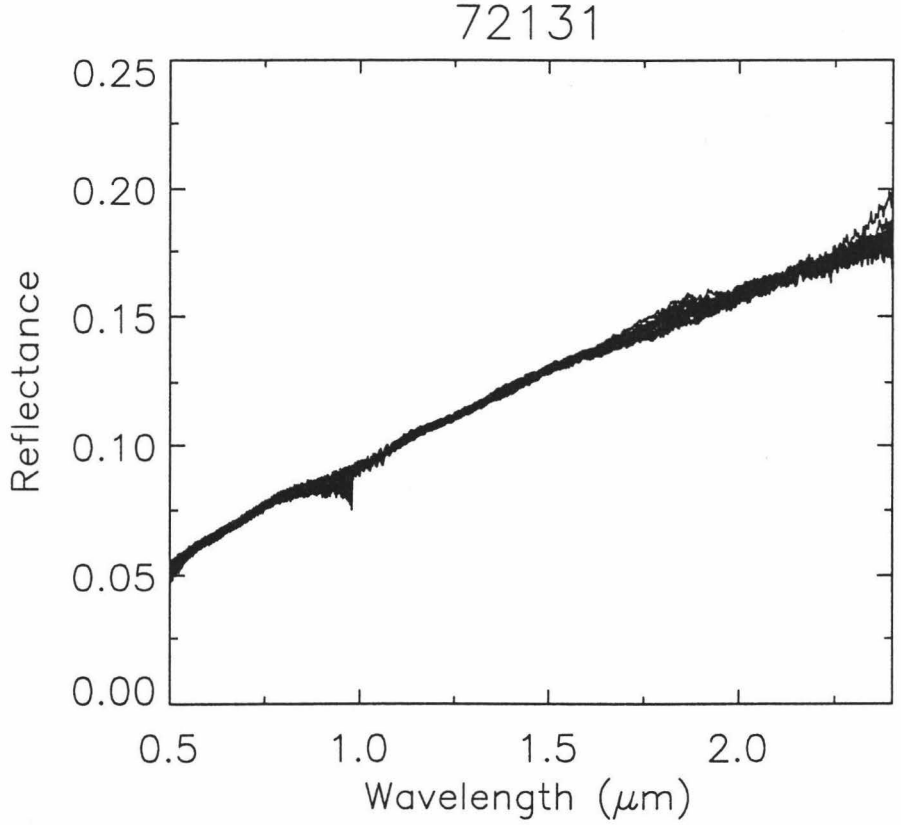

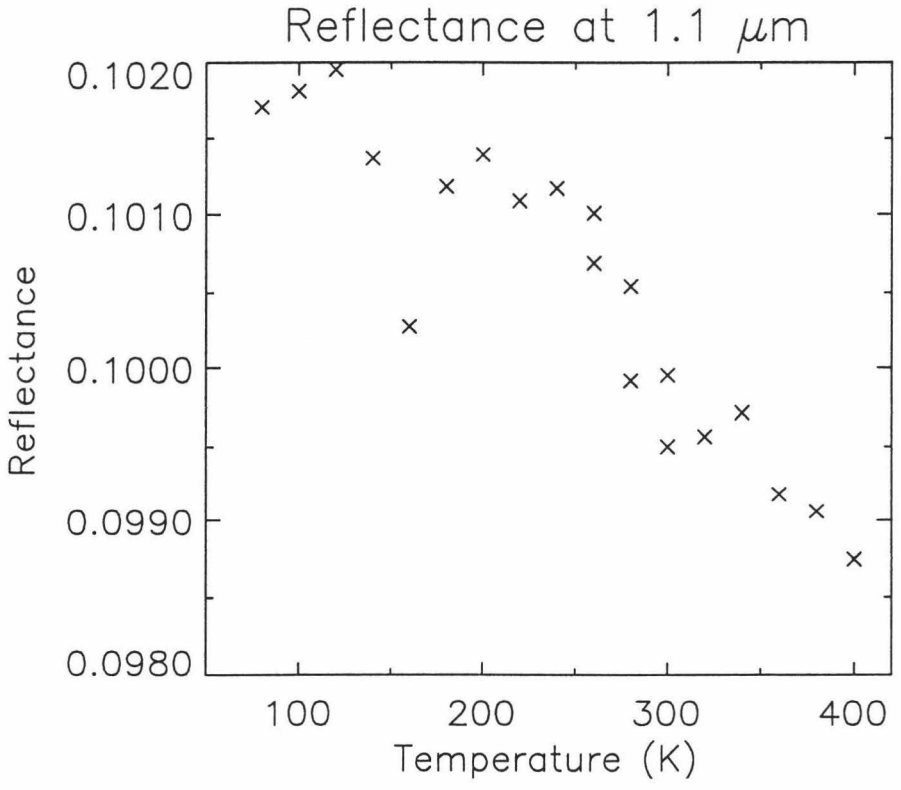

72501 – Mature mafic highland from base of South Massif, $I_s/FeO = 81$, Apollo 17.

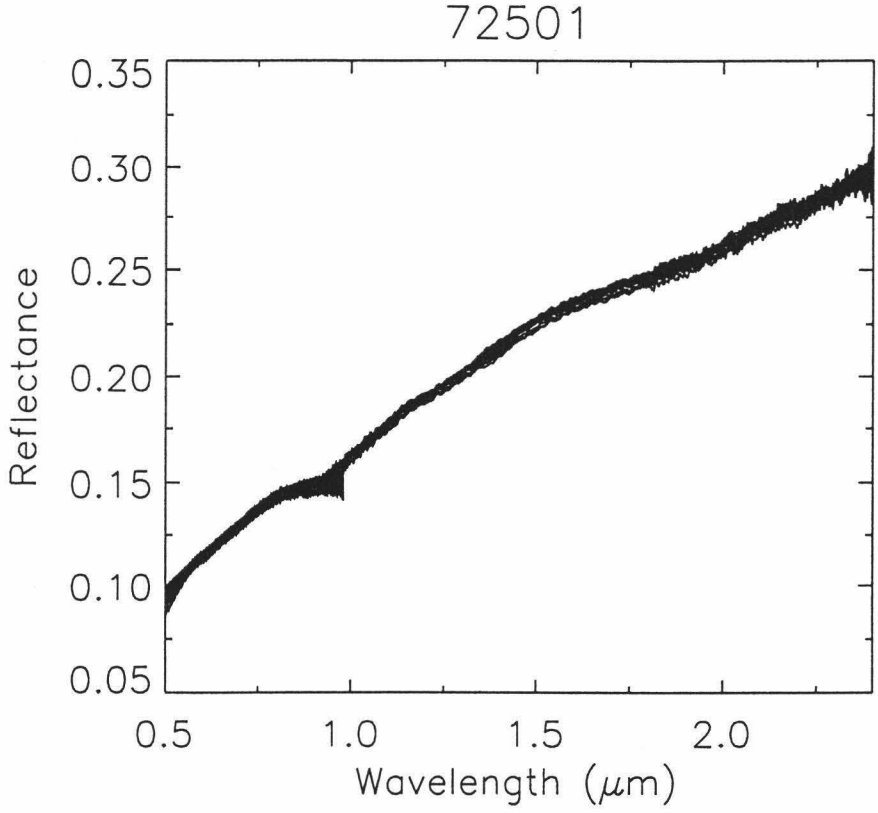

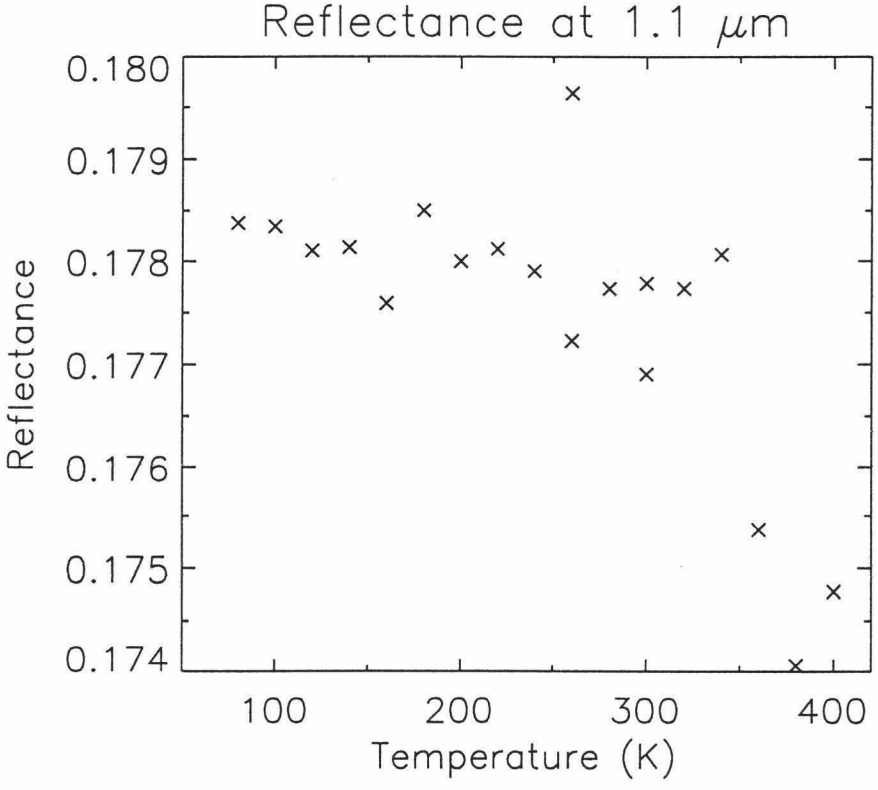

73241 – Immature mafic highland light mantle material, I_s/FeO = 18, Apollo 17.

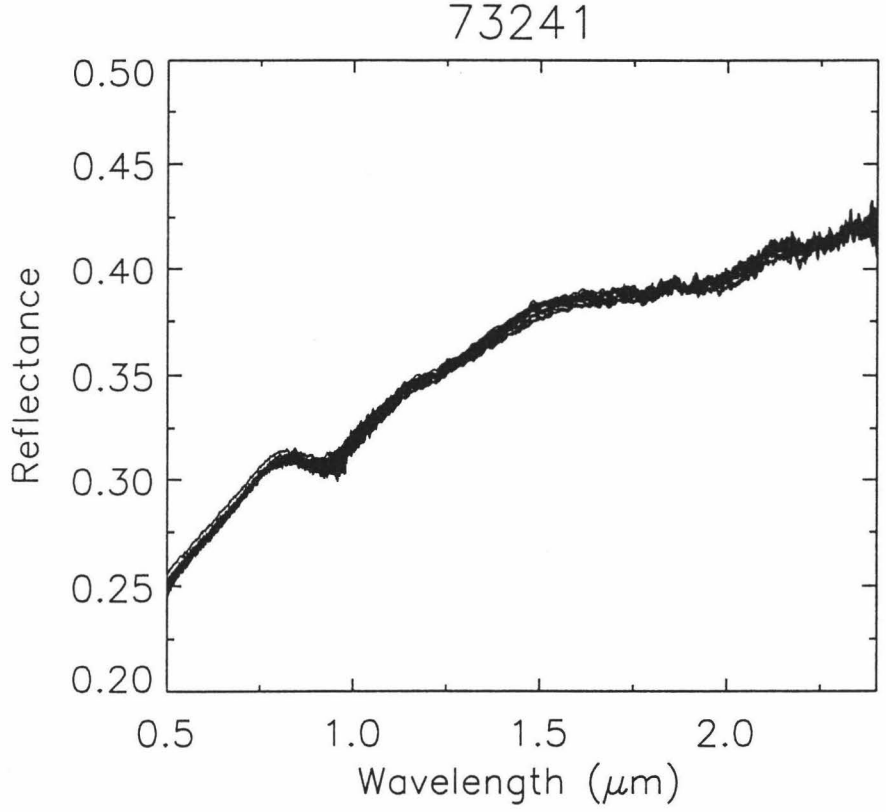

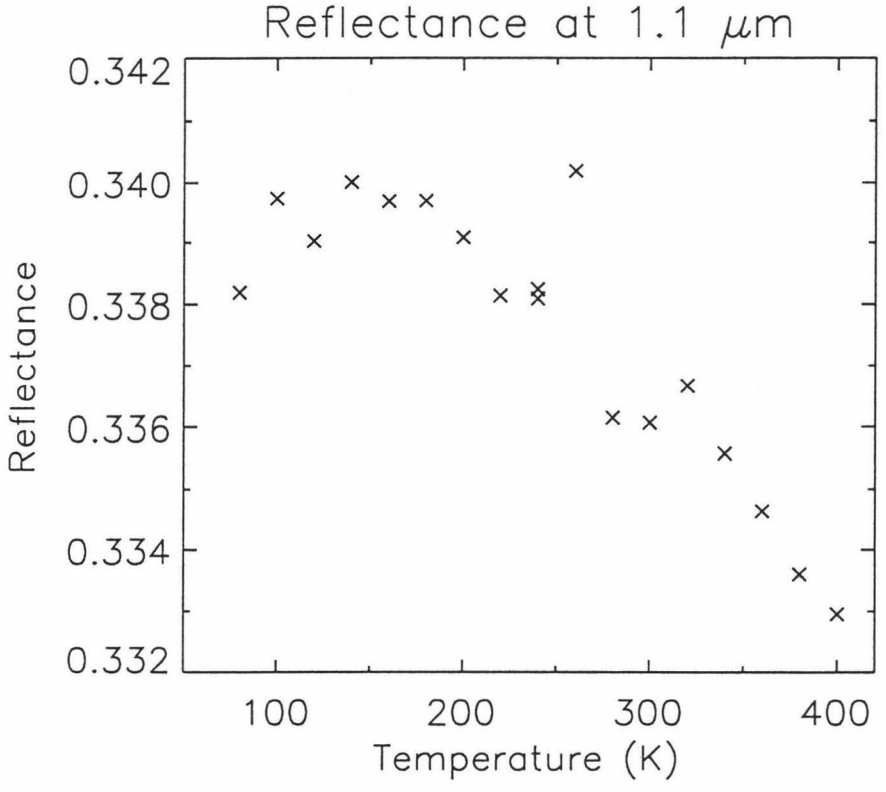

75061 – High Ti submature, I_s/FeO = 33, Apollo 17.

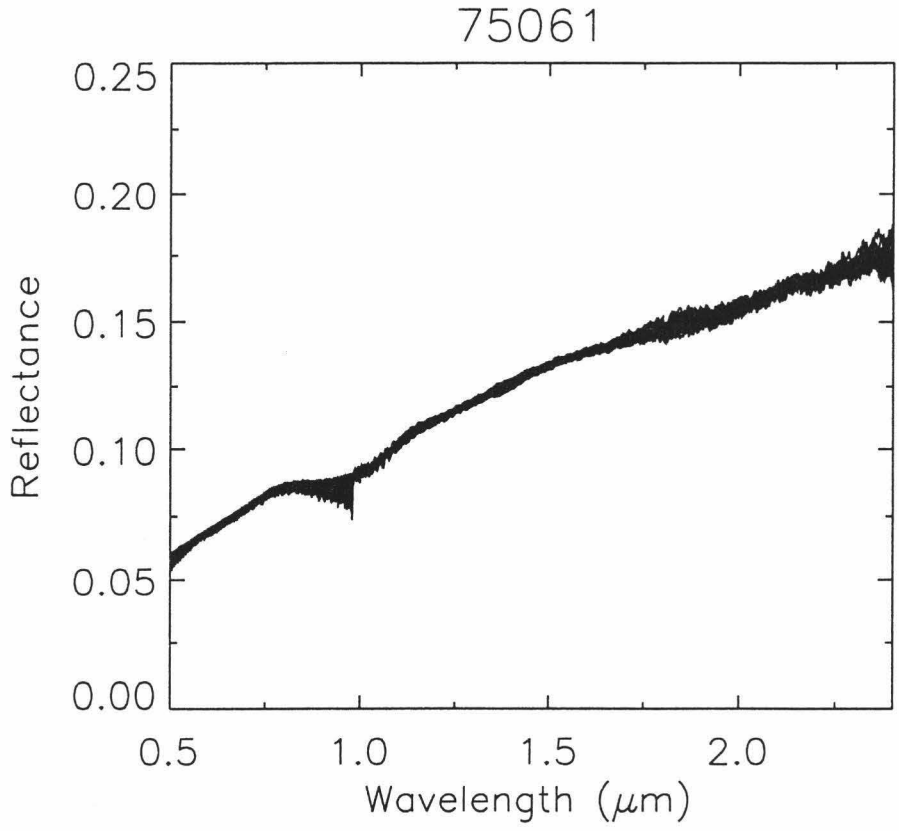

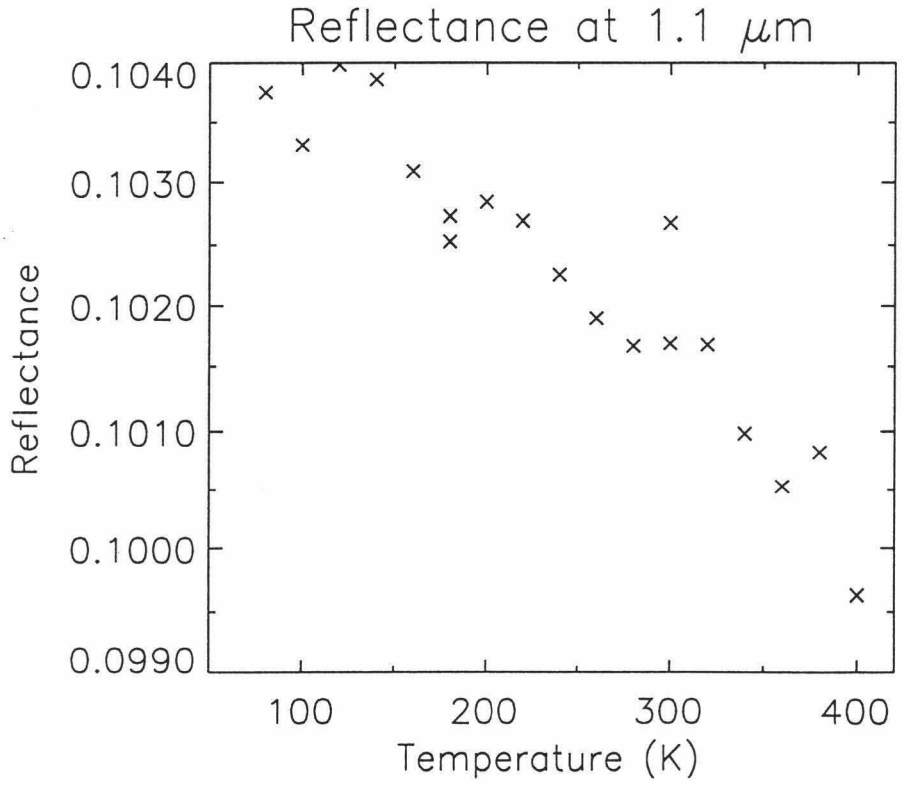

Conclusions

The results presented here, the first measurements of the temperature effect for the near-infrared spectra of lunar soils, show that although a small effect is present the amplitude of the effect is so small that it can be ignored in remote sensing analysis of the Moon. Reasons for the small amplitude of the effect are almost certainly the predominance of dark, spectrally neutral components in the lunar soils. Of course, the brighter feldspathic soils will have a smaller effect without the presence of as much dark, spectrally neutral, material because feldspar is not a mafic mineral and therefore does not experience Fe^{2+} absorptions susceptible to the temperature effect. The spectrally neutral components are most likely to be sub-micron reduced Fe, ilmenite, and a variety of glasses produced by impact processes and ancient volcanism.

Now that these comprehensive measurements have been made concerns about the affect of temperature on lunar remote sensing analysis may definitively be addressed with this data showing the effect is too small to be of any importance.

REFERENCES

[1] Roush, T.L., "Effects of temperature on remotely sensed mafic mineral absorption features", Masters Thesis, University of Hawaii, 1984.

[2] Singer, R.B. and T.L. Roush, "Effects of temperature on remotely sensed mineral absorption features", J. Geophys. Res. 90, B14, pp 12434-12444, 1985.

[3] Roush, T.L., and R.B. Singer, "Gaussian analysis of temperature effects on the reflectance spectra of mafic minerals in the 1-um region", J. Geophys. Res. 91, B10, pp10301-10308, 1986.

[4] Roush, T.L., and R.B. Singer, "Possible temperature variation effects on the interpretation of spatially resolved reflectance observations of asteroid surfaces", Icarus, 69, 571-574, 1987.

[5] Burns, Crystal Field theory

[6] Cloutis, E.A., and M.J. Gaffey, Spectral-compositional variations in the constituent minerals of mafic and ultramafic assemblages and remote sensing implications; *Earth, Moon, and Planets*; **53**, 11-53, 1991.

[7] Heiken, Vaniman, and French (Eds.), Luanr Sourcebook, Cambridge, 1991.

[8] Analytical Spectral Devices, Boulder CO, FeildSpec Manual, 1998.

[9] Sunshine, Jessica, personal communication.

[10] Roush, T.L., "Effects of temperature on remotely sensed mafic mineral absorption features", Masters Thesis, University of Hawaii, 1984.

[11] Roush, T.L., and R.B. Singer, "Possible temperature variation effects on the interpretation of spatially resolved reflectance observations of asteroid surfaces",Icarus, 69, 571-574, 1987

[12] Cruikshank, D.P and Hartmann, W.K., The meteorite-asteroid connection: Two olivine rich asteroids, *Science* **223**, 281-283, 1984.

[13] Lucey, P.G., K. Keil and R. Whiteley, "The influence of tempterature on the spectra of the A-asteroids and implications for their silicate chemistry", *JGR Planets*, **103**, E3, 5865-5871, 1998.

[14] Gaffey, M.J., J.F. Bell, R.H. Brown, T.H. Burbine, J.L. Piatek, K.L. Reed, and D.A.Chaky, Mineralogical variations within the S-type asteroid class, *Icarus*, **106**, 573-602, 1993.

[15] Hinrichs, J.L. P.G. Lucey, M.S. Robinson, A. Meibom, and A.N. Krot, "Implications of temperature-dependent near-IR spectral properties of common minerals and meteorites for remote sensing of asteroids". GRL **26** No. 12, pp.1661-1664, June 15,1999.

[16] Hapke, B., *Theory of Reflectance and Emittance Spectroscopy*, 455 pp., Cambridge Univ. Press, New York, 1993

[17] Cloutis, E.A., M.J. Gaffey, D.G.W. Smith, and R.S.J. Lambert, Reflectance spectra of mafic silicate-opaque assemblages with applications to meteorite spectra; *Icarus*, **84**, 315-333, 1990.

[18] Binzel R. P. and Xu S. Chips off of asteroid 4 Vesta: Evidence for the parent body of basaltic achondrite meteorites. *Science* **260**, 186-191, 1993.

[19] For a good overview look for Burbine et al., Vesta, Vestoids and HEDs: Relationships and the Origin of Spectral Differences, Meteoritics and Planetary Science, in press.

[20] Heiken, Vaniman, French, Eds. Lunar Sourcebook, Cambridge, p34, 1991.

[21] Morris, Score, Dardano and Heiken, Handbook of Lunar Soils, pts 1 and 2, NASA Planetary Materials Branch Publication 67, JSC pub. 19069, 1983.

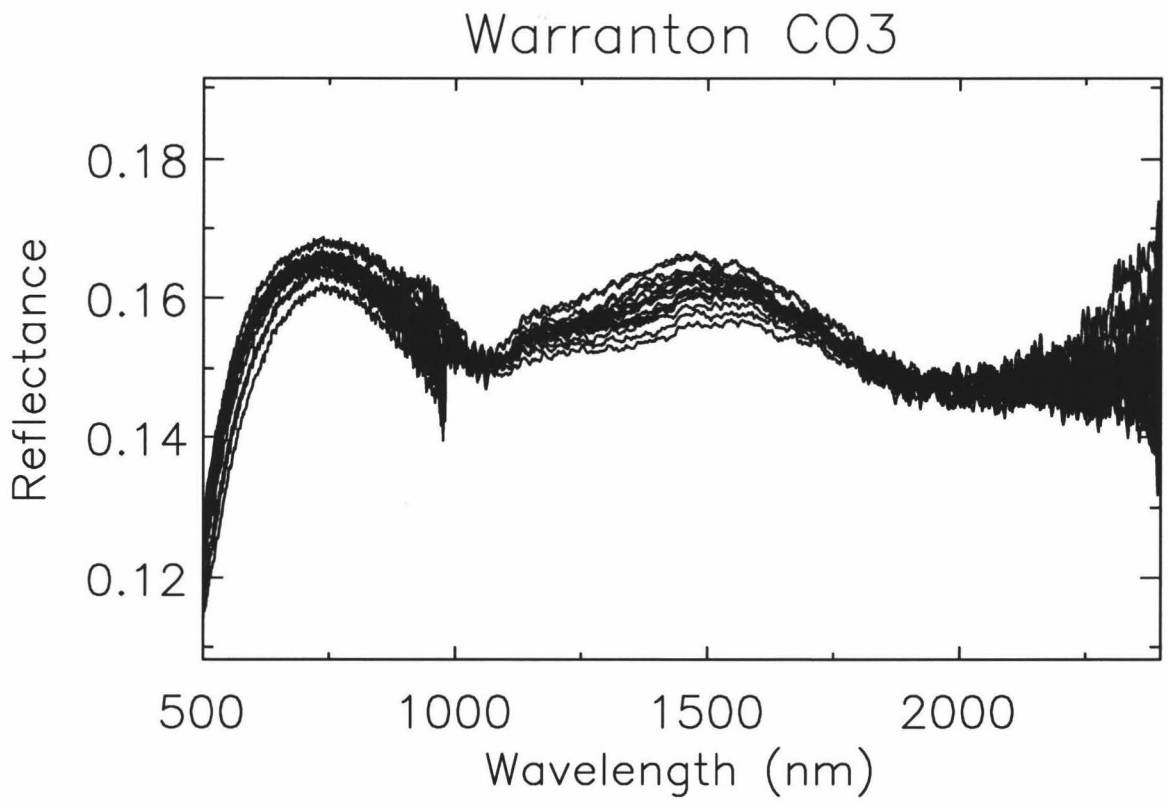
Warranton CO3
Reflectance
0.18
0.16
0.14
0.12
500
1000
1500
2000
Wavelength (nm)

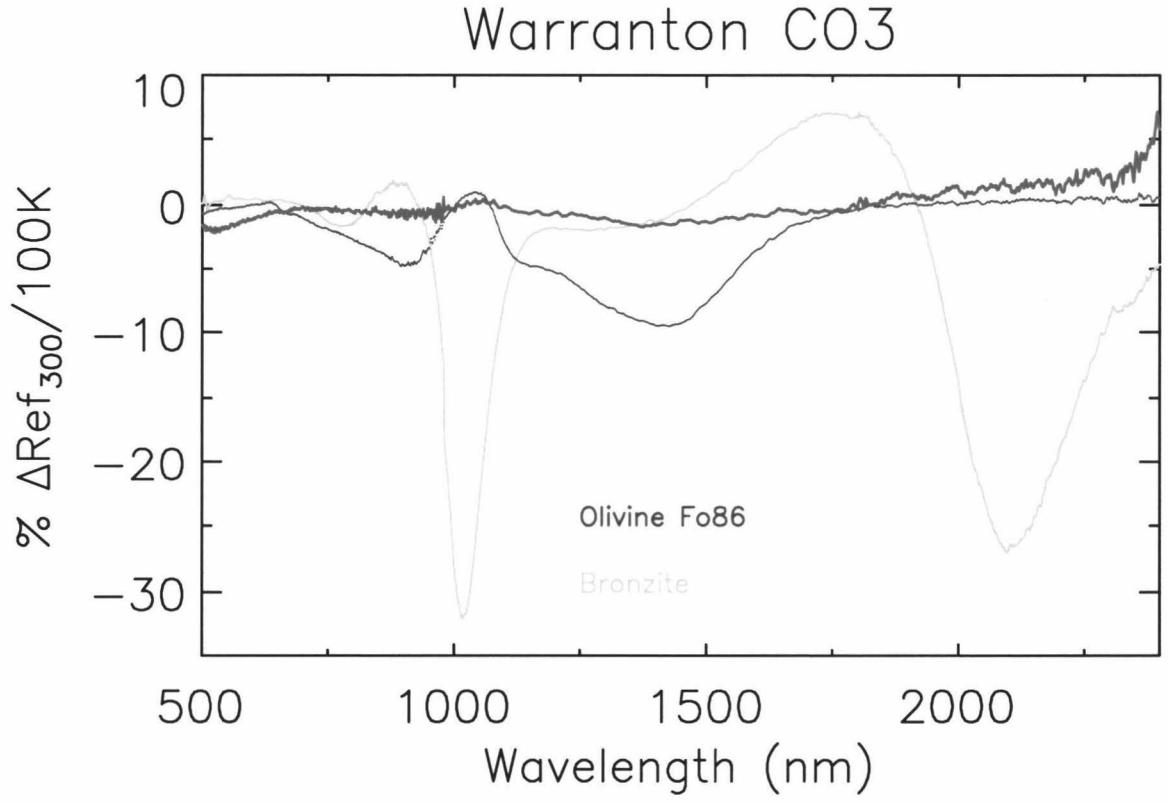
Warranton CO3
% ΔRef300/100K
10
0
−10
−20
−30
Olivine Fo86
Bronzite
500
1000
1500
2000
Wavelength (nm)